The molecular universe

A. G. G. M. Tielens*

Leiden Observatory, Leiden University, PO Box 9513, NL-2300RA Leiden, The Netherlands

(published 12 July 2013)

Molecular absorption and emission bands dominate the visible, infrared, and submillimeter spectra of most objects with associated gas. These observations reveal a surprisingly rich array of molecular species and attest to a complex chemistry taking place in the harsh environment of the interstellar medium of galaxies. Molecules are truly everywhere and an important component of interstellar gas. This review surveys molecular observations in the various spectral windows and summarizes the chemical and physical processes involved in the formation and evolution of interstellar molecules. The rich organic inventory of space reflects the multitude of chemical processes involved that, on the one hand, build up molecules an atom at a time and, on the other hand, break down large molecules injected by stars to smaller fragments. Both this bottom-up and the trickle-down chemistry are reviewed. The emphasis is on understanding the characteristics of complex polycyclic aromatic hydrocarbon molecules and fullerenes and their role in chemistry as well as the intricate interaction of gas-phase ion-molecule and neutral-neutral reactions and the chemistry taking place on grain surfaces in dense clouds in setting the organic inventory of regions of star and planet formation and their implications for the chemical history of the Solar System. Many aspects of molecular astrophysics are illustrated with recent observations of the HIFI instrument on the Herschel Space Observatory.

PACS numbers: 95.30.Ft, 98.38.Bn, 98.58.Bz

CONTENTS

*tielens@strw.leidenuniv.nl

I. INTRODUCTION

Over the last 20 years, we have discovered that we live in a molecular universe: a universe where molecules are abundant and widespread; a universe with a rich organic inventory particularly in regions of star and planet formation; a universe where the formation of stars and the evolution of galaxies is driven in many ways by the presence of molecules; a universe where prebiotic interstellar molecules may represent the first steps toward life; a universe where molecules can be used as "dye" to trace important processes in the interstellar medium; a universe where molecules provide unique information on the physical conditions of a wide variety of regions; and a universe where molecules can work together to form such complex species as you and me.

Diatomic molecules were first discovered in space as far back as the 1930s through their optical transitions. Starting in the 1960s, rotational transitions of simple molecules in the millimeter and submillimeter observations revealed the ubiquitous presence of molecular clouds and allowed detailed studies of their physical conditions. However, the realization that molecules permeate all of space was driven home only with the opening up of the infrared and submillimeter sky through space-based observatories, the Infrared Space Observatory launched by the European Space Agency (ESA) in 1995 and the Spitzer Space Telescope launched by the National Aeronautics and Space Agency (NASA) in 2005. These observatories clearly demonstrated that large complex molecules are ubiquitous and abundant components of the interstellar medium of galaxies and play an important role in the evolution of galaxies. And the future of studies of the molecular universe looks bright with the Herschel Space Observatory—launched by ESA in 2009—taking data, NASA's Stratospheric Observatory For Infrared Astronomy (SOFIA) just taking off, the Atacama Large Millimeter Array ready for early science, and NASA's James Webb Space Telescope on the horizon. In addition, over the last ten years, progress in our understanding of the molecular universe has been greatly aided by the close collaborations between astronomers, molecular physicists, physical chemists, molecular spectroscopists, surface scientists, solid-state physicists, quantum chemists, and astrochemists in a number of closely knit networks at both the national and the international level.

Over the years, a number of reviews have appeared on molecular astrophysics, ranging from the fundamental processes in the chemistry of space and their applications to the evolution of the molecular composition in regions of star formation (Watson, 1976; Herbst, 2005; Herbst and van Dishoeck, 2009; Smith, 2011). The fundamentals of the physics and chemistry of the interstellar medium are discussed in the textbook by Tielens (2005), while the symposia of the International Astronomical Union dedicated to astrochemistry provide a good cross cut of the field every ~5 years. Proceedings of the last two are Lis, Blake, and Herbst (2006) and Cernicharo and Bachiller (2011). Specific reviews have appeared on the chemistry of polycyclic aromatic hydrocarbon molecules (PAHs) and fullerenes (Bohme, 1992; Tielens, 2008) and on ion chemistry in space (Larsson, Geppert, and Nyman, 2012)

This paper provides an overview of the many facets of the molecular universe. It starts with the molecular inventory of the interstellar medium. In previous reviews, such discussions often focused on the gas-phase composition of molecular clouds as determined from studies of the (sub)millimeter rotational transitions of molecules. However, those studies are biased toward linear species with large dipole moments (e.g., radicals or species with eletronegative groups). Here care is taken to also provide an overview of the composition of ices—a main molecular reservoir in dense clouds—as determined from absorption features due to vibrational transitions in the midinfrared. In addition, the ubiquitous presence of very complex species such as PAHs, fullerenes (C_{60}, C_{70}), and nanodiamondoids has been revealed by their vibrational emission bands in the midinfrared. The presence of a diverse molecular inventory has also long been surmised from optical absorption bands, the diffuse interstellar bands (DIBs). All these components are reviewed in Sec. II. The chemistry of the interstellar medium has long been thought to result from bimolecular ion-molecule reactions driven by cosmic-ray ionization in the shielded environments of dense clouds. In more recent years, the important role of surface reactions of small dust grains has also been realized. This is a bottom-up approach to interstellar chemistry where small species keep reacting to form ever more complex species. However, it is now becoming clear that there are also top-down channels whereby large molecules, formed in stellar outflows, are broken down to smaller species, and this is particularly important in the harsh environment of the diffuse interstellar medium. These different views toward molecular complexity in the interstellar medium are summarized in Sec. III. After reviewing these different approaches to interstellar chemistry—gas-phase chemistry (Sec. IV), grain-surface chemistry (Sec. V), and PAH chemistry (Sec. VI)—the chemical implications for planet-forming zones around young stellar objects are discussed (Sec. VII). This is followed by an illustration of the potential of molecules as tracers of key astrophysical processes in the interstellar medium (ISM) (Sec. VIII.A) and the use of molecules as probes of the physical conditions in the ISM (Sec. VIII.B) and the elemental evolution[1] of galaxies (Sec. VIII.C). A short epilogue (Sec. IX) concludes this review.

II. THE MOLECULAR INVENTORY OF THE INTERSTELLAR MEDIUM

The ISM plays a central role in the evolution of galaxies. It is the repository of the ashes of previous generations of stars enriched by the nucleosynthetic products of the fiery cauldrons

---

[1]This is sometimes confusingly also called the chemical evolution of the galaxy.
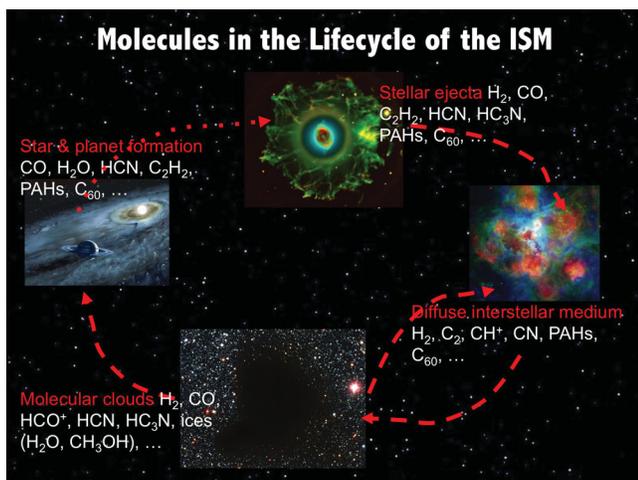
FIG. 1 (color). The life cycle of the interstellar medium starts with the injection of material from stars either in the form of wind or in an explosion. In the interstellar medium, material circulates rapidly ($\tau \sim 100$ Myr), and often between more diffuse phases and molecular clouds. Molecular clouds can become gravitationally unstable and form new stars and associated planetary systems. The central star eventually (on a few billion years time scale) evolves and in its death throes ejects much of its gas back into the ISM. The whole life cycle from old star to new star takes a few billion years. Each of these different phases in the life cycle of the ISM is characterized by often distinctive molecules, and illustrative examples are given.

in the stellar interiors. These are injected either with a bang, in a supernova (SN) explosion of massive stars, or with a whimper, in the much slower-moving winds of low-mass stars during the asymptotic giant-branch phase of stellar evolution (see Fig. 1). In this way, the abundances of heavy elements in the ISM slowly increase. This is part of the cycle of life for the stars of the galaxy, because the ISM itself is where future generations of stars are created. It is this constant recycling and its associated enrichment that drives the evolution of galaxies, both physically and in their emission characteristics.

Molecules are present in all different phases of this life cycle (see Fig. 1). Some 170 molecules have been identified through their rotational (millimeter), rovibrational (infrared), and/or electronic (ultraviolet or visible) transitions (Table I). We recognize simple hydrides such as H_2, H_2O, and NH_3, a diverse array of hydrocarbon chain species such as the cyanopolyynes (e.g., HC_3N), but also cyclic species including possibly benzene, common simple organics such as alcohols and aldehydes, highly reactive species such as ions and radicals, and very stable species such as the fullerenes C_{60} and C_{70}. Besides these specific molecules known to be present, we have also learned that, as a class of molecules, PAHs are the most abundant polyatomic species in space, although no individual PAH has yet been identified. Perusing this table makes it clear that interstellar chemistry is rich and diverse. It is also clear that kinetics rather than thermodynamics is playing a major role in setting the organic inventory in space.

In this section, I review the characteristics and molecular inventory of diffuse interstellar clouds (Sec. II.A) and dark molecular clouds (Sec. II.B). I then discuss in some detail the characteristics of the most complex species in space, PAHs (Sec. II.C), fullerenes (Sec. II.D) and nanodiamondoid

species (Sec. II.E). Finally, diffuse interstellar bands were discovered in stellar spectra almost 100 years ago and this was the first sign of the presence of a rich molecular inventory in space. The characteristics of these bands and their carriers are discussed in Sec. II.F.

A. Diffuse clouds

Diffuse interstellar clouds are regions of relatively low density $n \sim 50$ cm^{-3} and temperature $T \sim 80$ K corresponding to a thermal pressure of 4000 cm^{-3} K. Typical sizes and masses of diffuse clouds are ~ 10 pc and $\sim 500 M_\odot$ but actually diffuse clouds show a broad mass and size distribution which joins quite smoothly into those of molecular clouds (Dickey and Garwood, 1989) (Sec. II.B). With total hydrogen column densities of $N_H \sim 10^{21}$ cm^{-2}, they are quite transparent to the ambient interstellar radiation field (e.g., visual extinction $\simeq 0.5$). Hence, UV photons play an important role in their physics and chemistry. In addition, these low columns and extinction allow sensitive absorption line studies against bright stellar or extragalactic background sources in the UV, visible, infrared, and millimeter wavelength regions. Snow and McCall (2006) recently reviewed the characteristics of diffuse interstellar clouds as well as their chemistry.

Molecular hydrogen can be observed directly in diffuse clouds through the Lyman and Werner bands (see Fig. 2) in the UV and these provide a direct probe of the column density and excitation of this key species. The H_2 fractional abundance is observed to rise rapidly from $<10^{-4}$ to values of ~ 0.6 around total hydrogen columns of $\sim 5 \times 10^{20}$ cm^{-2}. The observations also reveal significant rotational and vibrational excitation of H_2. Diatomic radicals (e.g., CH, CH$^+$, CN) with electronic transitions in the visible were the first molecular species to be observed, back in the late 1930s [cf., Swings and Rosenfeld (1937)] but they have now also been observed through millimeter and submillimeter absorption lines (Liszt and Lucas, 2001, 2002; Gerin et al., 2012). Later on, C_2 and C_3 were added to this list of simple radicals detected through electronic transitions in the visible (Federman et al., 1994; Maier et al., 2001; Oka et al., 2003; Thorburn et al., 2003). CO and OH have been studied in diffuse clouds through both UV electronic and millimeter rotational transitions (Liszt, Lucas, and Pety, 2005). The nitrogen-bearing species NH and N_2 have been detected with great difficulty in the UV (Meyer and Roth, 1991; Knauth et al., 2004). Nitrogen hydrides have recently also been observed with HIFI/Herschel[2] (Hily-Blant et al., 2010; Persson et al., 2012). The hydride H_3^+ has been observed in diffuse clouds through its vibrational transitions in the near IR (McCall et al., 1998, 2003). A variety of polyatomic species have been detected through absorption and emission studies in the millimeter including HCN, H_2CO, C_2H, C_3H_2, H_2, and HCS$^+$ (Liszt and Lucas, 2001; Lucas and Liszt, 2002; Liszt, Lucas, and Pety, 2005).

As this summary shows, diffuse clouds show a wide variety of simple species and typical abundances are listed in Table II. There is a preponderance of simple radicals and ions. While molecular hydrogen is very abundant, most of the

---

[2]HIFI is the heterodyne instrument for the far infrared that has flown onboard of the Herschel Space Observatory.

TABLE I. Identified interstellar and circumstellar molecules. [Most molecules have been detected at radio and millimeter wavelengths, unless otherwise indicated (IR, VIS, or UV). Species labeled with a question mark await confirmation.]

Simple hydrides, oxides, sulfides, halogens				
H_2 (IR, UV)	CO	NH_3	CS	HCl
O_2	H_2O_2	PO	CO_2 (IR)	$NaCl^a$
H_2O	SO_2	OCS	H_2S	KCl^a
PN	SiO	$SiH_4{}^a$ (IR)	SiS	$AlCl^a$
N_2O	CH_4 (IR)	HSCN	HF	AlF^a
HONC	HNCO	AlOH		

Nitriles and acetylene derivatives				
C_2 (IR)	HCN	CH_3CN	HNC	$C_2H_4{}^a$ (IR)
C_3 (IR,UV)	HC_3N	CH_3C_3N	HNCO	C_2H_2 (IR)
$C_5{}^a$ (IR)	HC_5N	CH_3C_5N	HNCS	C_6H_2 (IR)
C_3O	HC_7N	CH_3C_2H	HNCCC	C_3H_6
C_3S	HC_9N	CH_3C_4H	CH_3NC	C_3H_7CN
C_4Si^a	$HC_{11}N$	CH_3C_6H	HCCNC	
H_2C_4	HC_2CHO	CH_2CHCN	CH_2CCHCN	

Aldehydes, alcohols, ethers, ketones, amides				
H_2CO	CH_3OH	HCOOH	HCOCN	CH_3CH_2CN
CH_3CHO	CH_3CH_2OH	$HCOOCH_3$	CH_3NH_2	NH_2CH_2CN
CH_3CH_2CHO	CH_2CCHOH	CH_3COOH	CH_3CONH_2	NH_2CN
NH_2CHO	$(CH_2OH)_2$	$(CH_3)_2O$	H_2CCO	CH_2CHCN
CH_2OHCHO	$(CH_3)_2CO$	H_2CS		
C_2H_5OCHO		CH_3SH		

Cyclic molecules				
C_3H_2	SiC_2	c-C_3H	CH_2OCH_2	C_6H_6 (IR) ?
c-SiC_3	H_2C_3O	C_2H_4O		

Molecular cations				
CH^+	CO^+	$HCNH^+$	OH^+	$HN_2{}^+$
$CH_3{}^+$	HCO^+	HC_3NH^+	H_2O^+	$H_3{}^+$ (IR)
HS^+	HOC^+	H_2COH^+	H_3O^+	SO^+
HCS^+	$HOCO^+$	CF^+	HCl^+	H_2Cl^+

Molecular antions		
C_4H^-	C_6H^-	C_8H^-
CN^-	C_3N^-	C_5N^-

Radicals				
OH	C_2H	CN	C_2O	C_2S
CH	C_3H	C_3N	NO	NS
CH_2	C_4H	$HCCN^a$	SO	SiC^a
NH (UV)	C_5H	CH_2CN	HCO	SiN^a
NH_2	C_6H	CH_2N	C_5N^a	CP^a
SH	C_7H	NaCN	KCN	MgCN
C_3H_2	C_8H	MgNC	FeCN	
C_4H_2	HNO	H_2CN	HNC_3	HO_2
C_6H_2	AlNC	SiNC	C_4Si	SiCN
HCP	CCP	AlO		

Fullerenes		
C_{60} (IR)	$C_{70}{}^a$ (IR)	$C_{60}{}^+$ (VIS) ?

[a]These species have been detected only in the circumstellar envelope of carbon-rich stars.

carbon, oxygen, and nitrogen are in atomic form. The most abundant molecular species CO locks up only 1% of the elemental carbon. Most of the gaseous carbon is in the form of C^+. This chemical simplicity reflects the harsh conditions (e.g., high UV radiation field). Conversely, this simplicity has been taken to imply that diffuse clouds provide convenient test beds for models of the initial chemical steps toward molecular complexity in the ISM. That expectation has, however, never fully been met. Notably, the high abundances of rotationally excited H_2 and CH^+ have proven very challenging for chemical models (cf., Sec. IV.I.4).

B. Molecular clouds

The CO $J = 1$-0 transition at 2.6 mm is commonly used as a tracer of molecular gas in the galaxy (see Fig. 3). Surveys
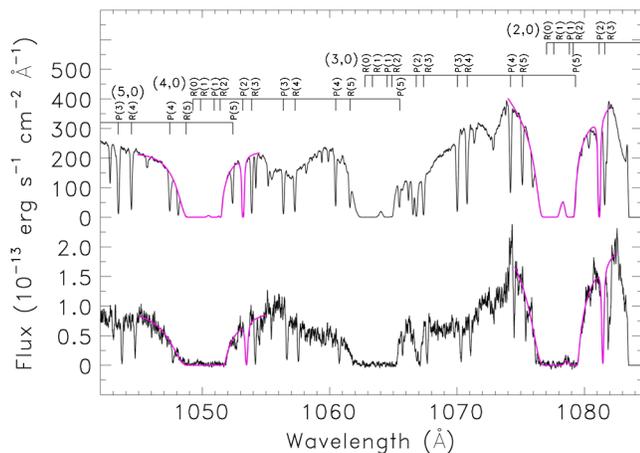
FIG. 2 (color online). Ultraviolet spectra covering the Lyman series (4, 0), (3, 0), and (2, 0) vibrational band heads of H_2. The numerous narrow lines are mostly due to rotationally excited H_2, as indicated by the series of tick marks above the spectra; exceptions include Ar I (1048, 1067 Å) and Fe II (1055 Å). The broad features at 1057 and 1073 Å as well as the weaker feature near 1067 Å are stellar in origin. Profile fits to the (4, 0) and (2, 0) bands are shown. From Rachford et al., 2002.

along this line have shown that much of the molecular gas in the Milky Way is localized in discrete giant molecular clouds with typical sizes of 40 pc, masses of $4 \times 10^5 M_\odot$, densities of ~ 150 cm^{-3}, and temperatures of 10 K (Dame et al., 1987). However, it should be understood that molecular clouds show a large range in each of these properties which at the low end join smoothly with diffuse clouds (Sec. II.A). Moreover, molecular clouds are not uniform but highly structured with large variations in density. The Taurus-Auriga molecular cloud complexes at a distance of only 140 pc, for example, break up into a large number of cloud cores, all spread over some 20×20 pc^2 with a total mass of $10^4 M_\odot$ (Ungerechts and Thaddeus, 1987; Pineda et al., 2010). Molecular clouds are characterized by high turbulent pressures—as indicated by the large linewidths of emission lines—and are self-gravitating rather than in pressure equilibrium with other phases in the ISM. While they are stable over time scales of $\simeq 3 \times 10^7$ yr, presumably due to a balance of magnetic or turbulent pressure and gravity, molecular clouds are the sites of active star formation and eventually the star formation process "destroys" molecular clouds through the combined action of stellar winds and jets and evaporation driven by radiative ionization and heating (see Fig. 4).

1. Prestellar cores and infrared dark clouds

Observations of molecular clouds in the rotational transitions of a variety of species allow a detailed study of their physical and chemical properties. These studies show that molecular clouds have spatial structure on all scales. In particular, molecular clouds contain cores with sizes of $\simeq 0.1$–1 pc, densities in excess of 10^4 cm^{-3}, and masses in the range $(10$–$10^3) M_\odot$ in which star formation is localized. Of particular interest are the so-called prestellar cores and infrared dark clouds which are generally thought to represent the earliest stages of star formation—the stage before gravitational collapse produces a central object.

TABLE II. The composition of diffuse clouds and molecular clouds. The entries in parentheses should be read as $a \, (-b) = a \times 10^{-b}$.

Species	Diffuse clouds[a]	Molecular cloud[b]
H	1.2	
H_2	1	1
HD	5 (−7)	
H_3^+	5 (−8)[e]	
O	1.6 (−4)	
OH	1.0 (−7)	3.0 (−7)
H_2O		5 (−9)[i]
OH^+	1 (−8)[f]	
H_2O^+	2 (−9)[f]	
H_3O^+	1.5 (−9)[f]	
O_2		5 (−8)[h]
C^+	2.6 (−4)	
C	7.0 (−6)	
C_2	3.3 (−8)	
C_3	3.5 (−9)	
CH	5 (−8)	
CH^+	6.3 (−8)	
C_2H	3 (−8)	5 (−8)
C_3H_2	1 (−9)	
CO	5 (−6)	5 (−5)
HCO^+	5 (−10)	8 (−9)
N	2.5 (−5)	
N_2	3 (−7)[c]	3 (−5)[d]
NH	2 (−9)	3 (−10)[g]
NH_2	2.0 (−9)	6 (−11)[g]
NH_3	2.0 (−9)	2 (−8)[g]
N_2H^+		5 (−10)
CN	5 (−8)	3 (−10)
HCN	3 (−9)	2 (−8)
HNC	6 (−10)	2 (−8)
HC_5N	<2 (−11)	1 (−10)
CS	3 (−9)	
SO	2 (−9)	
H_2CO	4.0 (−9)	2 (−8)
CH_3OH	<7 (−11)	2 (−9)
HCl	2 (−10)	

[a]Abundance relative to H_2 measured toward ζ Oph through UV absorption lines [cf., Snow (2005)] or toward B2200 + 420 in millimeter emission lines (Liszt, Pety, and Lucas, 2008), unless otherwise indicated.
[b]Abundance relative to H_2 measured toward the dark cloud core TMC-1, unless otherwise indicated.
[c]Measured toward the star HD 124314 (Knauth et al., 2004).
[d]Measured toward the dark cloud core B68 (Maret, Bergin, and Lada, 2006).
[e]Measured toward the star ζ Per (McCall et al., 2003).
[f]Measured in absorption against G10.6-0.4 (Gerin et al., 2010a).
[g]Measured in absorption against the protostar IRAS + 16293 − 2422 (Hily-Blant et al., 2010).
[h]Measured toward rho Oph (Liseau et al., 2012).
[i]Ortho H_2O measured toward the outer region of L1544 (Caselli et al., 2010).

Prestellar cores are centrally condensed cores in submillimeter dust-continuum emission of molecular clouds (Ward-Thompson et al., 1994). They are characterized by high number density in their centers ($\sim 3 \times 10^6$ cm^{-3}), low kinetic temperatures (~ 6 K), radii of $\sim 10^{17}$ cm, masses of $(1$–$3) M_\odot$, and, often, kinematic features in their molecular spectra indicative of collapse motion (Bergin and Tafalla, 2007; di Francesco et al., 2007). The Bok globule B68 is a well-known example of a prestellar core. The rotational emission from CO and other carbon-bearing molecules shows a central hole on the dust core, but the emission from
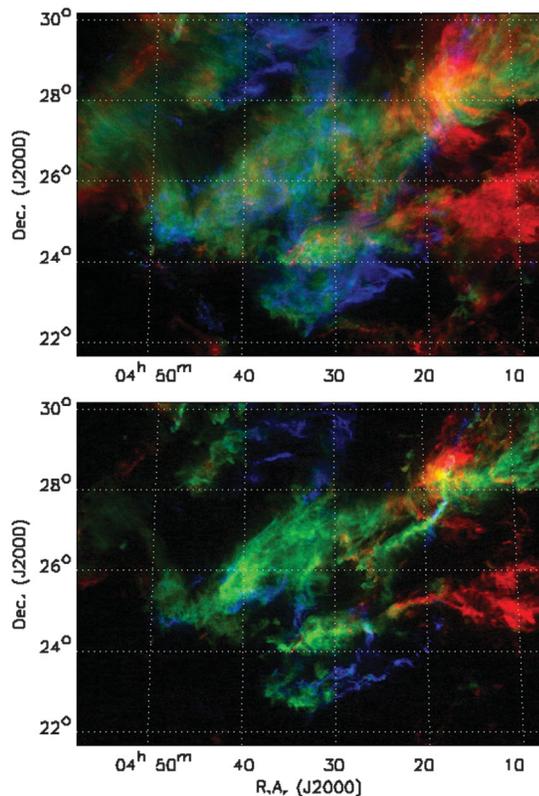
FIG. 3 (color). The dark molecular cloud system in Taurus as measured in the ^{12}CO (top) and ^{13}CO (bottom) $J = 1$-0 transition. Color coding according to velocity with blue coming toward us, red going away, and green at the cloud's rest velocity. Star formation is occurring along the denser filaments evident in the ^{13}CO emission, which traces the denser gas. These denser cores are embedded in a more diffuse halo visible in ^{12}CO. The total mass in this cloud (denser cores plus diffuser gas) is $\simeq 2 \times 10^4 M_\odot$. From Goldsmith et al., 2008.

N-bearing species (e.g., N_2H^+) is centrally peaked. In terms of abundances, these observations typically imply a factor of 10 decrease for CO in prestellar cores but only a modest factor of 2 for N_2H^+. Prestellar cores also show highly enhanced deuterium fractionation in molecules such as DCO^+ and N_2D^+.

Infrared dark clouds are cold dense molecular clouds seen in absorption against the bright midinfrared emission from the galactic plane (Perault et al., 1996; Egan et al., 1998). Infrared dark clouds have typical densities of $\sim 2 \times 10^3$ cm^{-3}, sizes of ~ 5 pc, and masses of $\sim 5 \times 10^3 M_\odot$. They are very filamentary and contain dense cores with median densities of $\sim 3 \times 10^4$ cm^{-3} and masses of $120 M_\odot$ (Rathborne, Jackson, and Simon, 2006). Infrared dark clouds have molecular abundances similar to those of prestellar cores, characterized by high depletion factors, bright emission in nitrogen-bearing molecules such as NH_3, and high deuterium fractionation (Pillai et al., 2006; Fontani et al., 2011, 2012; Vasyunina et al., 2011). In many ways, infrared dark cloud cores are thus the high-mass counterparts of prestellar cores and they are thought to be the site of future massive star formation.

2. Gas-phase composition

While CO is commonly used to trace interstellar molecular gas, H_2 is thought to be the dominant molecular species, with a H_2:CO ratio of 10^4–10^5. In addition (as of mid-2012), approximately 170 different molecular species have been detected—mainly through their rotational transitions in the submillimeter range—in the shielded environments of molecular clouds (see Fig. 5). Typical abundances of some characteristic species are summarized in Table II. Given the overabundance of hydrogen in the ISM, one might expect the molecular composition to be dominated by saturated hydrides such as H_2O, NH_3, and CH_4. Simple hydrides are indeed present at low levels in molecular clouds (cf. Table II). However, interstellar molecular clouds also contain a variety of unsaturated radicals and ions. These radicals are very reactive under terrestrial laboratory conditions. Acetylenic carbon chains and their derivatives figure prominently on the list of detected molecules. The degree of unsaturation is particularly striking. Largely, this reflects observational bias as the small partition functions and high dipole moments strongly favor detection of linear molecules with high electronegative groups such as HC_3N. Nevertheless, the molecular composition of dark clouds is far from thermodynamic equilibrium, attesting to the importance of kinetics over thermodynamics.

The abundances summarized in Table II are very typical for molecular clouds. However, compositional variations do exist. In particular, there is a class of dense cores, the so-called carbon-chain-rich cores, where the abundance of acetylenic derivatives is much higher than in other regions. The dense core TMC-1 in the Taurus molecular cloud is the best studied of these (Hirahara et al., 1992), but several others have now been identified through, e.g., a high CCS or NH_3 abundance (Hirota, Ohishi, and Yamamoto, 2009; Sakai et al., 2010; Hirota et al., 2011). These cores seem to lack embedded protostars and may also be linked to the presence of gradients in the atomic C abundance in the region (Maezawa et al., 1999). Both may reflect a relatively young age.

3. Ice mantle composition

Infrared spectra of protostars embedded in or of background stars located behind molecular clouds reveal broad absorption bands due to simple molecular ices (see Fig. 6). Comparison of these spectra with the spectra of laboratory analogs provides direct identification of the solid compounds present in space and allows measurement of accurate abundances and thus the composition of the ices (Boogert and Ehrenfreund, 2004; Tielens and Allamandola, 2011). Subtle profile details may reflect the interaction of these molecules with the matrix in which they are embedded. Table III summarizes the chemical makeup of interstellar ices along the lines of sight through several molecular clouds. The most striking aspect of the infrared spectrum in Fig. 6 is the apparent simplicity of the composition of interstellar ices. Many species are highly hydrogenated (H_2O, NH_3, and CH_4) but the spectra also show mixed oxidation-reduction patterns (CO, CO_2, H_2CO, CH_3OH, and CH_4). Water ice is the dominant ice component while carbon is divided between CO, CO_2, and CH_3OH. The abundances of CO and CO_2 are very stable relative to H_2O (Tielens et al., 1991; Chiar et al., 1998; Gerakines et al., 1999; Pontoppidan et al., 2003, 2008) while CH_3OH is highly variable from one sight line to the next (Whittet et al., 2011).

TABLE III. The composition of interstellar ice.

Species	Quiescent cloud[a]	Low-mass protostar[b]	High-mass protostar[c]	Comets[d]
H_2O	100	100	100	100
CO (total)	25	5	13	23
CO (H_2O ice)	3	10	6	$\cdots$
CO (pure CO)	22	4	3	$\cdots$
CO_2 (total)	21	19	13	6
CO_2 (H_2O ice)	18	?	9	$\cdots$
CO_2 (CO mix)	3	?	2	$\cdots$
CO_2-CH_3OH complex	$\cdots$	$\cdots$	1.2	$\cdots$
CO_2 (pure crystalline)	$\cdots$	$\cdots$	1.0	$\cdots$
CH_4	<3	<1.4	1.5	0.6
CH_3OH[e]	10	30	18	2.4
H_2CO	$\cdots$	$\cdots$	6	1.1
HCOOH	<1	<1	7	0.09
OCS	<0.2	<0.1	0.2	0.4
NH_3	<8	<11	15	0.7
OCN^-	<0.5	<0.2	3.5	0.1[f]

[a]Observations toward the star Elias 16 behind the Taurus cloud (Bergin *et al.*, 2005; Knez *et al.*, 2009).
[b]Observations toward the low mass protostar Elias 29 in the ρ Oph cloud (Boogert *et al.*, 2000; Boogert *et al.*, 2008; Pontoppidan *et al.*, 2008).
[c]Observations toward the luminous protostar, W33A (Pontoppidan *et al.*, 2003; 2008; Gibb *et al.*, 2004).
[d]Abundances measured for comet Hale-Bopp at 1 AU from the Sun (Bockelée-Morvan *et al.*, 2000).
[e]Methanol abundances are highly variable (Whittet *et al.*, 2011).
[f]Taken as HNCO.

This apparent simplicity is somewhat misleading as a detailed inspection of the absorption profiles reveals that there are multiple ice components along the same line of sight. Specifically, much of the solid CO is not mixed in with the (dominant) H_2O ice but rather in a component with only nonpolar molecules (Tielens *et al.*, 1991; Chiar *et al.*, 1998; Pontoppidan *et al.*, 2003). Solid CO_2 also shows multiple mixtures along the same sight lines, with most of the CO_2 in the H_2O-rich ice, but some is mixed in with the non-polar-CO

ice and in some sight lines there is evidence for CO_2 mixed with CH_3OH ice (Gerakines *et al.*, 1999; Boogert *et al.*, 2000; Bergin *et al.*, 2005; Pontoppidan *et al.*, 2008). These separate ice components are reported separately in Table III. In some sources, the spectra also show evidence for thermal processing in the detailed profile of the 3.07 μm ice band, and in the profiles of the 15.2 μm $^{12}CO_2$ band and the 4.4 μm $^{13}CO_2$ band (Smith, Sellgren, and Tokunaga, 1989; Gerakines *et al.*, 1999; Boogert *et al.*, 2000).

Absolute abundances of H_2O ice are $\simeq 10^{-4}$ relative to H_2 and, hence, an appreciable fraction of the available elements is locked up in ices inside molecular clouds. This is also apparent from gas-phase studies as the abundance of many gaseous molecules drops precipitously in the densest cores (Caselli *et al.*, 1999; Bergin *et al.*, 2001, 2002) (Sec. V.F.2). Finally, it should be noted that the composition of interstellar ice is very different from that in the gas phase (Tables II and III).

C. Interstellar polycyclic aromatic hydrocarbons

The infrared spectra of almost all interstellar objects, including regions of massive star formation such as HII regions and reflection nebulae (see Fig. 4), carbon-rich stars in the last phases of their evolution such as post-asymptotic-giant-branch stars and planetary nebulae, surfaces of dark clouds, the planet-forming disks of young stellar objects, the general interstellar medium, galactic nuclei, and (ultra)luminous infrared galaxies, are dominated by strong, broad emission features at 3.3, 6.2, 7.7, 8.6, 11.2, and 12.7 μm (see Fig. 7) (Mattila *et al.*, 1996; Hony *et al.*, 2001; Peeters *et al.*, 2002; Armus *et al.*, 2007; Lutz *et al.*, 2007; Sellgren, Uchida, and Werner, 2007; Galliano *et al.*, 2008). These strong emission features are accompanied by a plethora of weaker bands at 3.4, 5.2, 5.7, 6.0, 7.4, 12.0, 13.5, 14.2, 15.8, 16.4, 17.0, and 17.4 μm and are perched on very broad plateaus and a continuum that is sharply rising toward a longer wavelength [for a review, see Tielens (2008)]. These features are

FIG. 4 (color). The Perseus molecular cloud is being destroyed by jets and radiation from newly formed stars. Left: The optical image is dominated near the top left by (blue) light from a young massive star reflecting off small dust grains. Toward the lower right hundreds of low-mass stars are visible, ripping the cloud apart through their (red) jets and red-glowing gas. Figure courtesy of T. A. Rector, University of Alaska Anchorage, H. Schweiker, WIYN, and NOAO/AURA/NSF. Right: False color image of the same region obtained by the Spitzer Space Telescope. The red glow to the top left is due to IR fluorescence of polycyclic aromatic hydrocarbon molecules pumped by the UV radiation from the young massive star. The greenish-blue emission traces warm H_2 molecules heated by the jets and shocks traversing the region. Note that the optical image covers only the central 1/2 of the IR image. Figure courtesy of NASA, JPL-Caltech, R. A. Gutermuth (Harvard-Smithsonian CfA).
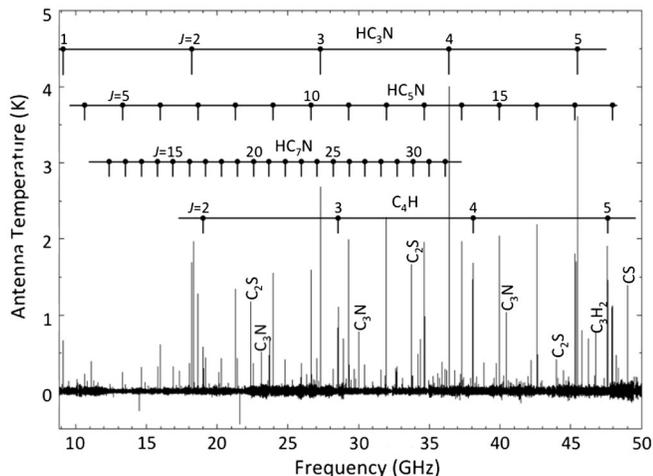
FIG. 5. Spectral survey of the dark cloud core TMC-1 in the 8.8–50 GHz region reveals a complex array of hydrocarbon species (Kaifu *et al.*, 2004). Figure courtesy of M. Ohishi.

ubiquitous in the interstellar medium on all scales from planet-forming disks around young stellar objects to the scale of whole galaxies (see Fig. 8). It is clear that the carriers represent an important component of the ISM.

1. The IR emission features and PAH molecules

These spectral features are very characteristic in peak position for polycyclic aromatic hydrocarbon materials and they are generally ascribed to IR fluorescence of UV-pumped large PAHs (Allamandola, Tielens, and Barker, 1989; Puget and Leger, 1989; Tielens, 2008). There are three pieces of evidence supporting the assignment of these features to large molecules (50–100 C atoms) rather than "bulk" materials (e.g., 10–300 nm grains). (1) In order to emit in the mid-IR, the carrier(s) of the IR emission features must be much hotter than the 15 K that characterizes the far-IR emission due to 10–300 nm grains in radiative equilibrium with the interstellar radiation field. Hence, a fluorescence process is implied in which a single photon highly excites the molecule, which then relaxes through the emission of IR photons. Analysis of the energetics involved implies then molecular-sized carriers
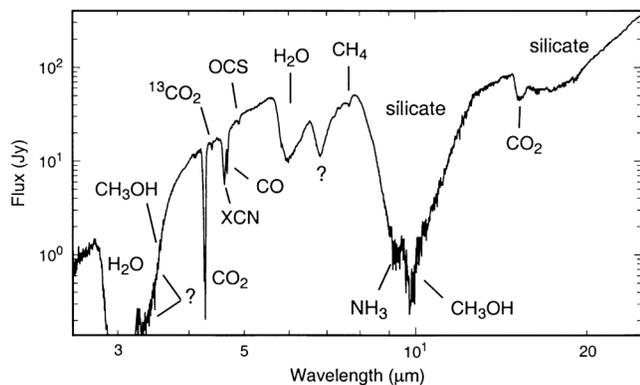
FIG. 6. The midinfrared spectrum of the protostar W33A observed with the short-wavelength spectrometer onboard the Infrared Space Observatory shows a variety of absorption features. Except for the 10 and 18 μm silicate bands, these features are due to simple molecules in an ice mantle. From Gibb *et al.*, 2000.
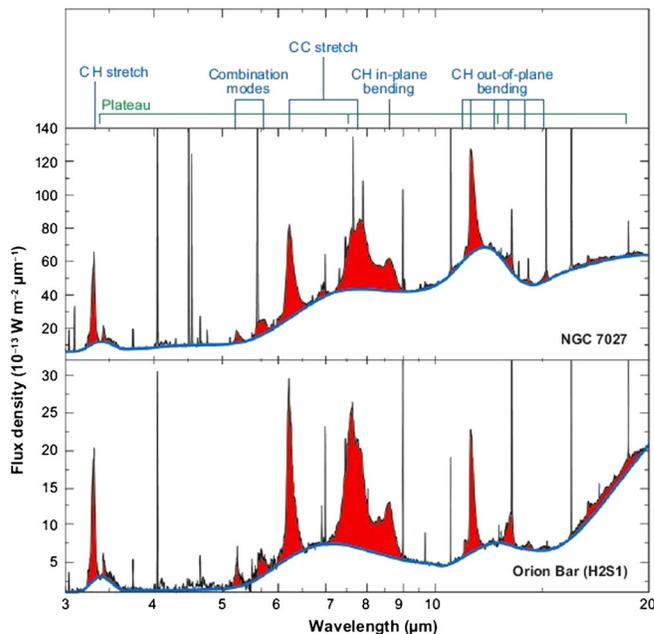
FIG. 7 (color online). The midinfrared spectra of the photodissociation region in the Orion bar and in the planetary nebula NGC 7027 are dominated by a rich set of infrared emission features. Assignments of these features with vibrational modes of PAH molecules are labeled at the top. These PAH features are perched on broad plateaus attributed to clusters of PAHs and on a midinfrared continuum likely due to nanograins. Adapted from Peeters *et al.*, 2002.

(50–100 C atoms). (2) Several of the IR emission features (e.g., the 6.2 and 11.2 μm features) show a pronounced redshaded profile. Such a profile is characteristic of anharmonicity, again a distinct signature for emission by highly vibrationally excited molecules (Barker, Allamandola, and Tielens, 1987; Cook and Saykally, 1998; Pech, Joblin, and Boissel, 2002). (3) The feature-to-continuum ratio is very high, exceeding 20 in many sources. This is quite typical for molecular compounds; bulk (carbonaceous) materials, in contrast, invariably have intrinsic feature-to-continuum ratios that are much smaller.

While the dominant midinfrared bands are due to molecular-sized species, the spectra also show evidence for underlying plateaus and a weak continuum and hence larger species. Specifically, these two emission components have been ascribed to clusters of (tens of) PAHs, probably bonded by van der Waals forces, and to very small grains (containing some 10^3–10^4 C atoms; Desert, Boulanger, and Puget, 1990; Rapacioli, Joblin, and Boissel, 2005; Berné *et al.*, 2007).

2. PAH excitation in the ISM

Thus, the dominant mid-IR emissions are thought to arise in small species that because of their limited heat capacity are instantaneously heated to a high temperature (~ 1000 K) by the absorption of a single UV photon (Sellgren, 1984). The highly excited species then cools rapidly (~ 1 s) through IR emission. The species remains very cold until the absorption of another UV photon, in the interstellar medium typically about a year later, but near a bright star photon absorption might occur once every hour. This is a solid-state description
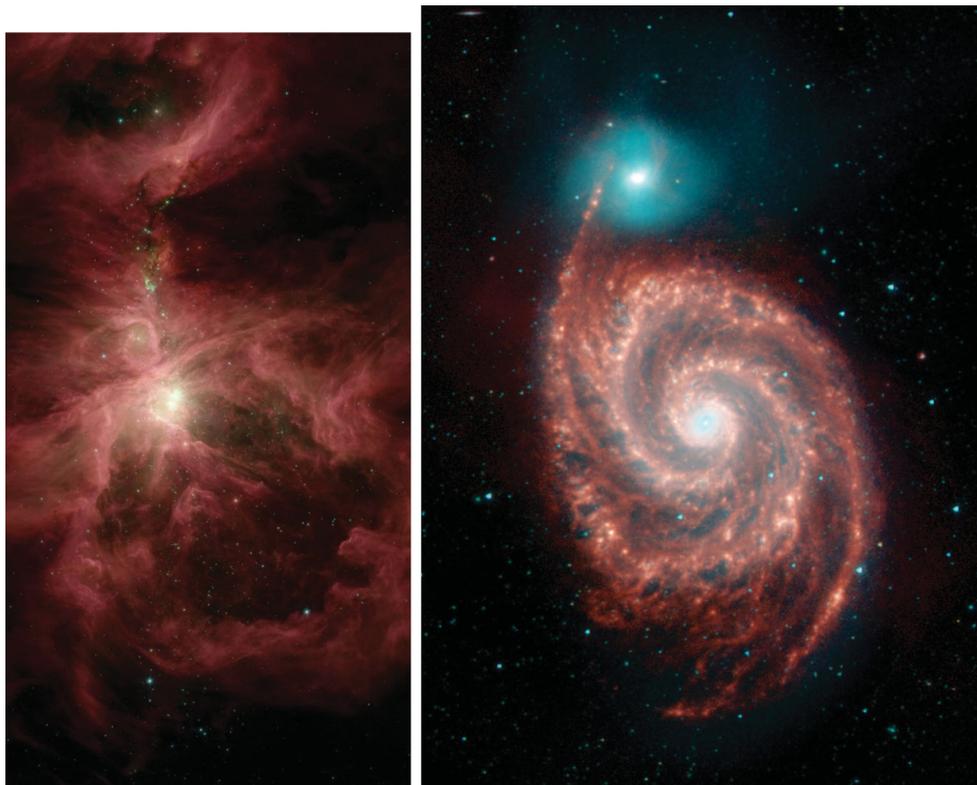
FIG. 8 (color). The midinfrared emission of (almost) all objects is dominated by fluorescence by large PAH molecules. Composite midinfrared images where the 8 μm (red) image traces primarily emission by PAH molecules in the 7.7 μm feature, while the 4.5 μm image (green) shows ionized gas and dust, and stars show up in 3.6 μm (blue). Left: The Orion star-forming region where massive stars at the center of a star cluster, the "trapezium," ionize the gas on a scale of $\simeq 0.2$ pc. The light from these (and other) stars also pumps the PAH molecules on much larger scale sizes ($\simeq 2$ pc). Right: The whirlpool galaxy M51 where the whole ISM on a scale size of 10 kpc is set aglow in the light of the PAHs. The spiral arms are dotted by individual regions of massive star formation akin to the Orion region (left). Images obtained with the IRAC on the Spitzer Space Telescope and courtesy of NASA, JPL-Caltech.

of what is essentially a molecular fluorescence process: A molecule absorbs a UV photon and this electronic energy is quickly transferred to the vibrational manifold of a lower-lying, electronic state (e.g., internal conversion). This excitation then decays through emission in the molecular vibrational bands (the IR emission features).

Using an appropriate model for the excitation, observed intensities of the various features can be translated into the sizes of the PAHs emitting in interstellar space. The excitation of the vibrational modes in large PAHs can be well described by a thermal model for this mode in contact with the larger heat bath of the other mode provided that the total energy in the mode under consideration is less than $\simeq 10\%$ of the total energy in the molecule (Allamandola, Tielens, and Barker, 1989). Detailed evaluations have been made for the density of states ρ of PAHs using direct counting techniques. The results are very similar to those derived from studies of graphite, once allowance is made for the finite size of the system and the presence of peripheral hydrogen (Leger, D'Hendecourt, and Defourneau, 1989; Schutte, Tielens, and Allamandola, 1993). The derived density of states can be approximated by

$$\ln[\rho(E)] = 2.84 \times 10^{-2} s\left(\frac{E}{s}\right)^{0.60} - 6.15 \qquad (1)$$

with s the number of degrees of freedom and E the internal energy in units of cm^{-1} (Tielens, 2005). This approximation is

valid over the energy range of 2.5×10^{-2}–3×10^2 cm^{-1} per mode ($\simeq 10^{-5}$–10^{-1} eV/C atom). A microcanonical temperature T_m can then be defined as (Klots, 1989)

$$\frac{1}{kT_m} = \frac{1}{k}\frac{dS}{dE} = \frac{d\ln[\rho(E)]}{dE}. \qquad (2)$$

The temperature of a species with an internal energy $\mathcal{E}$ in eV is

$$T_m = 2000\left(\frac{\mathcal{E}}{N_c}\right)^{0.4}, \qquad (3)$$

over the range 35–1000 K. The intensity I in a vibrational mode at frequency ν_i is given by

$$I(\nu_i) = \kappa_i N(E)B(\nu_i, T_m), \qquad (4)$$

where $N(E)$ is the number of species with internal energy E, T_m is the temperature that corresponds to this energy, and κ_i is the integrated strength of the mode. This expression has then to be integrated over the temperature cascade as the molecule cools through IR emission.

The abundance of the PAHs can be evaluated by comparing the observed intensity of the features to that of the dust and adopting the dust-to-gas abundance ratio measured for the ISM. Specifically, the fraction of the elemental carbon f_c locked up in a specific component is given by

$$f_c = 0.23\left(\frac{7 \times 10^{-18} \text{ cm}^{-2}}{\sigma_{\text{UV}}}\right)\frac{f_{\text{IR}}}{1 - f_{\text{IR}}}, \qquad (5)$$

with σ_{UV} the UV absorption cross section per C atom and f_{IR} the fraction of the IR energy emitted in the vibrational bands of this component (Tielens, 2005). This analysis shows that PAH molecules are very abundant; with an abundance of $\simeq 10^{-7}$ relative to H, they lock up some 10% of the elemental carbon. The PAH clusters and nanograins lock up somewhat smaller but comparable fractions of the elemental carbon. This analysis suggests that the abundance of large molecules, clusters, and nanograins smoothly joins to the interstellar grain size distribution (Tielens, 2008).

3. Spectral variations and the composition of interstellar PAHs

While the global spectral characteristics of the IR emission features are very similar from source to source, the spectra reveal subtle variations in profile, peak position, and relative strength within sources and from one source to another (see Fig. 9). This has stimulated detailed laboratory studies using a wide variety of experimental techniques [for a review, see Oomens (2011), and references therein]. These have been supplemented by extensive density functional theory (DFT) calculations, which are particularly useful to systematically evaluate the IR characteristics of PAHs (Langhoff, 1996; Malloci, Joblin, and Mulas, 2007; Bauschlicher, Jr., Peeters, and Allamandola, 2008, 2009; Ricca et al., 2012). While this has not led to the identification of specific PAHs present in the ISM, this has provided a number of key insights [for a review, see Tielens (2008), and references therein].

In particular, neutral PAHs have strong CH stretch and out-of-plane bending modes and weak CC stretch modes, while for PAH cations this is just reversed. Hence, the ratio of the interstellar bands at 3.3 and 11.2 μm to those at 6.2 and 7.7 μm are taken to measure the PAH neutral over ion abundance ratio in space (Peeters et al., 2002; Galliano et al., 2008). In addition, the ratio of the CH stretching mode and the CH out-of-plane bending mode is a particularly sensitive tool to determine the size of the emitting (neutral) PAHs in the ISM. For a species that has absorbed a photon with a given temperature, the intensity of the bands can then be calculated from Eq. (4) where the intrinsic strength of the modes is provided by laboratory and quantum chemical studies and the temperature follows from Eq. (3). The results can then be compared to the observations (see Fig. 10). The observed ratio of the 3.3:11.3 μm bands corresponds to sizes in the range 50 to 150 C atoms, depending on the source. The plateaus and the continuum in the 5–20 μm range observed in the interstellar spectra (see Fig. 7) can be evaluated in a similar way and are then carried by somewhat larger species [$\sim$ 400 C atoms for the plateaus (likely van de Waals PAH clusters) and nanosized (1–10 nm) carbonaceous grains for the continuum].

Observed variations in the relative strength of the CH out-of-plane modes in the 11–15 μm range are also relevant as they are related to the edge structure of the PAHs. The observations reveal a shift from the stable zigzag edge structure to the more labile armchair edge structure when going from stellar ejecta to ISM emission regions (Hony et al., 2001). The other variations to highlight are shifts in the

peak position of the CC modes near 6.2 and 7.7 μm (see Fig. 9) (Peeters et al., 2002; van Diedenhoven et al., 2004). The origin of these variations is not agreed upon but compositional variations are implicated. They may involve the incorporation of N into the PAH skeleton (Hudgins, Bauschlicher, Jr., and Allamandola, 2005), the effects of aliphatic side groups (Pino et al., 2008), and/or clustering of PAHs either with themselves or with metal atoms (Rapacioli, Joblin, and Boissel, 2005; Berné et al., 2007). The observations reveal that the spectral variations in these bands depend strongly on the color and strength of the radiation field (see Fig. 9) (Sloan et al., 2007; Keller et al., 2008; Boersma et al., 2009a). These variations are particularly prominent in regions of star and planet formation and reflect an active chemistry involving PAHs that locally modifies the organic inventory (cf. Secs. VI.C and VI.D).

It should be emphasized here that the spectrum of the IR emission features in the *interstellar medium* is very characteristic for highly aromatic molecules. Indeed, there is little direct observational evidence for the presence of other molecular groups in the spectra (Allamandola, Tielens, and Barker, 1989; Tielens, 2008). Aliphatic hydrocarbons are a case in point. There is a weak feature at 3.4 μm which has been interpreted as due to CH_3 groups attached to the PAH skeleton. Currently, most researchers tend to assign this feature to an additional H atom, puckering an edge C atom out of the plane, rather than an aliphatic CH_3 side group. Ignoring this here, we can derive an upper limit on the aliphatic character of PAHs from the observed strength of the 3.4 μm feature (aliphatic groups) to the 3.3 μm aromatic CH stretch. From such an analysis, we conclude that the ratio of aliphatic CH_3 to aromatic CH is 0.02 in the interstellar medium (Tielens, 2008). Spectra of some circumstellar regions are characterized by stronger 3.4 μm bands but even in these exceptional regions aliphatic CH_3 groups are at best a minor component compared to aromatic CH. As noted, spectral variations in the 6.2 μm (and 7.7 μm) band peak
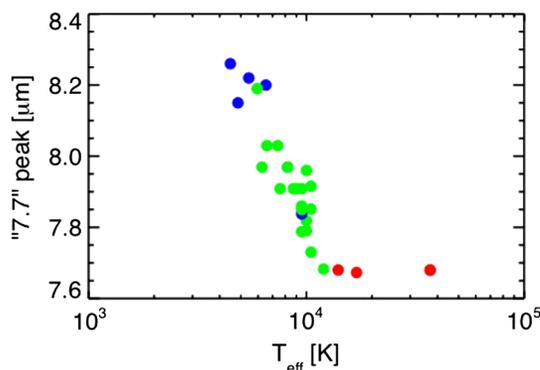
FIG. 9 (color online). Variation in the mean position of the 7.7 μm band as a function of the effective temperature of the exciting star, illustrating a chemical variation in the molecular carrier(s) (Sloan et al., 2007; Boersma et al., 2009a). Mean positions correspond to the wavelength where equal amounts of integrated flux are to shorter and longer wavelengths. All ISM sources have very similar peak positions. Since, for these hot sources, the FUV radiation field is largely independent of T_{eff}, a single point is shown.
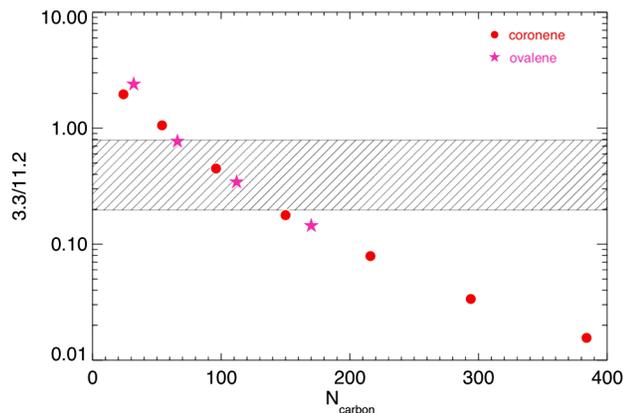
FIG. 10 (color online). Calculated ratio of the emission in the 3.3 μm stretching mode to that in the 11.2 μm out-of-plane bending mode as a function of PAH size. The intrinsic strength of these modes has been calculated using density functional theory. Sequential members of the coronene (ovalene) family are formed by adding additional rings of hexagons around coronene (ovalene). The observed range of this ratio in space in different sources is indicated by the shaded area (Peeters *et al.*, 2002). Adapted from Ricca *et al.*, 2012.

position have been interpreted as evidence for a larger contribution of aliphatic groups in some sources. This has, however, not been quantified. Every now and then, a result appears presenting a molecular structure for the emission carriers resembling that of hydrogenated amorphous carbon grains and characterized by a substantial fraction of aliphatic groups [cf. Kwok and Zhang (2011)]. However, these molecular structures bear no relationship to the observed interstellar IR emission spectrum and the postulated aliphatic component in these structures is excessive even for those regions characterized by shifted peak position.

While, overall, the consensus in the field seems to be that the interstellar PAH family is very diverse, there are signs that, actually, a few, large and compact "grand PAHs" dominate the PAH population. That is supported by the fairly simple 15–20 μm emission band pattern (Boersma *et al.*, 2010; Ricca *et al.*, 2010) and that many interstellar sources show almost identical emission spectra. In this view, only the most stable PAHs are expected to survive the harsh conditions of the ISM. Such a view of the survival of the fittest is in line with observed abundance variations of PAHs and fullerenes in the reflection nebula NGC 7023 (Sec. VI.C). However, attempts to fit this characteristic spectrum using only the most stable PAHs (e.g., circumcoronene, circumcircumcoronene) have not (yet) been successful, possibly because the photophysics of grand PAHs is not fully understood.

D. Fullerenes in space

The C_{60} fullerene molecule was "discovered" serendipitously in 1985 in the laboratory in a study driven by the quest of a laboratory spectroscopist who had become interested in molecular radio astronomy and wanted to understand how carbon-chain molecules formed in circumstellar envelopes (Kroto *et al.*, 1985). An important breakthrough came in 1990 when two other astronomers—in search of interstellar

dust analogs—demonstrated that gram quantities of fullerenes could be synthesized by striking an arc between two graphite electrodes in an inert atmosphere (Krätschmer *et al.*, 1990). Yet, until recently, the actual presence of fullerene molecules in space remained elusive. In the mid-1990s, two weak absorption bands in the far red were ascribed to electronic absorption of C_{60}^{+} (Foing and Ehrenfreund, 1994). However, this identification faces some issues that were never fully resolved (Maier, 1994). First, the identification was based upon matrix-isolation studies (Fulare, Jacobi, and Maier, 1993) and peak positions will shift due to matrix interaction and probably more than the comparison would "allow." Second, in the laboratory studies, the relative strength of the two bands varies depending on the experimental conditions and this has been attributed to the presence of two slightly different, distorted structures of C_{60}^{+} trapped in the matrix (Fulare, Jacobi, and Maier, 1993).

The difficulty in detecting interstellar fullerenes in the infrared largely reflects the dominance of the very rich vibrational spectrum of interstellar PAH molecules in the spectra of most objects (cf. Fig. 7), which swamps the signal of the small quantities of fullerenes present. Recently, however, the IR spectrum of the planetary nebula TC 1 was uncovered and this unusual spectrum is dominated by a few bands that are very different from the PAH bands normally seen (Cami *et al.*, 2010). These bands are characteristic of the fullerene molecules C_{60} and C_{70} (see Fig. 11) and this identification is now widely accepted. Now that these bands are recognized as signposts for the presence of fullerenes in space, they have also been extracted from the complex infrared spectrum of more objects in space, including reflection nebulae, HII regions, post–asymptotic-giant-branch (post-AGB) objects, and young stellar objects (Sellgren *et al.*, 2010; García-Hernández, Kameswara Rao, and Lambert, 2011; Gielen *et al.*, 2011; Boersma, Allamandola, and Rubin, 2012). Fullerenes are thus an important component of the interstellar organic inventory. Early studies overestimated the fullerene abundance by comparing the strength of the fullerene bands to those of the PAHs in the same spectrum and adopting the fact that interstellar PAHs lock up 10% of the elemental carbon. However, these estimates were based upon spectra
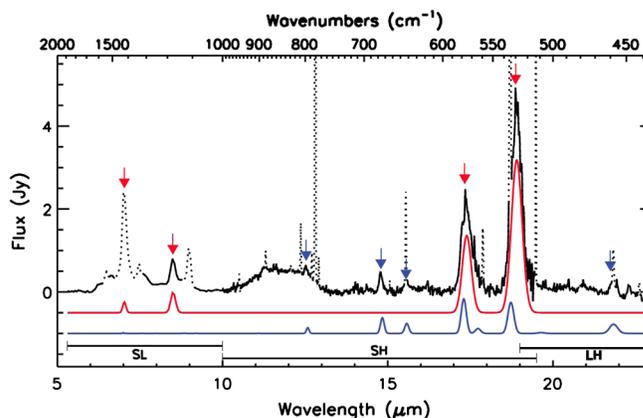

FIG. 11 (color online). The infrared spectrum of the planetary nebula TC 1 (upper trace) is dominated by a few bands which are well fitted by emission by C_{60} (middle trace) and C_{70} (lower trace) molecules. From Cami *et al.*, 2010.

of regions close to the central star where PAHs have been destroyed and the actual abundance of PAHs is only 10^{-2} of the elemental carbon (Berné and Tielens, 2012). Hence, fullerenes lock up only some 10^{-5} of the elemental carbon in the diffuse ISM as compared to $\sim 10^{-1}$ in (all) similar-sized PAH molecules, while close to bright stars, this shifts toward 10^{-4} of the elemental C in C_{60} and 10^{-2} in PAHs.

The observed relative strength of the C_{60} emission bands in TC 1 is somewhat puzzling. Unfortunately, there are no IR spectra of gaseous C_{60} for direct comparison. Measurements on C_{60} films as well as quantum chemical calculation show widely varying intrinsic ratios for the four bands (Menéndez and Page, 2000). Taking an average of these and adopting a Boltzmann distribution [note only appropriate for low temperatures (cf. Eq. (4)], the calculated excitation temperature of C_{60} in this source is estimated to be only 330 K (Cami et al., 2010), where it was suggested that the 7.04 μm band might be contaminated by an [ArII] fine-structure line originating from the ionized gas in this nebula and hence this emission temperature derives largely from the observed 8.6 to 18.9 μm band ratio. Using the density of states for C_{60}, the temperature and internal energy are related through a very similar equation as for the PAHs [cf. Eq. (3)],

$$T_m = 2000\left(\frac{E\,(\mathrm{eV})}{60}\right)^{0.36} \mathrm{K}, \qquad (6)$$

valid over the range $1 < E < 14$ eV. Hence, the derived emission temperature is much less than expected ($\simeq 1000$ K for a C_{60} molecule excited by a typical 10 eV photon, even after accounting for the energy cascade). This led Cami et al. (2010) to suggest that C_{60} in this source is present in the form of a film condensed on small dust grains in radiative equilibrium with the stellar radiation field.

However, a recent analysis of TC 1 plus two more planetary nebulae shows the same ratios for the C_{60} emission bands within the error bars (Bernard-Salas et al., 2012). Constant ratios of emission bands are a characteristic of a fluorescence process. Moreover, in TC 1, the C_{60} emission is observed to originate at a distance of $\simeq 8000$ a.u. (atomic units) from the illuminating star in TC 1 where radiative equilibrium dust temperatures are expected to be much less than 300 K (Bernard-Salas et al., 2012). If the actual temperature were indeed 330 K, rather than a film in contact with a thermal bath, this might imply the presence of C_{60} clusters in TC 1, and the observed temperature would then indicate a cluster size of ~ 10 C_{60} molecules [e.g., possibly the stable icosahedron $(C_{60})_{13}$ cluster; see Zhang, Liu, and Li (2000)]. More likely, the adopted, relative intrinsic strength of the C_{60} bands is incorrect as they are based upon calculations or film studies rather than measurements on gaseous species and the different studies show a large scatter.

In the ISM, the presence of C_{60} is recognized from the 18.9 μm band but the 7.04, 8.6, and 17.4 μm bands are more difficult to extract from among the strong PAHs bands invariably present as well. For NGC 7023, there is a weak, but distinct, feature at 7.04 μm present in regions with strong 18.9 μm bands. If due to C_{60}, the derived ratio of this band to the 18.9 μm band indicates an excitation temperature $\simeq 750$ K, in good agreement with models for the excitation of gaseous C_{60} molecules pumped by a single UV photon

(Sellgren et al., 2010). It is clear that further laboratory studies on the IR characteristics of gaseous C_{60} molecules and clusters of C_{60} molecules could be helpful in settling these issues. From the observational side, high spectral and spatial resolution studies are needed to isolate the emission characteristics of C_{60} bands from among those due to PAHs, in order to search for variations in their relative strength as an indicator of excitation temperature or energy and/or of cluster size.

E. Interstellar diamondoids

Some 25 years ago, analysis of meteorites revealed the presence of small (2 nm) diamond grains with an isotopic composition of trapped noble gases that is distinctly nonsolar (Lewis et al., 1987). Since then, it has been demonstrated that these are just one component of a wide array of stardust materials that derives directly from the stellar birth sites of these dust grains (Anders and Zinner, 1993). Apparently, these dust grains formed in stellar ejecta—enriched by the nucleosynthetic products of processes taking place in the deep interiors of these stars and then mixed to the surface—were injected into the ISM, processed by shocks and other energetic events, became part of a region of star formation that collapsed to form the Solar System, saw the hot gases swirl in the solar nebula, experienced possibly the shocks and lightning processes rampant in this environment, were incorporated into the planetary body from which the meteorite was derived, survived the collisional processes that comminuted this parent body in smaller fragments (the meteorites) that crashed on Earth. And through all this arduous and torturous history, these stardust grains never equilibrated fully with the gas and managed to preserve their stellar heritage.

Here the diamond grains isolated from meteorites are of particular interest since their sizes, 2 nm (~ 10 zepto carat), are close to molecular. They are also the most abundant stardust component in meteorites with an abundance of $\simeq 400$ parts per million (by mass). Observationally, there is little evidence for the presence of small diamonds in the interstellar medium. However, there are two, perhaps three, objects that show infrared emission features at 3.43 and 3.53 μm in their spectra that are telltale signs of H bonded to diamond surfaces (see Fig. 12) (Guillois, Ledoux, and Reynaud, 1999). While comparison to (bulk) diamond film studies imply nanodiamonds with sizes of 50 nm (Sheu et al., 2002; Jones et al., 2004a), much larger than the meteoritic diamonds, recent laboratory studies (Pirali et al., 2007) demonstrated that small diamondoid[3] molecules with T_d symmetry show bands in the near-IR similar to those observed in these two objects. DFT calculations revealed that the 3.43 μm band is due to the antisymmetric stretching vibration of CH_2 on the corners of these molecules while the 3.53 μm band is due to the stretching mode of CH groups on the facets. The relative strength of these two bands is then a measure of the surface to "corner" area and the size of the diamonds (see Fig. 12) (Pirali et al., 2007). Taking tetrahedral

---

[3]Hydrocarbon molecules that are largely superimposable on the diamond lattice. The smallest one in this class is adamantane ($C_{10}H_{16}$).
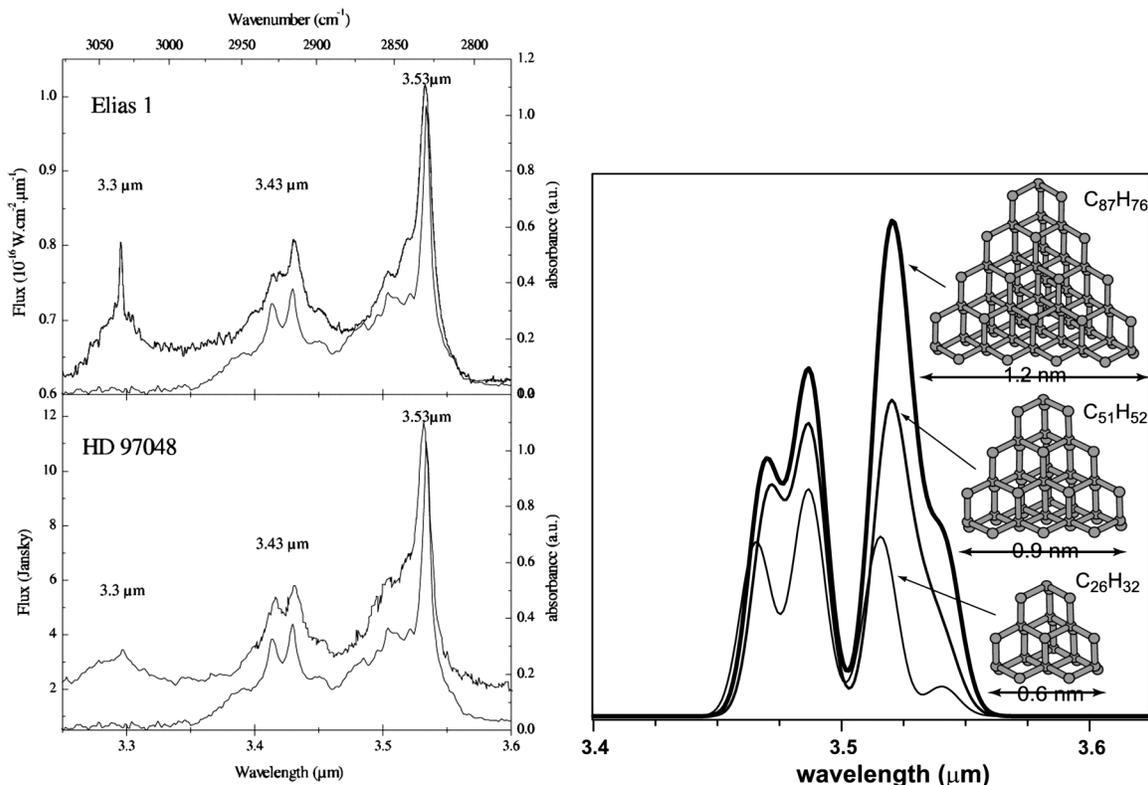
FIG. 12. Diamondoid species in space. Left: The newly formed stars Elias 1 and HD 97048 show a unique emission spectrum in the 3 μm region with strong bands at 3.43 and 3.53 μm (upper trace in each panel) that emanate from the inner regions of their circumstellar disk. These bands can be well fitted by laboratory spectra of diamond films (lower trace in each panel). From Guillois, Ledoux, and Reynaud, 1999. Right: Density functional theory calculations of the infrared spectra of small diamondoid molecules with T_d symmetry as a function of size. The 3.43 and 3.53 μm bands are due to CH$_2$ and CH groups on the edges and facets, respectively. See text for details. From Pirali et al., 2007.

molecules as a guide, the diamondoid $C_{136}H_{104}$ is (typically) implied by the observed 3.4:3.5 μm band ratio in the source HD 97048, quite comparable in size to that of interstellar PAHs.

F. Diffuse interstellar bands

DIBs are a set of several hundred absorption features in the visible wavelength range. They were recognized as due to interstellar material in the earliest spectra (Merrill, 1934). By now some 400 DIBs have been cataloged [cf., Hobbs et al. (2009)] and new ones are reported every year. The strongest and best-known bands occur at 4430, 5778, 5780, 5796, 6177, 6196, 6284, and 6614 Å. While most of the bands fall in the visible, they actually stretch from the near UV to the far red (Hobbs et al., 2009) and have recently been discovered in the near IR as well (Geballe et al., 2011). Reviews can be found by Herbig (1995) and in the proceedings edited by Tielens and Snow (1995).

The observed width of the DIBs varies from $\sim$0.5 to 30 Å but is typically 0.7 Å. Their strength (relative to the continuum) is expressed in terms of the equivalent width

$$W_\lambda = \int \frac{F_c - F_o}{F_c} d\lambda \qquad (7)$$

with F_c and F_o the continuum and observed flux, respectively. Most of the DIBs are weak to very weak

($W_\lambda/N_H \simeq 10^{-24}$ Å/H atom) but a subset of 30 have appreciable equivalent width ($W_\lambda/N_H \simeq 10^{-23}$ Å/H atom) and a few are strong ($W_\lambda/N_H \simeq 10^{-22}$ Å/H atom). Surveys are likely incomplete at the weak end and have not yet reached the spectral "confusion" noise but likely there is a (very weak) DIB at every wavelength.

Correlation studies have cut a well-worn swath through DIB country and much insight into the characteristics of the DIB carriers has been gained this way. Initial studies divided the strong DIBs in families where bands within one family correlate well together but not one to one with bands in other families (Chlewicki et al., 1987; Krelowski and Walker, 1987). However, subsequent studies revealed that these families were really "dysfunctional" and correlations between the strength of the strong DIBs are generally not perfect [cf., Fig. 13; see Cami et al. (1997), Ehrenfreund et al. (1997), and Moutou et al. (1999)]. This has been investigated well only for DIBs with appreciable strength and whether this pertains to the weaker ones as well is to be determined. The best correlation is found for the pair 6614 and 6196 Å, but even for these two DIBs the correlation is not truly perfect unless the influence of systematic errors has been underestimated (Moutou et al., 1999; McCall et al., 2010).

Most interstellar quantities trace each other and, in that sense, the strength of the DIBs scales with the dust visual extinction and with the total column density of hydrogen but these correlations are (also) not perfect. In fact, the DIBs
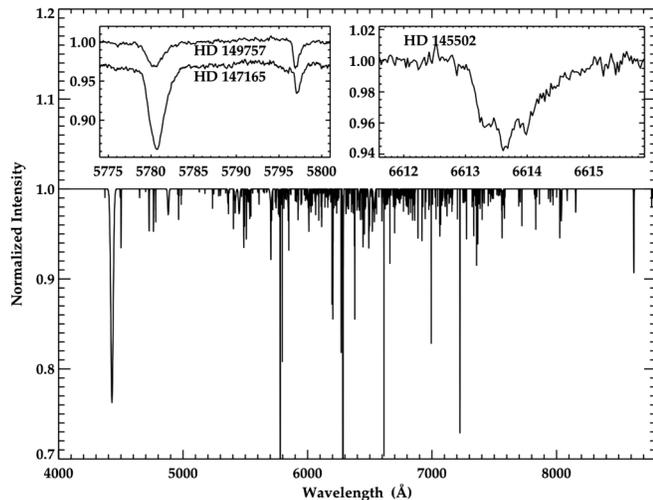
FIG. 13. Some 400 diffuse interstellar bands (DIBs) are present in visible absorption spectra of the interstellar medium. The synthesized spectrum of diffuse interstellar bands within the 4300–6800 Å wavelength range observed toward BD + 63 1964 (Ehrenfreund *et al.*, 1997) illustrates the great variety in relative strength and width of the DIBs. Inset right: Detailed profile of the 6614 Å DIB and its associated substructure observed toward the star HD 145502. Inset left: Variations in the strength of the DIB bands relative to each other for two well-studied DIBs (5780 and 5797 Å) on the basis of observations of the stars HD 149757 and HD 147165. Figure courtesy of J. Cami.

correlate much better with the column density of atomic hydrogen than with that of molecular hydrogen (Friedman *et al.*, 2011). However, outliers in these correlation studies indicate that, for example, the ambient radiation field may be a player in the strength of, e.g., the 5780 Å (Sonnentrucker *et al.*, 1997; Friedman *et al.*, 2011). In terms of the dust, there is a good but not perfect correlation with the dust column density. Considering specific DIBs, the measured band strength correlates with the characteristics of the dust extinction curve. That is, dust extinction curves have been divided into σ and ζ types, where the latter have much faster rising far-UV (FUV) extinction curves than the former. As an example, observations show that the 5780 Å DIB is much stronger in σ sight lines, while the 5797 Å correlates with the ζ-type extinction curves [cf., Fig. 13; see Sneden, Woszczyk, and Krelowski (1991) and Cami *et al.* (1997)]. This may again indicate that penetration of FUV photons plays a role in the presence of the carriers where σ carriers exist in the outer skins of diffuse clouds while ζ carriers are abundant in the shielded cores (Friedman *et al.*, 2011). Further studies confirm that the abundance ratios of DIBs are sensitive to the local physical conditions as traced by the abundance of simple diatomic molecules [e.g., CO, CH, C_2; see Krełowski *et al.* (1999), Thorburn *et al.* (2003), and Weselak *et al.* (2004)].

Following Douglas (1977), it is now generally accepted that the DIBs are due to electronic absorptions by molecules (rather than due to absorption by impurities in dielectric grains). Among the observational evidence is the absence of large variations in the peak position and profile of these bands between sight lines with very different dust properties (e.g., grain size). Also the detailed profiles of some DIBs show substructure which resembles the rotational substructure of

molecular transitions (Sarre *et al.*, 1995; Ehrenfreund and Foing, 1996; Galazutdinov *et al.*, 2003; Cami *et al.*, 2004; cf., Fig. 13). The peak position and relative strength of this substructure show weak variations, indicating varying excitation conditions. Finally, the enigmatic object, the red rectangle, shows *emission* bands at wavelengths which are near to, but not exactly at, the position of some (absorption) DIBs, suggesting that these transitions may be involved in a fluorescence process when the conditions are right (Scarrott *et al.*, 1992; Sarre, Miles, and Scarrott, 1995; Van Winckel, Cohen, and Gull, 2002).

The large number ($\simeq 20$) of strong DIBs and the absence of a detailed correlation between them has been taken to imply that there are at least some 20 different, abundant, complex molecules in diffuse interstellar clouds and probably many more (but see below). Per logarithmic interval of strength, the summed equivalent width is about constant (at least, until the completeness limit of $\simeq 10^{-24}$ Å/H atom) and all DIBs sum up to some 0.5% of the dust extinction over the same (4000–8500 Å) wavelength region. Taking the star HD 183143 as our guide, the equivalent width of the three strongest DIBs (4430, 6284, and 5780 Å) corresponds to molecular abundances relative to H of $4 \times 10^{-9}/f$, $7 \times 10^{-10}/f$, and $4 \times 10^{-10}/f$ with f the oscillator strength of the transitions involved. Summing over all DIBs, the abundance is $\sim 10^{-8}/\bar{f}$ with $\bar{f}$ an average oscillator strength. Typical measured oscillator strengths for the first transition ($S_0 \rightarrow S_1$) of small PAHs and hydrocarbon chains are 0.01–0.1 (Tuley *et al.*, 1998; Maier, Walker, and Bohlender, 2004; Gredel *et al.*, 2011). As the size of these species increases, the effective number of electrons involved in the transition is expected to increase and the oscillator strength per C atom is roughly constant at ~ 0.01 (Watson, 1994; Weisman *et al.*, 2003). In that case, the fraction of the C locked up in the three strongest DIBs is 10^{-4}–10^{-3} and for all DIBs it would be 2×10^{-3}. Higher oscillator strengths are obtained for higher transitions ($S_0 \rightarrow S_2 \cdots$) and for large enough species these would shift into the visible domain. However, these higher electronic states couple efficiently to lower electronic states, resulting in rapid internal conversion and lifetime broadening of the lines. For PAH cations, these nonradiative, fast relaxation channels lead to very broad lines whenever the energy difference is >1 eV (Pino *et al.*, 2011). Such transitions do not correspond to the known DIBs (as they are difficult to discern in interstellar spectra, they may well be there). In any case, the bottom line is that individual carriers of strong DIBs have to be as abundant as simple polyatomic molecules such as HCN in diffuse clouds (Table II). If we adopt the rule "one DIB, one molecule" and an average oscillator strength of 0.1, then as a class, the DIB carriers have an abundance of 10^{-7}. While there is no C-abundance crisis, this is an extremely high abundance, quite comparable to the total abundance of the PAH family.

Accepting that the DIB carriers will have strong FUV transitions with average absorption strengths per C atom comparable to the PAHs, they should have IR emission bands with an integrated strength that is a fraction $\sim 2 \times 10^{-2} \bar{N}_c$ of that of the PAH IR emission bands with $\bar{N}_C$ the average number of C atoms per DIB carrier (and we have adopted 50 C atoms as the typical size for interstellar PAHs). To be

even more specific, consider carbon chains as a class. Their characteristic C-C bands occur in the range 4.6–5.2 μm (Allamandola *et al.*, 1999). The infrared spectra of the Orion bar and M17 show weak emission features at 4.6, 5.2, and 5.75 μm. These have actually been ascribed to deuterated PAHs and combination modes involving the PAH out-of-plane CH bending modes (Peeters *et al.*, 2004; Boersma *et al.*, 2009b), but for the sake of argument, we sidestep this issue here and assume that they originate in hydrocarbon chain molecules. The integrated strength of these bands relative to the PAH bands is 6×10^{-2} in these sources and hence the abundance limit on carbon chains in these PDR[4] environments is $\sim 8 \times 10^{-7}/\overline{N_C}$ relative to H nuclei. The IRTS/AKARI as well as ISOCAM/ISO and DIRBE/COBE[5] provide limits on the carbon-chain feature strength in the IR spectrum of the diffuse ISM of a few percent, corresponding to an abundance limit of $4 \times 10^{-7}/\overline{N_C}$ (Allamandola *et al.*, 1999; Tielens *et al.*, 1999). Hence this analysis can be taken to imply that if carbon chains are involved in the DIBs, they have to be quite small in size in order to agree with the IR-derived abundance limits.

It is generally assumed that the DIBs are due to electronic transitions of gas-phase molecules with low internal temperatures and, hence, they are in their lowest vibrational state, with rotational temperature of 10–100 K, depending on the molecule. Small radicals may indeed radiatively relax before further (reactive) collisions occur or the species is photodissociated or -ionized (Maier *et al.*, 2011a). The excitation of PAHs, on the other hand, will depend on the physical conditions, e.g., the radiation field, of the region (Joblin *et al.*, 2002). Consider, UV pumping of PAHs will leave the species in a highly vibrationally excited state from which it will relax through IR emission (e.g., the IR emission features). Now, when the internal energy in the molecule drops below some critical value E_c the density of states will be so low that the modes will start to decouple (Felker and Zewail, 1983; Kuzmin and Stuchebrukhov, 1985). That will leave the molecule vibrationally excited in the lowest vibrational modes and, without rapid internal vibrational relaxation, energy in these modes can be lost only through radiation in these specific modes. For PAHs, the lowest (drumhead) mode occurs at $\simeq 59(50/N_c)$ cm^{-1} and has an integrated strength $\simeq 2.4 \times 10^{-19}(50/N_C)^{4/5}$ cm/molecule. This corresponds to an Einstein A of $9.5 \times 10^{-4}(50/N_c)^{14/5}$ s^{-1}. For magnetic-dipole or electric-quadrupole transitions, the decay rates will be a factor $\sim (1/137)^2 \simeq 5 \times 10^{-5}$ smaller. Although the rotational population ($J \sim 100$) is appreciable, Coriolis coupling between vibrational states is effective only for very closely spaced vibrational levels [e.g., $\nu_{\text{rot}} \sim 10^{-3}(50/N_c)^2$ cm^{-1}; see Rouan *et al.* (1992)]. Likewise, coupling of the vibrations to the rotational bath is expected to be

very slow given the large energy mismatch. Consider specifically the circumcoronene molecule ($C_{54}H_{18}$) with 1000 cm^{-1} of internal energy, the excitation temperature at decoupling will be ~ 150 K, several modes are accessible and will be appreciably populated, and the lowest mode at 40.6 cm^{-1} has no dipole-allowed transition. These deexcitation rates have to be compared to the UV pumping rates $k_{\text{UV}} \simeq 4 \times 10^{-7}(N_C/50)G_0$ s^{-1} and the collisional deexcitation rate $n\gamma_{\text{col}} \simeq 10^{-9}n$ s^{-1} with G_0 the average interstellar (UV) radiation field in the solar neighborhood and n the density (Tielens, 2005). With these values, levels with dipole-allowed transitions will depopulate quickly (compared to the pumping rate). However, the population of IR-dark levels is set by the balance of UV pumping into and out of these states. The excitation of these modes will then be set by the (UV) Franck-Condon factors involved, the temperature of the radiation field, and the molecular excitation temperature at the time of decoupling. It will thus be sensitive to the local physical conditions (e.g., G_0 and the UV radiation field temperature which in turn depend on, for example, dust shielding).

This has a number of potential implications. The relationship between DIBs originating from the ground vibrational state and from IR-dark states depends on the Franck-Condon factors involved in the DIB transition. If the molecular geometry of the molecule changes appreciably between the ground and excited electronic state, this will shift transitions originating from dark states well clear from the ground state absorption. No perfect correlation is expected for such DIBs even though they originate from the same species. If the ground and excited electronic states have similar molecular geometries, then shifts may be quite small but would likely still affect the band profile. This has, for example, been examined as a cause of the observed variations in the profile of the DIB-related emission bands in the red rectangle (Sharp *et al.*, 2006). Because the oscillator strength from IR-dark states may differ from that in the ground state, correlation studies would also be affected. The UV pumping process will dominate the rotational population (Rouan *et al.*, 1992; Ysard and Verstraete, 2010). Hence profiles of transitions controlled by rotations (rather than nonradiative processes) will be sensitive to the local conditions. While this discussion centers on PAHs, similar considerations pertain to other astrophysically relevant species. For example, the lowest vibration of pure carbon chains shifts through the 10 to 100 cm^{-1} range when the chain length increases from four to ten C atoms and for the larger carbon chains, deexcitation time scales may also approach the collisional, pumping, or chemical time scales. Finally, while this discussion does not affect the abundance considerations, it may imply that the interstellar complex molecule family is less diverse than the DIB correlation studies seem to imply.

Identification of the carriers of the DIBs has turned out to be very challenging as the list of potential candidates is large and laboratory studies are demanding. Among the leading candidates are hydrocarbon chains (Fulare *et al.*, 1993; Maier, Walker, and Bohlender, 2004), PAHs (Bréchignac and Pino, 1999; Biennier *et al.*, 2003; Kokkin *et al.*, 2008), and fullerenes (Sassara *et al.*, 2001), largely because there is independent evidence for the presence of these species in the ISM (and that is one way to limit the scope of the search). Electronic transitions in the visible require either open shell radicals, cations

---

[4]Photodissociation regions (PDRs) are the predominantly neutral atomic layers of clouds where UV photons from nearby stars or from the interstellar radiation field dissociate molecules and ionize atoms with low ionization potentials (e.g., C) as well as heat the gas through the photoelectric effect.

[5]IRTS is the infrared spectrograph onboard the Japanese satellite, AKARI. ISOCAM is the imaging spectrometer onboard ESA's Infrared Space Observatory, and DIRBE is the Diffuse Infrared Background Experiment onboard NASA's COBE satellite.

or anions, or very large species. Because these species are reactive or unstable in laboratory settings or are not very volatile, special techniques have to be used [for a review of these techniques, see Pino *et al.* (2011)]. Many laboratory studies employed matrix-isolation techniques but the matrix will shift and broaden the bands and, while this can provide tantalizing suggestions, identification requires further proof. A number of criteria can be formulated before an identification will be widely accepted by the community, including an exact match of peak positions, profiles, and relative strength of (at least) two DIBs with laboratory gas-phase spectra (Maier, 1994). But, as argued, IR-dark states can have appreciable populations. Hence, one or all of these criteria may have to be relaxed somewhat.

While a few specific species have been put forward as candidates for particular DIBs, invariably, these have fallen by the wayside if tested according to these criteria. Specifically, the coincidence of five of the seven vibronic bands in the lowest energy transition of the anion, C_7^- reinvigorated the field when it was announced in 1998 (Tuley *et al.*, 1998). However, later astronomical studies cast serious doubt on this identification since the observed peak position and width of the strongest (origin) band of this species (in fact, all weak vibronic bands as well) do not agree with calculated profiles (McCall *et al.*, 2001). The assignment of the 9577 and 9632 Å bands to C_{60}^+ (Foing and Ehrenfreund, 1994) still has to await laboratory (gas-phase) confirmation (see Sec. II.D). The origin band of the linear propadienylidene anion l-$C_3H_2^-$ at 6994 Å occurs close to a weak DIB (Güthe *et al.*, 2001), but there is no exact match in comparison with high resolution laboratory spectra (McCall *et al.*, 2002). Following a suggestion by Linnartz *et al.* (2010), broad DIBs at 4881 and 5450 Å have been attributed to vibronic absorptions by the radical, propadienylidene (l-C_3H_2) based on the excellent agreement in peak position and width (Maier *et al.*, 2011b). Subsequent studies revealed intensity variations between the astronomical bands, calling this identification into serious question (Krełowski, Galazutdinov, and Kołos, 2011). A weak DIB at 5069 Å has been attributed to the gas-phase origins transition of HC_4H^+ (Krełowski *et al.*, 2010). However, accurate profile calculations revealed differences in peak position and width with the observed DIB and this assignment, too, disappears (Maier *et al.*, 2011a). Finally, Gredel *et al.* (2011) and Salama *et al.* (2011) searched for laboratory-measured visible transitions of typically small PAHs to no avail and the species searched for are not abundant (typical upper limits of 3×10^{-10} but up to 3×10^{-8} for the weakest transitions) in the interstellar PAH family.

Over the last 80 years, it has proven difficult to delineate a path forward. From an astronomical point of view, clearly, the focus should be on identifying strong DIBs since there is a weak ($W_\lambda / N_H \sim 10^{-24}$ Å/H atom) band at any wavelength and coincidences will make such an assignment meaningless. It may also pay to study those bands that show rotational structure. These are not broadened by internal conversion and may well correspond to the $S_0 \rightarrow S_1$. Moreover, the rotational structure may help "seal" the identification. The DIBs with emission counterparts in the spectrum of the red rectangle also show rotational broadening behavior [but see Sharp *et al.* (2006)]. A high fluorescence yield implies that internal conversion is not important and again points toward a first electronic transition. Of course, aromatic cations have fluorescent quantum yields close to zero and hence would be purposely deselected this way. These DIBs with emission counterparts might therefore be a prime carbon-chain hunting ground. But this really turns the issue upside down: identifications have to be initiated from laboratory studies and, in order to do so, we have to know already which molecule is a good candidate and our intuition has not been a successful guide in the past. Perhaps, a growing understanding of trickle-down chemistry (Sec. VI.C) will help us focus our laboratory studies.

III. PATHWAYS TO MOLECULAR COMPLEXITY

Much of the carbon in regions of star and planet formation is locked up in very stable species that do not readily partake in chemical reactions. The story of interstellar organic chemistry is therefore by necessity a story that starts with breaking the carbon out of these species. The two main molecular reservoirs are CO and PAH molecules. Figure 14 illustrates relevant chemical routes. In dark clouds, ion-molecule chemistry converts gaseous carbon into predominantly carbon monoxide. Traces of hydrocarbon chains are also formed but on an overall "budget" scale, they are not important (Table II). After accretion onto grains, hydrogenation reactions convert CO efficiently into formaldehyde and methanol as well as traces of other species in an icy grain mantle. Energetic processing of these ices by UV photons and cosmic rays can convert these molecules into more complex species, while heating by the protostar can initiate thermal polymerization reactions.
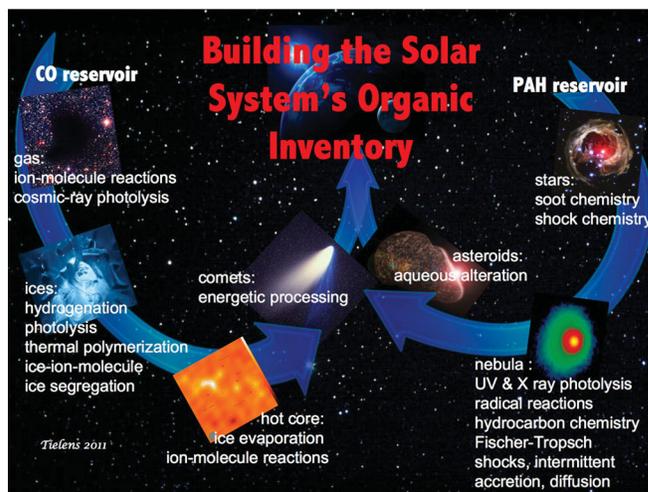
FIG. 14 (color). The organic inventory of the Solar System derives from a vast array of processes acting in a wide range of environments. Globally, two independent routes can be recognized. The first one builds up complex species from small radicals and starts with CO in dark clouds. Ion-molecule reactions, grain-surface chemistry, and photoprocessing converts the main gaseous reservoir CO into complex species. The other route breaks down very complex species (e.g., PAHs) injected into the interstellar medium by stars into smaller and smaller species. Eventually, the species produced by either of these two chemical routes can become part of planetesimals and cometesimals in a protoplanetary disk environment which delivers this organic inventory to the nascent planets in the habitable zone.

The newly formed protostar will sublime these ices and fast ions in shocks can sputter some molecules into the gas phase. Subsequent ion-neutral and neutral-neutral reactions in the warm dense gas of the hot core surrounding the protostar may convert, in particular, methanol into more complex species such as dimethyl ether and methyl formate. These can then accrete again into ices and other planetesimals. Thus, in this route, complex species are built up by continued adding of small compounds, leading to a rich organic mixture.

The other route starts with the formation of PAHs and other large, complex molecules in stellar ejecta through chemical processes akin to soot chemistry. The injected PAH family is further processed in the interstellar medium by energetic photons and particles, weeding out the less stable members. Further processing can occur in the photosphere of the protoplanetary disk by stellar UV and x-ray photons. Furthermore, in the inner, hot, and dense (midplane) regions, H and OH radicals will break down these complex species into acetylene, methane, and carbon monoxide and carbon dioxide. Turbulence will diffuse these species and their daughter products, formed through neutral-neutral reactions, throughout the protoplanetary disk. Hence, this is a top-down chemistry where complex species are injected by stars and then broken down by (energetic) processing in the ISM to smaller and smaller species. Eventually, the species produced in these two chemical routes can become part of planetesimals and cometesimals where further processing may occur before this organic inventory is delivered to nascent planets.

IV. GAS-PHASE CHEMISTRY

In this section, I briefly review a few key aspects of gas-phase chemistry in the ISM followed by discussions of the initial steps in the chemistry of oxygen, carbon, and nitrogen, as well as deuterium fractionation, the formation of acetylenic derivatives, and the role of molecular anions. As gas-phase chemistry is essentially ion-molecule chemistry driven by cosmic-ray ionization, molecular observations can be used to determine the cosmic-ray ionization rate and various studies deriving the cosmic-ray ionization rate are summarized next. This section ends with a review of the contributions of HIFI/Herschel studies to our understanding of the initial chemical steps toward molecular complexity in the gas phase.

At the low temperatures and densities of the ISM, kinetics is a key issue and reactions with activation barriers are generally inhibited but can become important in shocks, photodissociation regions, or hot cores. However, pervasive cosmic rays and also penetrating ultraviolet photons produce a low level of ionization. As ions can use the Coulomb energy to overcome activation barriers in reactions with neutral ions, gas-phase chemistry in diffuse and dark clouds is generally dominated by ion-molecule reactions (Herbst and Klemperer, 1973; Watson, 1973). Reactions occur then at the Langevin rate, $\simeq 10^{-9}$ cm^3 s^{-1}. Ionization is counteracted by dissociative electron recombination at a rate of $\simeq 10^{-7}$ cm^3 s^{-1} for molecular ions. Electron recombinations for atomic ions are radiative and hence much slower, $\simeq 10^{-11}$ cm^3 s^{-1}. In recent years, it has become clear that anions can be abundant and, in particular, PAH anions might be the dominant negative charge carriers. In that case, mutual neutralization reactions can become important. Neutral radical-radical reactions, at the collision rate (if no barriers are involved) of $\simeq 10^{-10}$ cm^3 s^{-1}, are important as well. The buildup of molecules is counteracted by photodissociation with a rate of typically $\simeq 10^{-10}$ s^{-1} in the ambient interstellar radiation field but a factor of $\simeq 5 \times 10^{-4}$ lower deep inside dark clouds where only cosmic-ray-produced photons are available.

With these rates as a guide, a set of simple rules governs the chemical routes, taking also into account the high H$_2$ abundance and the electron fraction of $\simeq 10^{-4}$ in cloud surfaces and $\simeq 10^{-7}$ inside cloud cores. For ions, reactions with H$_2$ are most important unless they are inhibited by an activation barrier. Dissociative recombination takes over then. For neutral species, proton transfer from cationic species such as H$_3^+$, HCO$^+$, and H$_3$O$^+$ is important, while reactions with He$^+$ often provide a loss channel. If proton transfer is inhibited, neutral-neutral reactions with small radicals have to be considered. If all else fails, the general consensus is that the "scoundrel" rule applies and grain-surface chemistry may be invoked (Sec. V). At the moment that is only generally accepted for the formation of molecular hydrogen and for the formation of hydrides, such as H$_2$O, NH$_3$, CH$_4$, H$_2$CO, and CH$_3$OH, which are abundant in ices.

A. Oxygen chemistry

The high abundance of atomic H in diffuse clouds makes H$^+$, produced through cosmic-ray ionization, the starting point of O chemistry. Because of the small energy difference, charge exchange of neutral O with H$^+$ is slow at low temperatures (< 100 K) for O in the ground state ($J = 2$) but very rapid for O in the $J = 1$ or $J = 0$ fine-structure levels (Stancil et al., 1999). Once O$^+$ has formed, reaction with H$_2$ then quickly leads to OH$^+$, H$_2$O$^+$, and then H$_3$O$^+$ (see Fig. 15). The latter dissociatively recombines to OH and H$_2$O. Reactions with C$^+$ then lead to CO$^+$ and HCO$^+$ and, eventually, CO. In diffuse clouds, molecule formation is strongly counteracted by FUV photodestruction.

Deeper in the cloud where H$_2$ is an important species, cosmic-ray ionization of H$_2$ eventually leads to the formation of H$_3^+$ which readily reacts with O to form OH$^+$ and, from there on, chemistry follows the same route. CO is a very stable molecule and almost all of the C is rapidly converted into CO; e.g., essentially for every C atom, one H$_2$ has to be ionized and the time scale is then

$$\tau_{\text{chem}} \simeq \frac{\mathcal{A}_\mathcal{C}}{\zeta_{\text{CR}}} \simeq 2 \times 10^6 \text{ yr,} \tag{8}$$

where $\mathcal{A}_\mathcal{C}$ is the carbon abundance and ζ_{CR} is the cosmic-ray ionization rate. In the gas phase, some excess oxygen is predicted to be converted into O$_2$ through reactions of OH and O. However, O$_2$ is observed to have a low abundance in dense clouds (Liseau et al., 2012) and this is thought to reflect the rapid sequestering of oxygen into H$_2$O ice mantles (Hollenbach et al., 2009) (cf., Sec. V.B.2).

B. Carbon chemistry

There are distinct differences in the initial chemical steps involved in the formation of oxygen- and carbon-bearing
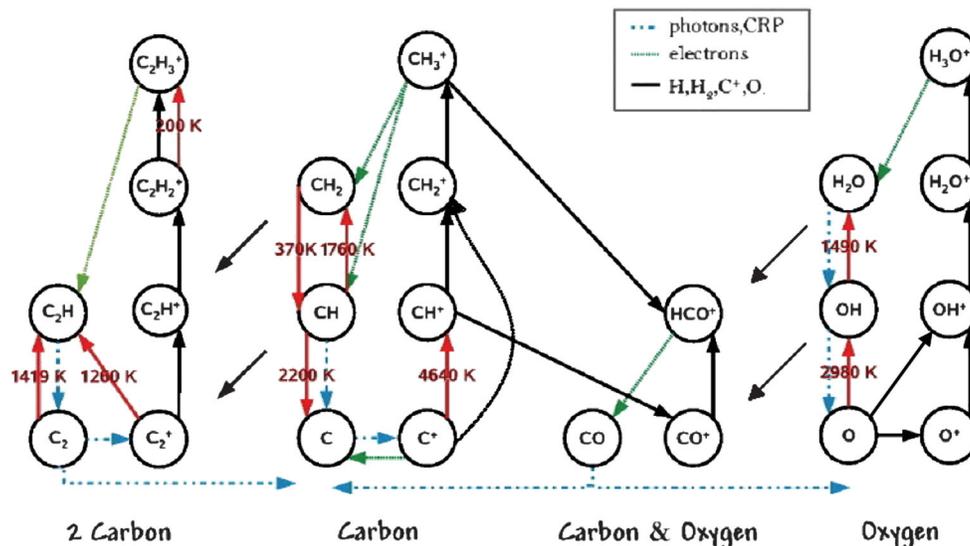
FIG. 15 (color). Key reactions in the buildup of molecules involving oxygen and carbon. Gas-phase chemistry is initiated by ionization, followed by a reaction with H_2 (if rapid) and electrons. These reactions convert C and O rapidly into small hydride radicals and then CO, which is very stable. The color code indicates reactions with H_2, C^+, H, and H^+ (black), reactions involving UV photons or cosmic rays (blue), and electron recombination (green). Reaction barriers are indicated in red. See text for details. Adapted from Godard, Falgarone, and Pineau Des Forêts, 2009.

species in diffuse clouds. First, most of the oxygen is neutral and the chemistry starts by charge transfer between O and H^+ (produced by cosmic rays) while carbon is largely in the form of C^+ (due to photoionization). Second, the buildup of oxygen-bearing species is driven by the reaction of O^+ with H_2. The analogous reaction of carbon-bearing species, H_2 reaction starting with C^+, is inhibited by a high activation barrier (see Fig. 15). Instead, small hydrocarbon radicals have to be formed through the slow radiative association reaction of C^+ with H_2 forming CH_2^+ (only 1 in $\sim 10^6$ collisions will result in reaction). This ion can react quickly with H_2 to CH_3^+ but further reaction with H_2 is again inhibited by an activation barrier. Radiative association to CH_5^+ is slow (1 in $\sim 10^4$ collisions) but can still be relevant. However, CH_5^+ dissociatively recombines to CH_3 rather than CH_4. Thus, in contrast to H_2O, the direct gas-phase route to CH_4 is effectively closed. The small hydrocarbon ions that result from this route can react with atomic O, eventually resulting in CO, or they may dissociatively recombine to small, neutral, hydrocarbon radicals. Reaction of these with C^+ will then lead to acetylenic species and longer chains can be built up from there through self-reaction of acetylenic radicals and ions and through C^+ or C-insertion reactions (see Fig. 15). Thus while the high abundance of H_2 and thermodynamics would argue for CH_4, kinetics leads to CO as the preferred carbon-bearing species in dense clouds, with an array of hydrocarbon radicals and carbon chains at much lower abundances.

C. Nitrogen chemistry

Neutral radical-radical reactions play a key role in nitrogen chemistry (see Fig. 16). Atomic N reacts with CH to form CN or with OH to form NO. These will react again with N to form N_2, which is a very stable molecule. Models predict that most of the nitrogen in molecular clouds is locked up in N_2.

Reaction of N_2 with H_3^+ forms N_2H^+. The product of the dissociative electron recombination of N_2H^+ is expected to be mainly N_2, but there has been some discussion on the breaking of the strong N_2 bond in this process. Early flowing afterglow Langmuir probe experiments (Adams et al., 1991) report the absence of NH as a product and assumed that N_2 is the only channel while storage ring experiments (Geppert et al., 2004) concluded that a considerable fraction of the recombinations form NH (and initiate interstellar nitrogen chemistry). Recent storage ring experiments suggest that the earlier studies were obfuscated by (inadvertent) $^{14}N^{15}N^+$ recombination and support the conclusion that dissociative recombination of N_2H^+ leads predominantly to N_2 ($93^{+4}_{-2}\%$) with a very minor contribution of NH ($7^{+2}_{-4}\%$) (Vigren et al., 2012).

The reaction pathway to NH_3 in the gas phase is not well understood. Dissociative recombination of N_2H^+ may lead to NH (see above) but reactions with H_2 will occur only in warm gas (cf., Fig. 16). Hence formation of NH_3 will have to start with the breakup of N_2 through reaction with cosmic-ray-produced He^+, forming N^+ and N. The route analogous to that for oxygen-bearing hydrides, starting with proton transfer to N from H_3^+ followed by rapid hydrogen abstraction from H_2 to eventually form NH_4^+, which dissociatively recombines to NH_3, has two bottlenecks: The initial step, forming NH^+, is endothermic, while the last hydrogen abstraction reaction, forming NH_4^+, has an activation barrier. NH_4^+ formation may instead be initiated by reaction of N^+ with H_2, which has a small activation barrier of $\simeq 200$ K for para H_2, but N^+ may react more efficiently with ortho H_2, which lies about 170 K above the para ground state (Luine and Dunn, 1985). The start of this route toward NH_3 depends then critically on the ortho-to-para ratio of H_2 in molecular clouds (Le Bourlot, 1991; Dislaire et al., 2012). Essentially, ortho and para H_2 are distinct chemical species in cold dense
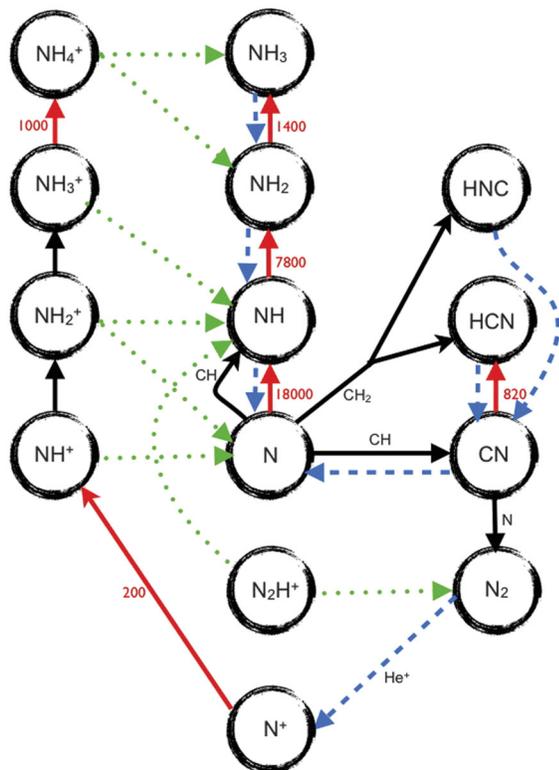
FIG. 16 (color). First chemical steps in gas-phase routes for nitrogen-bearing species. The color code indicates reactions with H_2, C^+, H, and H^+ (black), reactions involving UV photons or cosmic rays (blue), and electron recombination (green). Reaction barriers are indicated in red. See text for details.

clouds, which are related through scrambling reactions involving the exchange of an H atom with H_3^+ (Hugo, Asvany, and Schlemmer, 2009), and the H_2 ortho-to-para ratio is not well known. The activation barrier ($\simeq 1000$ K) in the $NH_3^+ + H_2$ reaction is of lesser concern as tunneling can assist this reaction ($k = 10^{-12}$ cm^3 s^{-1} at 10 K). In the competition between dissociative electron recombination and hydrogen abstraction from H_2, the latter will then win when the electron abundance is small ($x \ll 10^{-6}$, e.g., $n \gg 10^2$ cm^{-3}). So, only in diffuse gas will this latter reaction hamper ammonia formation.

As all hydrides, ammonia is also often considered a grain-surface chemistry product (Sec. V.B).

D. Deuterium chemistry

Originally, observational studies of interstellar deuterated molecules were inspired by the constraints provided by the deuterium abundance on cosmology and on stellar nucleosynthesis. However, observations quickly revealed that isotopologs of molecules with a hydrogen replaced by a deuterium atom typically have abundances far in excess of the cosmological D/H ratio. Hence, it was realized that instead of probing cosmology deuterated molecules provide direct insight into chemical routes in the ISM. This high deuteration reflects the slightly higher stability of deuterated species as a result of the zero-point-energy difference; i.e., deuterium sits slightly deeper in the potential well than hydrogen.

The reactions of interest are of the form,

$$X H^+ + HD \leftrightarrow X D^+ + H_2 + \Delta E. \quad (9)$$
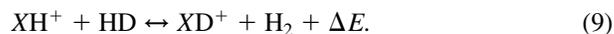
The energy difference $\Delta E/k$ is of the order of a few hundred degrees and these reactions play a role only at low temperatures. The route involving H_3^+ is of particular interest (see Fig. 17),

$$H_3^+ + HD \leftrightarrow H_2 D^+ + H_2 + \Delta E. \quad (10)$$
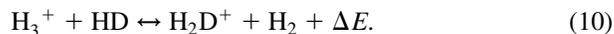
The endothermicity of this reaction is 232 K when all species are in their ground state.[6] Ignoring reactions with other species for the moment, we find in the local thermodynamic equilibrium (LTE)

$$\frac{H_2 D^+}{H_3^+} = \frac{HD}{H_2} \exp[\Delta E/kT]. \quad (11)$$

As HD and H_2 are the main reservoirs of H and D, at a temperature of 10 K, the $H_2 D^+/H_3^+$ ratio is greatly enhanced over the elemental abundance ratio (1.5×10^{-5}). Including kinetics, deuterium fractionation is limited by electron recombination and proton or deuteron transfer to other species. Typically, in one-third of the collisions, the enhanced fractionation of $H_2 D^+$ is passed on to neutral molecules with deuteron affinities larger than H_2 such as DCO^+,

$$H_2 D^+ + CO \rightarrow DCO^+ + H_2. \quad (12)$$
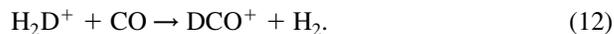
We find then for the deuterium fractionation,

$$\frac{X(H_2 D^+)}{X(H_3^+)} = \frac{k_f X(HD)}{k_b X(H_2) + k_e X(e^-) + k_{CO} X(CO) + \cdots}, \quad (13)$$

and

$$\frac{X(DCO^+)}{X(HCO^+)}$$
$$= \frac{X(H_2 D^+)}{3 X(H_3^+)}$$
$$= \frac{2}{3} \frac{\mathcal{A}_D}{\exp[-\Delta E/kT] + 193 X(e^-) + 1.2 X(CO) + \cdots}, \quad (14)$$

here $\mathcal{A}_D$ is the elemental deuterium abundance and we have used the reaction rates $k_f = 1.4 \times 10^{-9}$ cm^3 s^{-1}, $k_e = 6 \times 10^{-8} \sqrt{300/T}$ cm^3 s^{-1}, and $k_{CO} = 1.7 \times 10^{-9}$ cm^3 s^{-1}. For typical electron abundances [$X(e^-) = 10^{-8}$–10^{-6}] and CO abundances [$X(CO) = 10^{-5}$–10^{-4}], the fractionation of deuterated molecules can much exceed [$X(DCO^+)/X(HCO^+) \sim 3 \times 10^{-2}$] the elemental deuterium abundance.

It is now recognized that, when most of the CO and other gas-phase species are depleted out in an ice mantle, the proton

---

[6]Note that H_2, H_3^+, and $H_2 D^+$ all have ortho and para states which should be treated as distinct chemical species. This complicates the analysis of this reaction system (Oka and Epp, 2004; Flower, Pineau des Forêts, and Walmsley, 2006; Hugo, Asvany, and Schlemmer, 2009; Pagani, Roueff, and Lesaffre, 2011) but does not change the general principle: the zero-point-energy difference in this reaction drives the system to the right and this can lead to large deuterium fractionations.

FIG. 17 (color online). Gas-phase reactions involving H_3^+ that lead to deuterium fractionation of molecules (Watson, 1974). Cosmic rays ionize H_2 and the resulting H_2^+ reacts with H_2 to form protonated molecular hydrogen. Because of the difference in zero-point energy ($\simeq 180$ K), reactions with HD drive deuterium into H_2D^+. Proton (deuteron) transfer to HCO^+ (DCO^+) followed by dissociative recombination lead to atomic D and H. In highly depleted regions, D can be further concentrated in HD_2^+ or even D_3^+ (Roberts, Herbst, and Millar, 2003). From Taquet, Ceccarelli, and Kahane, 2012b.

and deuteron transfer channel to CO and other species is closed and instead H_2D^+ will react with HD to form HD_2^+ and even D_3^+ (see Fig. 17). As these species are then the dominant cations, the deuterium balance can be combined with the ionization balance,

$$\frac{X(H_2D^+)}{X(H_3^+)} = k_f X(HD)\left(\frac{n}{\zeta_{CR}k_e}\right)^{1/2}$$

$$= 7 \times 10^{-1}\left(\frac{n}{10^4 \text{ cm}^{-3}}\right)^{1/2}. \quad (15)$$

In fact, in this case, sequential reactions of the isotopologs of H_3^+ with HD can drive the deuteration of this species all the way to D_3^+ (Roberts, Herbst, and Millar, 2003). Actually, the gas-phase chemistry involving H_3^+ is slightly more complex since all different spin states [ortho, para (and meta)] of these species have to be taken into account (Hugo, Asvany, and Schlemmer, 2009), but the basic point remains that high densities, high depletions, and high deuterium fractionation of H_3^+ go hand in hand. Of course, there will be very few heavy species around to hand this enhanced fractionation to and the effects of this deuteration, and high gas-phase depletion, may best be studied through observations of H_3^+ and its isotopologs. Supported by extensive theoretical models (Walmsley, Flower, and Pineau des Forts, 2004; Pagani et al., 2009; Sipilä et al., 2010), the two isotopomers H_2D^+ and HD_2^+ have been observed and used to measure the characteristics of very dense molecular cloud cores (Caselli et al., 2003, 2008; Vastel, Phillips, and Yoshida, 2004; Roberts and Millar, 2007; Parise et al., 2011).

Finally, it should be noted that, given the important role of H_3^+ in interstellar ion-molecule chemistry, reaction (10) dominates deuterium fractionation at low temperatures. However, as the temperature increases, this reaction "shuts" off and other reactions take over; notably,

$$CH_3^+ + HD \leftrightarrow CH_2D^+ + H_2 + \Delta E \quad (16)$$

and

$$C_2H_2^+ + HD \leftrightarrow C_2HD^+ + H_2 + \Delta E \quad (17)$$

with exothermicities of 370 and 550 K, respectively (Roberts and Millar, 2000)

E. The chemistry of carbon isotopes

In diffuse clouds, CO photodissociation is a key process affecting the carbon-isotope distribution. CO photodissociation occurs through line absorption into predissociative excited states. As a result, the CO photodissociation rate is affected by self-shielding. For CO column densities of $\sim 10^{15}$ cm^{-2} these lines become saturated and the photodissociation rate decreases rapidly (van Dishoeck and Black, 1988). This is an isotope selective effect that will lead to fractionation (Bally and Langer, 1982). Hence, the abundance of ^{13}CO (and other isotopologs) will be decreased in the surface layer of a cloud relative to that of ^{12}CO. A CO column density of $\sim 10^{15}$ cm^{-2} corresponds typically to a H column density of 3×10^{20} cm^{-2} (Sheffer et al., 2008). For the diffuse cloud toward ζ Oph, the difference in the photodissociation rate is calculated to amount to a factor of 3 to 6 (Visser, van Dishoeck, and Black, 2009). The precise value depends on the excitation temperatures of H_2 and CO, the Doppler broadening of the lines, and the dust properties. The "excess" of ^{12}CO is also passed on to daughter products such as HCO^+. The photodissociation of CO will preferentially produce ^{13}C (and ^{17}O and ^{18}O) for depth in excess of this column density of $\sim 10^{15}$ cm^{-2} and this fractionation can be passed on to C daughter products, including, for example, acetylenic products formed through C-insertion reactions (Secs. IV.B and IV.F). However, mostly C will be ionized by penetrating UV photons and C^+ is the main (e.g., unfractionated) carbon reservoir.

As for hydrogen, isotope exchange reactions can fractionate carbon-bearing species because of the zero-point energy difference. The main reaction of interest is

$$^{13}C^+ + {}^{12}CO \leftrightarrow {}^{12}C^+ + {}^{13}CO + \Delta E. \quad (18)$$

Because the zero-point energy difference is much smaller (35 K) than for hydrogen-bearing species, fractionation effects will be much more modest. When C^+ is the main carbon reservoir, this process by itself will lead to a fractionation $R(CO)$ of ^{13}CO relative to ^{12}CO, given by

$$R(CO) = K(T). \quad (19)$$

The equilibrium constant $K(T)$ is approximately given by $\exp[\Delta E/kT]$, which for a typical temperature of a diffuse cloud (50 K) amounts to $R \simeq 2$. This will counteract the effect of photofractionation described above.

In dense clouds, CO is the main carbon reservoir and C^+ is generated through reactions of cosmic-ray produced He$^+$

with $CO(\rightarrow C^+ + O)$ which breaks out both isotopes equally facile. If CO is the main reaction partner for C^+, reaction (18) will preferentially deplete $^{13}C^+$ and a fractionation factor $R(C^+)$ given by

$$R(C^+) = K(T), \tag{20}$$

which is about 30 at 10 K. Thus, $^{13}C^+$ is rapidly sequestered back into CO, the species derived from C^+ will be isotopically light, and carbon-isotope fractionation can be much more important inside dense clouds. As the resulting C^+/CO ratio is $<10^{-3}$, the isotope ratio of CO is not affected. Species derived from CO can be fractionated in a similar fashion through ion-molecule reactions; viz.,

$$^{13}CO + H^{12}CO^+ \leftrightarrow {}^{12}CO + H^{13}CO^+ + \Delta E, \tag{21}$$

but ΔE is only 8 K and this amounts to a factor of 2 fractionation. Note that this reaction can also fractionate in diffuse clouds but there the effect is at the 10%–20% level as $T \simeq$ 50 K. Grain-surface products from CO (e.g., H_2CO, CH_3OH, CO_2; see Sec. V.B.1) will not be fractionated (Wirström et al., 2011). Cosmic rays also produce UV photons (through excitation and/or fluorescence of the Lyman-Werner bands of H_2) and these can photodissociate CO into C and O. The isotopic effects of this depend on the details of the line overlap of the CO isotopes with the H_2 lines as well as with the main CO isotope (through the shielding factor) and this has not yet been calculated but one might expect a factor of a few. As neutral carbon does not flow directly back to CO, carbon-bearing species deriving from C may show a different behavior than those deriving from C^+. Given that C is very unreactive in dark clouds, it may be mainly destroyed through reactions on grain surfaces forming, for example, methane or ethanol. We note that He^+ is some 50 times more important than cosmic-ray photons in the destruction of CO (Liszt and Ziurys, 2012). Observationally, species such as CN, HCN, and CS do not show fractionation in dense clouds relative to CO (Milam et al., 2005; Liszt and Ziurys, 2012). Perhaps they are formed early on when C^+ is the main (and unfractionated) reservoir or C rather than C^+ is involved in their formation (and cosmic-ray-induced photons do not fractionate). It remains puzzling though that the effects of reaction (18) are not obvious and possibly this suggests the importance of other loss routes for C^+ in dense clouds such as mutual neutralization with PAH anions that can be important if PAHs are the dominant negative charge carriers and CO is mildly depleted (Sec. IV.G).

Finally, we consider scrambling of the C isotopes within carbon-chain molecules. In contrast to CN, CS, and HCN, observations revealed that CCH is isotopically light but that the abundance ratio of $C^{13}CH/^{13}CCH$ is larger than unity ($\simeq 1.6$) (Sakia et al., 2010). Here the reaction

$$H + {}^{13}CCH \leftrightarrow H + C^{13}CH + \Delta E, \tag{22}$$
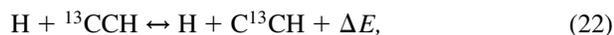
where ΔE is 8 K, may play a key role (Furuya et al., 2011). Similar fractionation of C_2S has been observed (Sakai et al., 2007) but is not as readily explained as atomic S is not an abundant reaction partner (Furuya et al., 2011).

F. Acetylene derivatives

The abundance of complex hydrocarbons and cyanopolyynes is directly linked to the C, not locked up in CO. In a dense core, the abundance of atomic C is regulated by cosmic-ray ionization which produces primary and secondary energetic electrons that can electronically excite H_2. Radiative decay in the Lyman-Werner bands produces then a weak, internal far-UV radiation field at a level of $\simeq 5 \times 10^{-5}$ of the average interstellar radiation field, or some 5×10^3 far-UV photons $cm^{-2} s^{-1}$ (Prasad and Tarafdar, 1983; Gredel et al., 1989). These photons can dissociate CO, forming atomic C. The resulting C/CO ratio is then approximately 6×10^{-3}, independent of density. Cosmic rays can also ionize helium and He^+ can break C^+ out of CO but this process is much less efficient. Given the low C and C^+ abundance, calculated abundances of acetylenic derivatives are low.

Somewhat higher abundances of carbon-chain molecules are obtained in model studies that start with all atomic initial conditions. During the initial phase, when CO is being built up from C^+, the high abundance of small hydrocarbon radicals can lead to abundances of carbon-chain molecules 4 orders of magnitude higher at early times ($\sim 10^5$ yr) than at late times and in reasonable agreement with observations (Table II) (Leung, Herbst, and Huebner, 1984).

High abundances of hydrocarbons are also obtained in models which have gas-phase C/O abundances exceeding 1. All the oxygen is then locked up in CO and the "free" carbon can be used to drive hydrocarbon formation.

G. Molecular anions

The first theoretical discussions on anion chemistry in the interstellar medium date back to the 1960s and 1970s (McDowell, 1961; Dalgarno and McCray, 1973) and the role of the H^- anion in the formation of H_2 in the early Universe has long been appreciated (Peebles and Dicke, 1968). Yet, detection of the first anionic molecular species had to await the early 21st century when sensitive laboratory spectroscopy studies pinned down their rotational spectra and allowed astronomical searches (McCarthy et al., 2006). At this point in time, six carbon-chain anions have been detected in space (Table I). Observed abundance ratios between the anion and its parent species can be as high as 0.1 for the largest species (Table II). Recent reviews provide entries to relevant laboratory and theoretical astrochemistry studies (Herbst, 2009; Bierbaum, 2011).

Molecular anions are formed through radiative attachment reactions,

$$A + e^- \leftrightarrow (A^-)^* \rightarrow A^-, \tag{23}$$

where $(A^-)^*$ is an excited molecular anion which can autoionize or radiatively stabilize. The rate coefficient for electron attachment k_{ea} is then given by (Herbst, 1981; Tielens, 2005)

$$k_{ea} = \left(\frac{k_r}{k_r + k_b}\right) k_f, \tag{24}$$

where k_f, k_b, and k_r are the forward (association), backward (autoionization), and radiative stabilization reaction rate coefficient. Evaluation of the latter requires knowledge of the vibrational transitions and their lifetimes as well as of the excitation of the species. The former can follow from quantum chemical calculations while the latter can be evaluated

with the ergodic assumption for (large) species. The capture and autoionization rate coefficients are related through the principle of detailed balance,

$$\frac{k_b}{k_f} = \frac{\rho^o}{\rho^-}, \tag{25}$$

with ρ^- and ρ^o the density of states of the anion and that of the neutral plus electron, respectively. Assuming that the neutral is in its vibrational ground state after loss of the electron, its density of states is that of the free electron,

$$\rho^o = \rho(e) = \frac{m^2 v}{\pi^2 \hbar^3}. \tag{26}$$

The density of states for the anion at the internal energy corresponding to the electron affinity of the neutral can be estimated from quantum chemically calculated vibrational frequencies. Radiative attachment is thus promoted by large electron affinities and/or by a large number of modes. For the open shell, carbon-chain radicals, electron affinities are typically 3–4 eV. When the backward reaction is slow compared to radiative stabilization, the radiative attachment rate coefficient is given by the forward rate, which (for a large species) is often assumed to be given by the Langevin rate,

$$k_f = 2\pi \left(\frac{\alpha e^2}{m_e} \right)^{1/2}, \tag{27}$$

with α the polarizability of the neutral. However, that approximation ignores the discrete character of the orbital momentum, which can enhance the electron attachment rate by a factor of 2 to 4 (Turulski and Niedzielskil, 1994; Petrie and Herbst, 1997). For the larger hydrocarbon chains considered here, reaction rate coefficients a few times 10^{-7} cm^3 s^{-1} at 10 K are indicated and provide reasonable agreement with the observed ratios of the abundances of the anion and its parent (Herbst, 2009).

The presence of carbon-chain anions promotes growth of larger chains through, for example, associative electron detachment reactions with carbon and hydrogen atoms. For small carbon-chain anions, carbon is lost in the reaction with oxygen and nitrogen to CO and CN$^-$. For larger chains, associative detachment is also observed (Eichelberger et al., 2007). Overall, the effect of carbon-chain anions in models is quite modest.

PAH anions have a much more pronounced effect in models of interstellar chemistry. The electron affinity of PAHs is a function of size scaling approximately with $N_c^{1/2}$ (Leach, 1987; Tielens, 2005). For astrophysically relevant PAHs (e.g., with $N_c \sim 50$), radiative stabilization should dominate over autoionization and the rate is then approximately the Langevin rate. In that case, PAH anions are the dominant negative charge carriers in dense ($n > 10^4$ cm^{-3}) cloud cores (Lepp and Dalgarno, 1988; Tielens, 2005; Wakelam and Herbst, 2008). The degree of ionization is then set by the balance of cosmic-ray ionization with mutual neutralization reactions of cations and PAH anions. As the latter are much faster than the other available recombination channel for metal cations (radiative recombination), this has the effect of greatly suppressing the degree of ionization (Tielens, 2005). In fact, the presence of PAH anions resolves one of the outstanding issues of astrochemical modeling; e.g.,

models with metal abundances typical for diffuse clouds but without PAHs predict too high degree of ionization and hence such pre-PAH models had to assume that metals were highly depleted while models with PAHs fare much better in the comparison to observations (Lepp and Dalgarno, 1988; Wakelam and Herbst, 2008).

H. The cosmic-ray ionization rate

Cosmic-ray ionization is the cornerstone of gas-phase chemistry routes. Conversely, molecular observations can be used to determine the cosmic-ray ionization rate. Diffuse molecular clouds are often used for this purpose because of their simple chemistry. A number of ways have been devised, resulting in similar results, within the (large) uncertainties. In each case, the formation rate of a species is related back to the cosmic-ray ionization of H or H$_2$. Using estimated destruction rates of the molecule under consideration, the observed abundances result then in a estimate of the cosmic-ray ionization rate ζ_{CR}. I focus here on the well-studied diffuse cloud toward ζ Per. A detailed analysis for the cosmic-ray ionization rate in this sight line is provided by Le Petit, Roueff, and Herbst (2004).

Chemically, the simplest determination is through the observations of H$_3^+$ (McCall et al., 2003). Referring back to Fig. 17, the primary cosmic-ray ionization rate is given by

$$\zeta_{CR} = \frac{k_e n(e) n(H_3^+)}{2.3 n(H_2)} = 7 \times 10^{-8} \frac{N(C^+) N(H_3^+)}{N(H_2)} \frac{1}{L}$$
$$= 3.5 \times 10^{-16} \text{ s}^{-1}, \tag{28}$$

where the numerical factor (2.3) takes secondary ionization into account and L is the path length through the cloud. The right-hand side of this equation assumes that the electrons come from C$^+$ and that the cloud is uniform (e.g., H$_2$ is coexistent), adopts an electron recombination coefficient of $k_e = 10^{-6} T^{-0.45}$ and column densities of H$_2$ (5×10^{20} cm^{-2}) (Savage et al., 1977) and C$^+$ (1.8×10^{17} cm^{-2}) (Cardelli et al., 1996) have been taken from observations. Various tracers indicate that this cloud is quite dense, 200–400 cm^{-3}, for a diffuse cloud. Adopting a density of 250 cm^{-3}, the total hydrogen column of 1.6×10^{21} cm^{-2} implies a scale size of $L = 2$ pc.

For OH, we make the assumption that every ionization of H is passed on to O and eventually forms OH which is then photodestroyed (see Fig. 15). The primary cosmic-ray ionization rate ζ_{CR} per H nucleus is then

$$\zeta_{CR} = 0.67 k_{UV}(OH) \frac{N(OH)}{N(H)} \simeq 6 \times 10^{-17} \text{ s}^{-1}, \tag{29}$$

where the numerical factor takes secondary ionizations into account. The unshielded photodissociation rate of OH is $7.6 \times 10^{-10} G_o$ s^{-1} and G_o is estimated to be $\simeq 6$ from observations. The total FUV dust optical depth of these clouds is $\simeq 2$ and hence dust shielding reduces this rate by a factor of $\simeq 3$. The derived cosmic-ray ionization rate adopts this value and the observed column densities of OH (4×10^{13} cm^{-2}) (Felenbok and Roueff, 1996) and H (6.5×10^{20} cm^{-2}) (Savage et al., 1977). As the charge exchange reaction with ground state O is quite slow (Stancil et al., 1999), some of the

H^+ may be lost through neutralization reactions with PAHs and the derived cosmic-ray ionization rate is really a lower limit.

Recent observations of OH^+ with HIFI/Herschel (Sec. IV.I.3) have provided a new handle on the cosmic-ray ionization rate (Gerin *et al.*, 2010a; Neufeld *et al.*, 2010b). As for OH, we make the assumption that every ionization of H is passed on to O and eventually forms OH^+ but this species is destroyed by dissociative electron recombination (see Fig. 15). We then have

$$\zeta_{CR} = 0.67 \frac{n(OH^+)n(e^-)k_e}{n(H)}$$
$$\simeq 6 \times 10^{-16} \left(\frac{100 \text{ K}}{T}\right)^{1/2} \frac{N(OH^+)}{3 \times 10^{14} \text{ cm}^{-2}} \frac{1}{L}, \quad (30)$$

where the factor 0.67 takes secondary ionizations into account, L is the path length in parsec, standard reaction rate coefficients have been adopted, and the electron fraction is assumed to be 3×10^{-4} (Sec. IV.I.3). These observations toward the molecular ring probably probe the atomic surfaces of molecular clouds with typical densities of 1000 cm^{-3} and L is then $\simeq 10$ pc. The observed integrated column density of 3×10^{14} cm^{-2} requires a cosmic-ray ionization rate of 6×10^{-17} s^{-1}.

The chemistry of HD is more involved (see Fig. 15). It also starts with H^+ and assuming that its abundance is set by cosmic-ray ionization and charge exchange with O, we have

$$\zeta_{CR} = \frac{n(HD)n(O)k_O k_{UV}(HD)}{n(H)n(D)k_D}$$
$$= 2.3 \times 10^{-16} G_o \exp[-\tau_{ext}] \frac{N(HD)}{N(H)}$$
$$\simeq 5 \times 10^{-16} \text{ s}^{-1}, \quad (31)$$

where we have adopted an O abundance of 3×10^{-4}, the observed HD (3.8×10^{15} cm^{-2}) (Snow, Jr., 1977) and H (6.5×10^{20} cm^{-2}) (Savage *et al.*, 1977) column densities, an unshielded HD photodissociation rate of $2.6 \times 10^{-11} G_o$ s^{-1}, $G_o = 6$, a reduction due to UV extinction by a factor of 3, and a deuterium elemental abundance of 1.5×10^{-5}.

H_3^+ provides the most direct observation of the cosmic-ray ionization rate. The cosmic-ray ionization rates derived from the H_3^+ and HD observations are (perhaps, fortuitously) in good agreement but the OH and OH^+ values are about a factor of 10 lower. Possibly this is because only a fraction of the H ionizations flow to OH and most H^+ neutralizes, for example, with PAH anions (Hollenbach *et al.*, 2012).

I. HIFI and hydride radical chemistry

The HIFI instrument on the Herschel Space Observatory has opened up the THz window for systematic surveys of light hydrides. As these species represent the first steps in the chemistry of space, this has provided new insight and tests of our chemical understanding of the interstellar medium. The Herschel key program PRISMAS has been designed to exploit this new opportunity through absorption studies

involving the ground state of these species toward bright background sources (Gerin *et al.*, 2012).

1. Tracing H_2 with small hydrides

It is well understood that CO is not a good tracer of H_2 in diffuse and translucent clouds as CO needs an appreciably larger column density of gas to be shielded against dissociating UV photons than H_2 (Sheffer *et al.*, 2008). This is particularly true for a low metallicity environment such as dwarf galaxies where the mass of CO-dark gas can be a dominant component of the ISM (Madden *et al.*, 1997). More recently, the Fermi gamma ray space telescope also unveiled extensive clouds of CO-dark gas in the solar neighborhood (Grenier, Casandjian, and Terrier, 2005). As H_2 is difficult to trace directly, other tracers than CO are imperative to get a good handle on the inventory of the ISM of galaxies.

It has long been known from optical ground-based studies that the CH column density correlates well with that of H_2 (Federman, 1982; Sheffer *et al.*, 2008) and indeed the CH column density has often been used as a proxy for the H_2 column density. HIFI extended these observations from nearby stars to absorption line studies along sight lines throughout the galaxy (Gerin *et al.*, 2010b). Referring back to Fig. 15, every reaction of C^+ with H_2 will eventually lead to CH and the CH abundance is given by

$$X(CH) \simeq \frac{k_{ra}}{k_{UV}(CH)} n(C^+) \simeq 3 \times 10^{-10} \frac{n_o}{G_o}, \quad (32)$$

with k_{ra} the radiative association rate (4×10^{-16} cm^3 s^{-1}) and k_{UV} the photodestruction rate of CH ($\simeq 1.6 \times 10^{-9}$ s^{-1}) and an abundance of 1.5×10^{-4} has been adopted for C^+. In the solar neighborhood, $n_o/G_o \simeq 100$ cm^{-3} and the predicted CH abundance is in good agreement with the observed one (Table II). In a pressure driven ISM, n_o/G_o is approximately constant and the CH column density will indeed track the H_2 column density reasonably well, although variations of a factor of 3 are observed.

Fluorine atoms react exothermally with molecular hydrogen. As HF is only slowly destroyed through reactions with C^+, H_3^+, and He^+, HF is predicted to be the dominant reservoir of fluorine in the diffuse and dense interstellar medium (Neufeld and Wolfire, 2009). HIFI observed the ground state HF line at 1232 GHz in absorption toward bright background sources. Analysis of the data reveals that HF is indeed the main F reservoir in the diffuse gas along these sight lines (Neufeld *et al.*, 2010a; Sonnentrucker *et al.*, 2010). Hence, observations of HF may be used as a proxy for H_2.

2. Nitrogen hydrides

HIFI/Herschel provide, for the first time, access to all three nitrogen hydrides, NH, NH_2, and NH_3 (Hily-Blant *et al.*, 2010; Persson *et al.*, 2010). These studies show that the NH/NH_2 ratio is unexpectedly high, $\simeq 5$. In diffuse clouds, the NH/NH_3 is also high, $\simeq 1$, while in dark cloud cores and protostellar envelopes this ratio has shifted toward NH_3 ($\simeq 3 \times 10^{-3}$). Models based upon the scheme outlined in Fig. 16 predict an NH/NH_2 abundance ratio typically less than 1 for dense clouds. Much better agreement is obtained

if it is assumed that dissociative electron recombination of N_2H^+ breaks the N_2 bond 10% of the time (Dislaire *et al.*, 2012).

3. Oxygen-bearing hydrides

HIFI/Herschel have measured the three oxygen-bearing hydrides involved in the formation of OH and H_2O in the gas, OH^+, H_2O^+, and H_3O^+, with a typical abundance ratio of 6:1.5:1 (Gerin *et al.*, 2010a; Neufeld *et al.*, 2010b). The abundances of these species are simply related through H-abstraction reactions with H_2 and dissociative electron recombination. Specifically, we can write

$$\frac{n(OH^+)}{n(H_2O^+)} = 0.64 + 7.3 \times 10^3 \left(\frac{100 \text{ K}}{T}\right)^{1/2} \frac{X(e^-)}{X(H_2)}, \quad (33)$$

where standard reaction rate coefficients have been used and a typical diffuse cloud temperature of 100 K is assumed. The first term on the right-hand side represents reactions with H_2, while the second term is due to electron recombination. It is clear that high OH^+ to the H_2O^+ ratio occurs only if recombination is much faster than reactions with H_2. The electron abundance is somewhat uncertain as, besides photoionization of C, also cosmic-ray ionization of H can be important, but a typical value is $X(e^-) \simeq 3 \times 10^{-4}$. The conclusion is therefore inescapable: these simple oxygen-bearing hydrides reside in gas with a very low H_2 fraction: $X(H_2) \lesssim 7 \times 10^{-2}$ (Gerin *et al.*, 2010a; Neufeld *et al.*, 2010b). So, surprisingly, these ions seem to be related to largely atomic rather than molecular gas. For comparison, toward local stars, UV absorption line studies reveal such low molecular hydrogen fraction only for low column densities ($N_H < 5 \times 10^{20}$ cm^{-2}) of hydrogen nuclei (Savage *et al.*, 1977).

4. CH^+ and turbulent dissipation regions

CH^+ was one of the first molecules discovered in the ISM. Yet understanding its chemical origin has long remained enigmatic. For diffuse clouds, direct pathways to CH^+ are closed by the high energy barrier involved (see Fig. 15). As the abundance of CH is well matched by models (Sec. IV.I.1), the basic carbon chemistry seems understood and the presence of warm gas is indicated. First models relied on heating by shock waves to produce the high temperatures required (Elitzur and Watson, 1978), but such models have largely been discounted as there are no obvious velocity shifts with respect to other molecular lines and the CH^+ column density shows a rough correlation with the total H column (Gredel, van Dishoeck, and Black, 1993).

It is now thought that CH^+ traces turbulent dissipation regions as viscous dissipation of turbulence is not uniform in time but rather occurs in bursts. As regions of large velocity shear [rather than (compressible) shocks] dissipate the suprathermal energy stored in supersonic turbulence, chemistry in the resulting warm gas can drive the formation of CH^+, as well as other species (Joulain *et al.*, 1998; Godard, Falgarone, and Pineau Des Forêts, 2009; Pan and Padoan, 2009). Models for turbulent dissipation regions are in good agreement with the observations of CH^+ (Godard, Falgarone, and Pineau Des Forêts, 2009) with $n \sim 50$ cm^{-3}, sizes of $\sim 10^2$ AU and strain rates of $\sim 10^{-11}$ s^{-1}. The number of active regions along the sight line (per unit parsec) is set by the average energy transfer rate in the cascade (obtained from observations), the average turbulent heating rate, and the size of the active vortices. Turbulent dissipation regions may also be the source of rotational excited H_2 in the diffuse ISM. So, chemistry provides a memory of the warm dissipation phase which persists for some 2000 years and, in order to explain the observations, these (remnants of the) turbulent dissipation regions fill a few percent of the sight lines in the diffuse ISM.

Intermittent turbulence may have a wider influence than the diffuse regions probed by CH^+ observations. In particular, turbulent heating may also provide an important energy source for the molecular gas in high-mass star-forming cores far from the central star (where much of the mass resides). Since temperature controls the Jeans mass, turbulence influences the star formation process. As turbulence and turbulent dissipation are key aspects of many regions of the interstellar medium, molecular chemistry may provide convenient tools to understand their role in star formation and the evolution of the ISM (Mac Low and Klessen, 2004; Pan and Padoan, 2009).

J. Gas-phase chemistry models

Detailed models have been devised to calculate the gas-phase composition of molecular clouds. Such models generally lean heavily on data bases of astrophysically relevant reactions—some 5000 reactions between some 450 species. There are three such data bases: UDfA at http://www.udfa.net/ maintained by Tom Millar and co-workers, OSU at http://www.physics.ohio-state.edu/~eric/research.html maintained by Eric Herbst and co-workers, and KIDA at http://kida.obs.u-bordeaux1.fr/ maintained by Valentine Wakelam and co-workers. With qualifications, gas-phase models of interstellar clouds have been very successful. Among the key successes are explanations for the high abundance of CO, the presence of ions such as H_3^+ and HCO^+, the presence of radicals such as OH and CH, the presence of isomers such as HNC/HCN, the rich array of acetylenic derivatives present, including the cyano-polyynes, and the high observed deuteration levels in species such as DCO^+. Qualitatively, the agreement between gas-phase models and the observations is impressive. Quantitatively, however, the agreement is wanting: they reach an order of magnitude agreement with observed abundances for some 80% of the species.

To some extent, this limited agreement reflects our imperfect chemical knowledge: less than 20% of the reactions included in these data bases have actually been studied in the laboratory. The remainder are educated guesses. It is not even known whether all the important chemical routes are included and whether perhaps some routes have been included that are inhibited at low temperature. In order to make progress in this area, the field should, over the coming decade, focus its attention on this aspect by supporting, coordinated programs between astrochemical modelers and chemists likely at the international level; such a program is led by Wakelam *et al.* (2010). Specifically, this program entails a characterization of the uncertainty in the reactions, propagation of these uncertainties through the models,

followed by a sensitivity analysis that can identify key but very uncertain reactions. These can then be studied in detail in the laboratory.

In addition to the uncertainties in reaction routes and the relevant rates, this "agreement" is somewhat misleading because often observations (of particularly the complex hydrocarbons) are compared to models which relate to an early time ($\sim 10^5$ yr) in a time-dependent calculation (Hasegawa, Herbst, and Leung, 1992). Gas-phase models really have difficulty explaining observations of complex hydrocarbons at late time because almost all the carbon tends to be locked up in the unreactive CO. At early times, this problem is "circumvented" because these models start with all the carbon initially available as C^+. Once some H_2 is formed, hydrocarbon radical chemistry really takes off but in less than 10^6 yr all of these hydrocarbons are converted into CO (Sec. IV.B). There are alternative solutions to the issue of the complex hydrocarbon abundances. One class of models has C/O elemental abundance ratios that are larger than 1. In that case, the formation of CO does not consume all of the C and hydrocarbon chemistry will be very efficient. Such a large C/O ratio is sometimes attributed to the formation of ice mantles, but there is little observational support for a preferential depletion of oxygen compared to carbon (Table III). Other models invoke the effects of shocks or turbulence to drive the chemistry away from CO toward hydrocarbons. Of these models, the early time chemistry models may be the most relevant, as the observations of carbon-chain-rich cores seem to indicate a relatively young age (Maezawa *et al.*, 1999). This explicitly introduces the cloud's history in the chemical analysis. On the one hand, this poses a challenge for the models. On the other hand, this provides an opportunity to study global aspects in the evolution of the ISM. Finally, grain-surface chemistry is only now becoming amenable to systematic laboratory studies (cf., Sec. V) but it has long been surmised that grains are an efficient way to "activate" the C in CO (Sec. V.B).

As the relative importance of these different scenarios for breaking the carbon out of CO is unclear, good agreement between models and observations cannot be expected. Nevertheless, I would summarize the situation in which, qualitatively, we do understand gas-phase chemistry and the ion-molecule and neutral-neutral reaction networks outlined in the previous sections are key. With HIFI, we have the tool to probe the initial steps in detail. It can be expected that understanding the quantitative aspects of astrochemistry may bring new insights in the physics and evolution of molecular clouds and the ISM.

In this assessment, it should also be understood that the goal of chemical models is not to reproduce the observations. The system is too complex, there are too many interacting variables, there are too many poorly known reaction rates, and the physical reality of sources is much more complex than we will ever care to model. Rather the goal of chemical models is to identify key chemical species, understand the chemical processes that play a role in their formation and destruction, predict trends for abundances, establish diagnostic diagrams to aid astronomers, and understand what molecules are telling us about the origin and evolution of the Universe, particularly of course in regions of star and planet formation. Within this mind set, astrochemical models are performing excellently.

V. GRAIN-SURFACE CHEMISTRY

In this section, I briefly review grain-surface chemistry with a focus on the formation of interstellar ices inside dense molecular clouds and the formation of H_2 on bare silicate and graphite grains. Mobility is the key aspect of grain-surface chemistry as it sets the reaction networks. A short discussion on mobility is followed by summaries of the initial steps in the chemical networks including hydrogenation of CO, H_2O formation, CO_2 formation, as well as deuterium fractionation and the formation of complex organic molecules. Because grain-surface chemistry is in the diffusion limit—reactions are limited by the rate at which coreactants can be brought to the surface—models need to take special care and various techniques for this are discussed at some length. The section is concluded with a discussion on H_2 formation and a summary of the results for the composition of interstellar ices and the contribution of grain-surface chemistry to the gas-phase composition.

A. Mobility

Interstellar grains provide a surface on which accreted species can meet and react and to which they can donate excess reaction energy (Tielens, 2005). Grain-surface chemistry is thus governed by the accretion rate, which sets the overall time scale for the process, and the surface migration rate, which governs the reaction network. For typical interstellar cloud conditions ($n = 10^4$ cm^{-3}, $T = 10$ K), the flux of reactive species of 10^5 species/(cm^2/s) on a single grain corresponds to one H atom accreting every couple of months (for a 50 Å grain) to one H atom every day (for a 1000 Å grain). Generally, reactive species have to wait for a (mobile) coreactant to arrive. Thus, surface chemistry on interstellar grains occurs in the diffusion limit where transport of material to the surface controls the chemistry (Tielens and Hagen, 1982). In contrast, in the laboratory, surface chemistry is studied at much higher fluxes as an ultrahigh vacuum background pressure of $P \sim 10^{-13}$ bar still corresponds to a flux of 10^{11} species/cm^2/s. Moreover, experiments are generally conducted on bulk samples and hence large surface concentrations of reactants build up and chemistry occurs in the reaction limit where surface "collisions" among accreted species is the limiting factor.

Surface migration is set by the potential energy surface of the species on the grain and, for ice surfaces, binding will occur in physisorbed sites with typical binding energies E_b of 400 to 4000 K. In general, estimates for the barrier against migration range from 0.1 to $0.5E_b$, depending on surface and adsorbate involved (Seebauer and Allen, 1995). For physisorption, migration barriers are often assumed to be one-third of the binding energy. Higher barriers may occur when an adsorbate is bonded near a kink or step in the surface. In principle, reactions can occur either through surface migration (Langmuir-Hinshelwood mechanism) or through direct reaction with an incoming gaseous species (Eley-Rideal mechanism) but generally only the former is considered in models. We note that, in laboratory studies, atoms come in with

excess kinetic energy and during the initial accommodation process such a hot atom may diffuse some 30–50 Å (Al-Halabi and van Dishoeck, 2007). For moderately high surface coverages ($\sim 10^{-3}$), this hot atom process may facilitate reaction. However, in the ISM, the limited excess energy of incoming species will have no influence. Hot species processes may play a role, though, as reaction products may have considerable excess energy. Translationally hot species migration followed by reaction will then compete with other mechanisms that dissipate the excess energy and this is an area that has not been studied much. Limiting ourselves to the Langmuir-Hinshelwood mechanism, at 10 K, species can in essence then be divided in "migrators" and trapped species depending on whether the surface migration time scale is much faster than the accretion time scale of coreactants or not. The former species can quickly scan a grain surface for a coreactant; the latter has to await the arrival of coreactants.

A number of experimental studies have been performed related to the mobility and recombination of hydrogen atoms to form H_2 on ice surfaces (Hornekaer et al., 2003, 2005; Perets et al., 2005; Matar et al., 2008; Dulieu et al., 2010). While these studies have not always been interpreted in the same way, the consensus emerging from them is that surface mobility is much affected by the structure and surface morphology of the ice. Specifically, H_2O deposited at 10 K forms high density amorphous solid water with a very porous open structure and a distribution of binding sites for H_2 ($E_b \simeq$ 500–700 K). Upon warmup to temperatures above 60 K, this ice is annealed to low density amorphous solid water with low porosity and somewhat lower binding energy for H_2 ($E_b \simeq$ 400–600 K) (Amiaud et al., 2006; Matar et al., 2008). The binding energy of atomic H is generally not measured directly but from polarizability arguments one might expect that it is $\simeq 15\%$ lower than for H_2. Detailed theoretical calculations yield a binding energy of 500–800 K on porous amorphous solid water for H (Al-Halabi and van Dishoeck, 2007). On both types of ice surfaces, the H_2-recombination experiments and even more the reactions with O_2 and CO provide direct evidence that atomic H is highly mobile and migrates readily even at 8 K with a barrier against migration on porous amorphous solid water estimated to be only 240 K (Matar et al., 2008). Much of the molecular hydrogen formed on porous amorphous solid water is, however, retained in the pores and, in thermal programmed desorption (TPD) experiments, not released until warmup in a random-walk process of sublimation and condensation in the pores. Because of the high porosity, H atoms can "penetrate" several monolayers into the ice and the density of surface sites is several times (5–10) larger than the nominal 2×10^{15} sites/cm^2.

There are few experiments specifically on the mobility of other important reactants on interstellar ice analogs. The polarizability of atomic oxygen is very similar to that of atomic H. However, the binding energy of atomic oxygen to hexagonal ice has been calculated to be much higher, 1320 K (Murray, 2003). Molecular thermoluminescence experiments involving oxygen in noble gas matrices (Fournier et al., 1979) provide some insight in binding and mobility of atomic oxygen on interstellar ices (Tielens and Hagen, 1982). These data suggest that, in these matrices, atomic O behaves similar to atomic H (see Fig. 18). These data are, however,
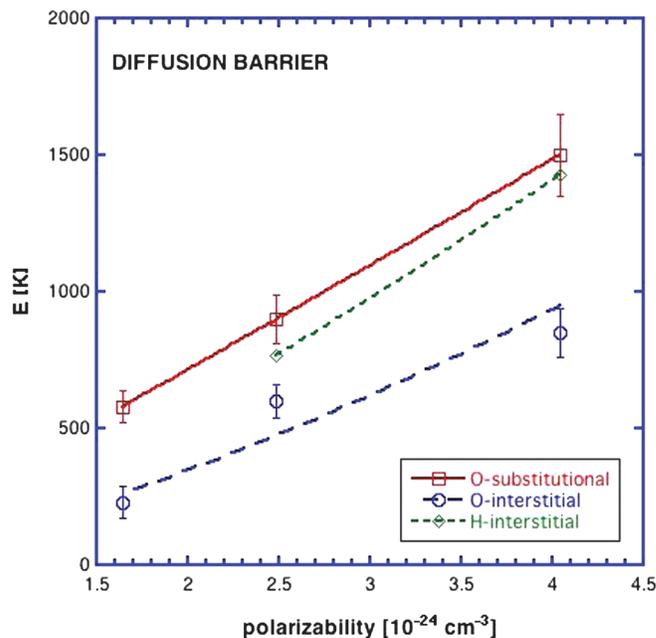

FIG. 18 (color). Barriers against migration for oxygen and hydrogen atoms trapped in noble gas matrices as a function of the polarizability of the matrix. Migration barriers have been estimated from molecular thermoluminescence, laser induced fluorescence, or electron paramagnetic resonance (Danilychev and Apkarian, 1993; Schrimpf et al., 1996; Vaskonen et al., 1999; Gumenchuk, 2007).

notoriously difficult to interpret. Specifically, the data reveal that atomic oxygen recombination occurs as a first order reaction despite the fact that often these O atoms have to diffuse some 300 Å. It has been suggested that this enhanced mobility reflects the (thermal) excitation of atomic oxygen from the triplet to the singlet state and O(^1D) is expected to be much more mobile in view of its smaller interaction radii (Danilychev and Apkarian, 1993; Apkarian and Schwentner, 1999). Alternatively, the mobility of oxygen trapped in interstitial or substitutional sites may be triggered by local phonon excitation, releasing the atom, which then may "ride" this phonon wave "ballistically" until a coreactant is encountered. Experimental studies on surface chemistry show that atomic oxygen can diffuse (and react) at 10 K on ice surfaces (Roser et al., 2001; Raut and Baragiola, 2011) but migration barriers have not been determined—they seem to be low, though—and it is therefore difficult to extrapolate these results to astrophysically relevant conditions (e.g., time scales and fluxes). Besides these uncertainties associated with the binding energy and migration barrier, it is also unknown whether atomic oxygen (like atomic H) can penetrate deeply into the porous structure of amorphous solid water.

B. Grain-surface chemical routes

1. Hydrogenation of CO

Grain-surface chemistry involves predominantly hydrogenation and oxidation reactions and leads to the formation of simple species; e.g., H_2O, CO, CO_2, CH_3OH, H_2CO, CH_4, and NH_3. Focusing on hydrogenation, atomic hydrogen is mobile, has an appreciable residence time, and because it is

so light can tunnel through appreciable activation barriers (Tielens and Hagen, 1982). Hence, H will "collide" often with coreactants on a grain surface and is very reactive. Of particular interest are reactions of H with CO to form H_2CO and, further, to CH_3OH (see Fig. 19). The importance of hydrogenation of CO was realized early on (Tielens and Hagen, 1982) based largely upon the low energy barrier for the gas-phase three body reaction ($E_a \simeq 1000$ K) and supported by thermoluminescence studies on cryogenic matrices where this reaction readily occurs (van IJzendoorn et al., 1983). Over the past 10 years, these theoretical ideas have been extensively investigated in the laboratory and the viability of this activation route of CO is now well established (Hiraoka et al., 1998; Hidaka et al., 2004, 2009; Ioppolo et al., 2008; Fuchs et al., 2009). Thus, while initial studies only observed efficient H_2CO formation, later studies (Hidaka et al., 2004; Fuchs et al., 2009) demonstrated that this reflected the H flux in these particular experiments and that actually under interstellar conditions full hydrogenation of CO to CH_3OH is expected to be efficient.

Reaction rate coefficients have been derived from the time-dependent behavior of the products and reactants in these experiments. These have to be used to extrapolate toward the much lower H-atom coverage expected in the interstellar medium. However, since the surface coverage of atomic hydrogen is unknown in these experiments (it is set by deposition balancing H_2 formation), only an effective rate constant can be determined (Watanabe and Kouchi, 2008) which is the product of the reaction rate coefficient and the surface coverage. In addition, some experiments have been analyzed in terms of thermally driven diffusion and, in that case, derived activation barriers are severely underestimated as quantum mechanical tunneling may be dominant. The tunneling probability depends on the height and the width of the activation barrier, the reduced mass along the reaction coordinate, and the detailed shape of the potential energy surface around the barrier region. Expressions have been derived for the "effective mass" necessary for the computation of tunneling corrections adopting simple one-dimensional models (Gonzalez, Allison, and Louis, 2001). For the $CO/H_2CO/CH_3OH$ system, the activation barriers and tunneling rates have been studied with quantum chemical methods at different levels of sophistication (Woon, 2002; Goumans and Kästner, 2011; Goumans, 2012). Du, Parise, and Tielens (2012) analyzed the experimental data in terms of a model for the hydrogen coverage in the experiments to derive the barrier width and hence the reaction rates relevant for interstellar conditions. As the different rates involved in hydrogenation of CO and in the formation of water have been "calibrated" in the experiments relative to each other, much of the uncertainty in this extrapolation tends to cancel out.

2. H_2O formation

In the initial theoretical studies (Tielens and Hagen, 1982), atomic O was assumed to be mobile and water formation then proceeds through reactions of H with O_2 and O_3 (see Fig. 19). Essentially, accreted atomic oxygen migrates and reacts to form molecular oxygen. Once a small amount of molecular oxygen is present, further accreted O will react to form O_3. Atomic H will then preferentially react with O_3, forming OH, which reacts immediately with H_2 present on the surface to form H_2O. This reforms O_2 and the oxidation-hydrogenation cycle can repeat itself. In these particular models, the barrier for hydrogenation of O_2 is assumed to be higher than that for O_3. Nevertheless, once enough O_2 has built up, the hydrogen peroxide channel to water formation also opened up with hydrogenation of O_2 leading to H_2O_2, which reacts then on with H to form H_2O and OH (see Fig. 19). The OH produced reacts immediately with H_2 to form H_2O as well (Tielens and Hagen, 1982).

In recent years, a number of surface chemistry experiments have been performed to study the formation of H_2O on interstellar ice analogs and the results provide support for, and also extend, the chemical routes outlined above. As expected, these studies reveal efficient water formation from direct recombination of atomic H and O on porous water ice and other cryogenic matrices (Hiraoka et al., 1998; Dulieu et al., 2010). The hydrogenation steps in the peroxide route have been investigated by Ioppolo et al. (2008) and Miyauchi et al. (2008) and shown to form water readily. The first step in the ozone channel, the reaction of O with O_2, is known to readily occur in cryogenic matrices (Benderskii and Wight, 1996; Hiraoka et al., 1998; Kiviniemi et al., 2004). Experiments show that hydrogenation of O_2 has no barrier. Hydrogenation of O_3 ($O_3 + H \rightarrow OH + O_2$) also possesses no barrier but is affected by steric hindrance. Experiments show that, assisted by tunneling, this reaction proceeds rapidly on ice surfaces at 10 K (Mokrane et al., 2009).

The final step in most of these routes toward water is the reaction of $OH + H_2$. This reaction has a large activation barrier (3000 K) (Atkinson et al., 2004; Nguyen, Stanton, and Barker, 2011) but a recent laboratory study shows that it occurs rapidly on 10 K surfaces through tunneling (Oba et al., 2012). Interstellar grain surfaces are expected to have
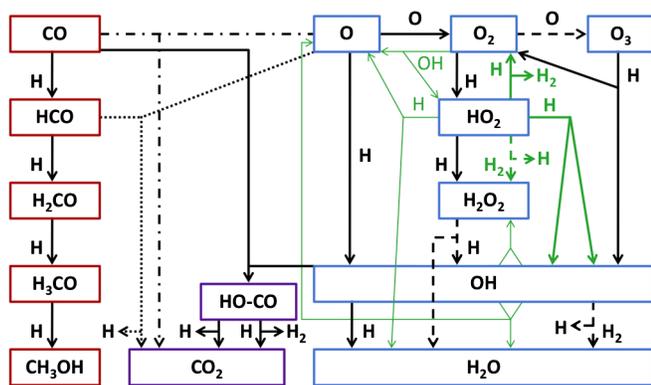

FIG. 19 (color online). Reactions involved in the hydrogenation of CO (left branch) leading to the formation of H_2CO and CH_3OH and the formation of H_2O (right branch) on grain surfaces. Reactions in the original network (Tielens and Hagen, 1982) are indicated by arrows. Laboratory studies revealed a much richer chemistry. Reactions with small or no barrier are shown with a solid line. Reactions with high barriers are dashed. Reactions which are inefficient in the laboratory experiments are shown with thin lines. Reactions which have not yet been studied are shown as dotted lines. Adapted from Ioppolo et al., 2008.

an appreciable abundance of H_2 [$\theta(H_2) \simeq 0.3$] (Govers, Mattera, and Scoles, 1980; Tielens and Hagen, 1982; Matar et al., 2008) which will readily react with OH and other species with appreciable activation barriers. Parenthetically, this H_2 will preferentially bind and block the strongest binding sites (such as kinks), affecting chemistry in ways that have not yet been investigated.

The laboratory experiments show evidence for a number of additional reactions that may also be involved in water formation (see Fig. 19). These center on the reaction $H + O_2H$. The channel that leads to 2OH may be the preferred route ($\simeq 0.6$) rather than H_2O_2 ($\simeq 0.4$) (Cuppen et al., 2010). The resulting OH would then directly react on H_2. Effective rate constants have also been estimated for some of these reactions (Watanabe and Kouchi, 2008), calibrated to the CO experiments, and analyzed for astrochemistry (Du, Parise, and Tielens, 2012).

3. CO_2 formation

In water formation, some of the oxygen can be lost through reactions with CO forming CO_2 (see Fig. 19). The reaction of $O(^3P)$ with $CO(^1\Sigma^+)$ occurs on the triplet potential energy surface, leading to CO_2 in the excited $^3A'$ or $1^3A''$ bound states from where it can relax through the matrix interaction to the $^1A'$ ground state. These two reaction pathways are inhibited by small activation barriers ($\simeq 2300$ and 3500 K) (Braunstein and Duff, 2000). Ground state CO_2 connects to ground state $CO(^1\Sigma^+)$ with $O(^1D)$ without an activation barrier. Thermoluminescence studies provide experimental support that ground state atomic oxygen can diffuse and react with ground state CO in low temperature matrices to form CO_2 (Fournier et al., 1979). The reaction of an isotopically labeled atomic oxygen beam with an H_2O-CO mixture has been studied under UHV conditions and inefficient ($< 2.5\%$ of the atomic O) formation of CO_2 was observed after warmup and ascribed to migration of the reactants through the porous structure and a reaction with an activation barrier of only 290 K. The remainder of O was probably lost to O_2 formation or sublimation (Roser et al., 2001). Codeposition of CO and cooled O and O_2 into thin films at 20 K also produced traces of CO_2 (Raut and Baragiola, 2011). Most of the O goes, however, into forming O_2 and O_3. Efficient reaction of migrating O atoms with other species (e.g., O_2) than CO probably also limited CO_2 formation in $Ar/CO/O_2$ matrix experiments (Grim and D'Hendecourt, 1986). The efficiency of tunneling on interstellar ice surfaces was investigated by Goumans and Andersson (2010) using harmonic quantum transition state theory and was found wanting: At most, 1 in 10^5 O atoms were expected to react with CO. This discrepancy between theory and experiments is not understood but may implicate the migration characteristics of atomic oxygen in low temperature matrices [e.g., involvement of exciton or $O(^1D)$].

In view of the low efficiency of the reaction of O with CO, other routes to CO_2 on interstellar ice surfaces have been explored; specifically, the reaction of OH with CO. Ioppolo et al. (2011) studied hydrogenation reactions in mixed CO/O_2 ices and identified this reaction as an efficient route toward CO_2 (see Fig. 19). Oba et al. (2010) observed efficient formation of CO_2 from codeposited, cold OH, and CO on

surfaces. It should be noted that, while OH cannot diffuse at 10 K on a grain surface, in general, the hydroxyl radical will be formed in an excited state on grain surfaces and one might speculate that it migrates a few sites before its excess energy is dissipated. During this migration process, OH may encounter a nearby trapped CO and react to form CO_2 (Keane, 2002). Thus, CO competes with H_2 for OH (Sec. V.B.2). This competition has not yet been investigated in the laboratory.

Observationally, interstellar solid CO_2 is present in three different environments. The CO_2 present in H_2O-rich ice is likely formed through reactions of OH plus CO. The origin of CO_2 in the CO matrix is less clear. Perhaps the inefficiency of the O plus CO reaction is balanced on interstellar grain surfaces by the long accretion time scales, effectively closing down the O plus O channel and forcing the O into the CO_2 channel. This would imply though that there is little O_2 around (which is reasonable). Finally, the interstellar CO_2/CH_3OH component likely reflects the effect of warmup. Experiments show that, upon heating to ~ 100 K, mixed $H_2O/CH_3OH/CO_2$ ices rearrange and molecules start to be mobile (Ehrenfreund et al., 1998). The IR spectra show evidence for the formation of "pure" CO_2 clusters in a H_2O/CH_3OH ice environment as well as a direct complex of CO_2 and CH_3OH. The miscibility of (fluid) water and carbon dioxide with methanol is of interest to supercritical fluid chromatography (Lee, Reighart, and Olesik, 1996) and with ethanol this process has been widely studied near Reims (Robinson, 2006). These studies revealed that methanol is well miscible with H_2O and CO_2 but H_2O does not mix well with CO_2 except at low concentrations. In ternary mixtures, the presence of methanol enhances the miscibility of CO_2 in H_2O. However, interstellar ice studies have not been placed within this context, yet.

4. Deuterium grain-surface chemistry

While there is a dependence on the reaction barriers involved, deuterium fractionation on grain surfaces is largely driven by the relative accretion probability of atomic H and D from the gas. The atomic H and D abundances are set by dissociative electron recombination of ions (see Fig. 17) and can then be directly linked to the abundance ratio of the intermediaries (Sec. IV.D) that can be observed directly, $X(D)/X(H) \simeq X(DCO^+)/X(HCO^+) \simeq 3 \times 10^{-2}$, where the value follows directly from observations of the formyl ion and its deuterated counterpart in dense clouds. The atomic D/H ratio in the gas phase is thus very much enhanced above the elemental abundance ratio ($\mathcal{A}_D \simeq 1.5 \times 10^{-5}$). After accretion, this enhanced atomic D/H ratio can be passed on to grain-surface chemistry products.

Experimentally, deuterium fractionation has long provided a convenient tool to probe reaction networks in detail. Astronomically, the important role of interstellar grain-surface chemistry in the deuteration of species such as H_2O, H_2CO, and NH_3 was recognized early on (Tielens, 1983). Driven by observations of high abundances of deuterated molecules in the warm gas of hot cores (cf., Sec. V.F.1), thought to reflect evaporating ices accreted in a preceding prestellar core phase, the early CO hydrogenation reaction network was expanded to include deuterium and the astronomical implications assessed (Charnley, Tielens, and

Rodgers, 1997). Subsequently, extensive laboratory studies confirmed the general schemes as outlined and quantified the reactions involved (Watanabe and Kouchi, 2008; Hidaka et al., 2009). These results are summarized in Fig. 20. These experimental studies also revealed new routes toward deuterium fractionation of methanol, e.g., exchange reactions of D with various isotopomers of methanol. Exposure of methanol to beams of atomic D shows that isotope exchange on the methyl group is rapid (see Fig. 20) (Nagaoka, Watanabe, and Kouchi, 2007). Substitution on the OH group, on the other hand, is not observed. Nor is the backward reaction of atomic H and deuterated methanol observed to occur under the experimental conditions, and analysis of the experiments using quantum chemically calculated barriers (Goumans and Kästner, 2011) shows that these reactions are 10^4 to 10^6 times slower (Du, Parise, and Tielens, 2012).

Finally, hydrogen-deuterium exchange was studied in mixed H_2O/CD_3OD ices (Souda et al., 2003; Souda, 2004; Ratajczak et al., 2009). In this case, rapid exchange is observed on the hydroxyl group forming HDO and CD_3OH at temperatures above 120 K before crystallization of H_2O ice. Such H/D exchange has been studied for other hydrogen bonding systems (H_2O/D_2O and NH_3/D_2O) and is related to proton transfer and ion defects (Bertie and Devlin, 1983; Collier, Ritzhaupt, and Devlin, 1984; Wooldridge and Devlin, 1988). Since charge separation seems to be important in interstellar ices and since heating and sublimation of ices near newly formed stars is a key ingredient in models for the warm gas in these environments (Sec. V.F.1), these reactions may be very relevant as well. Both types of reactions can result in different deuterium fractionation on the groups within one molecule or between molecules in the same ices. Observationally, fractionation of the deuteration between the methyl and hydroxyl groups of methanol and between methanol and water have been observed around some protostars (Parise et al., 2005, 2006).
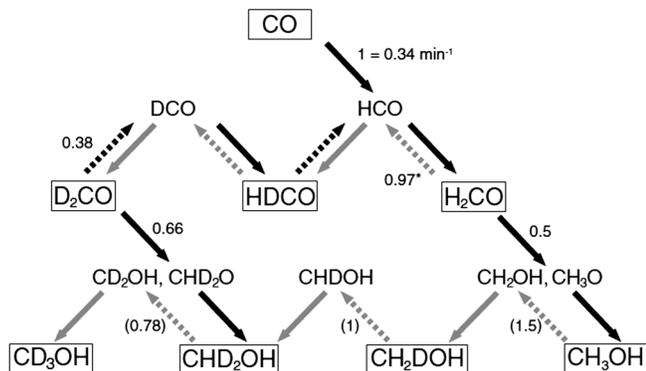

FIG. 20. Reactions involved in the hydrogenation and deuteration of CO on grain surfaces leading to the formation of H_2CO and CH_3OH and their isotopologs. Solid arrows indicate H and D addition reactions. Dashed arrows indicate H and D abstraction reactions forming HD. The numbers shown are the reaction rates relative to the H + CO reaction (measured to be 0.34 min^{-1} under the laboratory conditions). Values in brackets are the reaction rates for pure CH_3OH studies. From Hidaka et al., 2009.

5. Complex organic molecules

The mobility of C and O atoms on a grain surface are not well known and matrix studies yield puzzling results (Sec. V.A), but if these atoms are mobile a rich chemistry can be initiated (Tielens and Hagen, 1982; Charnley and Rodgers, 2009). Possible grain-surface routes toward larger organic compounds involve reactions of these atoms with, for example, the intermediate radicals HCO and CH_3O (see Fig. 21). With O and N, this can, for example, lead to formic acid (HCOOH) and formamide ($HCONH_2$). With atomic C, a host of molecules come into play, including dimethyl ether (CH_3OCH_3), ethanol (CH_3CH_2OH), acetaldehyde (CH_3CHO), and methyl formate (CH_3COOH). These routes toward further chemical complexity have not been tested experimentally and, if there are no activation barriers involved, isomerization at intermediate steps may preferentially lead to the most stable products instead (Lattelais et al., 2009). Characterizing the precise chemical routes in the laboratory may be a prime tool for understanding the complex inventory of interstellar ices produced by grain-surface chemistry (cf., Sec. V.F.1).

C. Modeling surface chemistry

Interstellar grain-surface chemistry is in the diffusion limit where the chemical reactions are limited by the rate at which reactants can be brought to the surface. Often, the kinetics of a chemical network, in the gas phase or on a surface, is evaluated using rate equations describing the rate of change of the (average) number density $n(i)$ of the species present in terms of the reactive binary collisions between them,

$$\frac{dn(i)}{dt} = -n(i)\sum_j n(j)k_{ij} + \sum_{j,k} n(j)n(k)k_{ik} + k_{ac}n_g(i) - k_{sub}n(i),$$ (34)

where the first sum includes all coreactants for species i, while the second sum pertains to all bimolecular reactions resulting in the formation of species i, and the last two terms refer to accretion of species i from the gas phase and sublimation into the gas phase. The reaction rate coefficient has to be treated with care. Considering a migrator "searching" the surface for a coreactant with which it can react upon collision (e.g., without activation barrier), say, H plus H, the reaction is limited by migration on the surface and the reaction rate coefficient is given by the migration rate k_{mig}. The rate at which a species, say H_2, is formed is then

$$R(H_2) = \tfrac{1}{2}k_{mig}n^2(H),$$ (35)

where the factor $1/2$ is to avoid counting each reaction twice. In case evaporation is not important, the average time scale to visit every site on the grain scales with $N_{max} \ln(N_{max})$ and this factor enters into the migration rate (Tielens, 2005; Lohmar, Krug, and Biham, 2009). In case evaporation is important, this correction factor to the rate at which species move from site to site has to be slightly adjusted. However, often relevant hydrogenation reactions possess an activation barrier and the probability for reaction p_{ij} in any collision is small. In that case, the reaction rate coefficient is given by $k_{ij} = k_{mig}p_{ij}$. This reaction probability depends on how long the migrator is
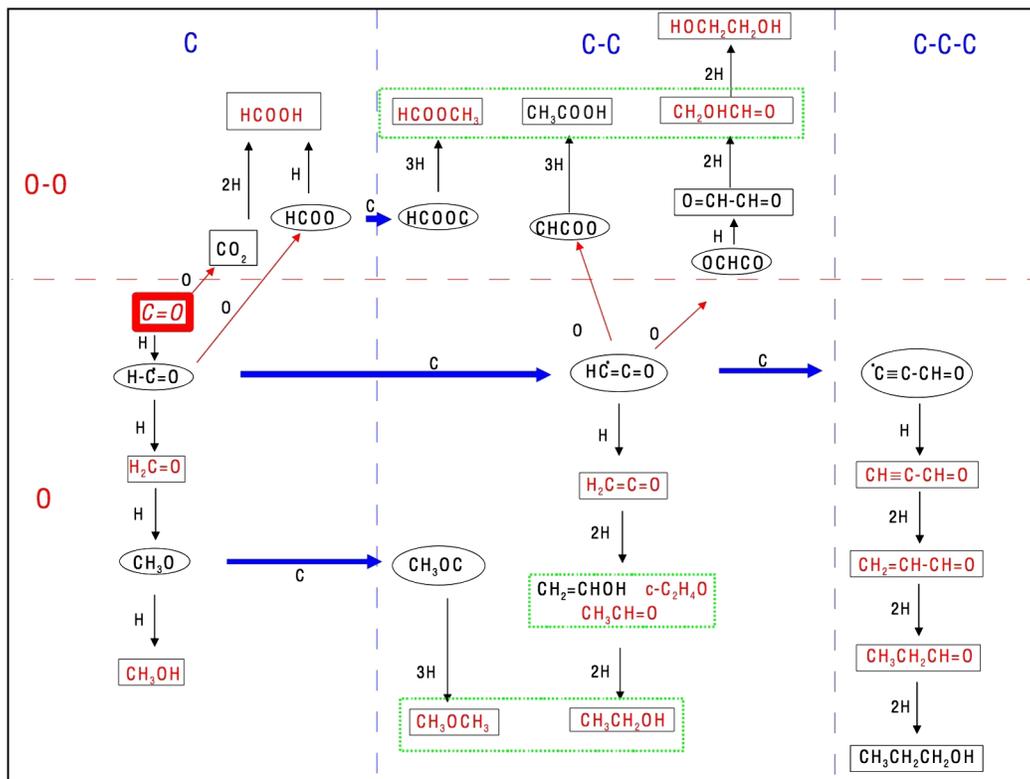
FIG. 21 (color online).   CO accreted on a grain surface is activated through reactions with H (vertical arrows). Eventually these H reactions will form H_2CO and CH_3OH. Intermediate radicals such as HCO and CH_3O can react with other atoms leading to larger organic molecules [reactions with C (O) are indicated by thick horizontal (thin slanted) arrows] and possible routes toward, among others, HCOOH, CH_3CH_2OH, and CH_3OCH_3 are indicated. Many of these molecules are observed to be abundant in hot cores (Sec. V.F.1). Molecules in dotted boxes are isomers. From Requena-Torres *et al.*, 2008.

associated with the reaction site and as this is inversely proportional to the migration rate, the reaction rate is independent of the migration rate (Tielens, 2005; Garrod *et al.*, 2009; Du, Parise, and Tielens, 2012).

For interstellar grain surfaces this "collisional" approach to chemistry has inherent problems as the surface area of the individual grains is exceedingly small (10^{-12}–10^{-10} cm^2 corresponding to 10^3–10^5 surface sites) and fluctuations in the concentration of (particularly migrating, reactive) species can become very large. It is clear that, when the actual number of species present on an individual grain surface flips between 0 and 1, reaction rates are set by the stochastic nature of the problem and rate equations provide an inadequate description of the evolution of the system (Tielens and Hagen, 1982; Tielens, 2005). Additionally, studies show that "cascade" effects can become important where, under conditions of low H fluxes, an appreciable abundance of a species is built up (e.g., O_3). Once an H lands and reacts, the resulting OH can react with H_2 releasing a new H atom that can react with another O_3 molecule. This process can then continue until the H atom is lost to another reactant which does not react with H_2. The resulting avalanche leads to strong fluctuations in the abundance of even immobile species (Tielens and Hagen, 1982; Keane, 2002; Du, Parise, and Bergman, 2012). Various methods have been devised to deal with the discrete stochastic nature of the system under these conditions, each with their advantages and disadvantages (Herbst and Shematovich, 2003).

In the Monte Carlo approach, random number generators are used to explicitly evaluate the accretion history of the different species from the gas phase and their subsequent reaction sequences with coreactants present on the surface (Tielens and Hagen, 1982). Using a large number of drawings, the system provides the surface concentrations of the species involved. The advantage of this method is that it takes the discrete nature of the problem fully into account. Moreover, Monte Carlo methods are versatile and allow the inclusion of many different aspects that influence the reaction probability, such as the presence of multiple binding sites and porosity and/or morphology effects (Cuppen and Herbst, 2005, 2007; Cuppen *et al.*, 2009). A disadvantage is that it is very time consuming and that it is difficult to integrate this approach with the rate equation method often used in evaluating chemical abundances in the gas phase.

In the master equation approach, the state of the surface is represented by a probability vector of the surface concentration of all species. The rate equations [Eq. (34)] are then replaced by time derivatives for these probabilities, which are constructed by properly accounting for the reactions involved (Biham *et al.*, 2001; Stantcheva and Herbst, 2004). As an example, in case that only one type of species (H) can be present on a grain with N_{max} sites, there will be N_{max} equations describing the time evolution of the system. The rate of formation of H_2 is then given by

$$R(H_2) = A(\langle N_H^2 \rangle - \langle N_H \rangle), \qquad (36)$$

with A constant and the moment $\langle N_{\mathrm{H}}^k \rangle$ given by

$$\langle N_{\mathrm{H}}^k \rangle = \sum_{N_{\mathrm{H}}=0}^{N_{\mathrm{max}}} N_{\mathrm{H}}^k p(N_{\mathrm{H}}), \qquad (37)$$

and $p(N_{\mathrm{H}})$ is the probability to have N_{H} species on the surface. Comparing Eqs. (35) and (36), the inherent incompatability between these approaches when $\langle N_{\mathrm{H}} \rangle$ is small is clear. This set of equations can then be solved with appropriate boundary conditions using, for example, Runga-Kutta techniques. Because of the computational effort involved, this method has been applied only to the simple system of H_2 formation (Biham *et al.*, 2001). The stochastic evolution can also be sampled using a Monte Carlo method and gas and grain-surface chemistry can then be evaluated simultaneously if needed (Charnley, 1998, 2001; Vasyunin *et al.*, 2009), but in practice this approach is too time consuming and has been used only sparingly in astrophysics. An alternative approach to solving the master equation was proposed by Lipshtat and Biham (2003). In this method, the master equation is rewritten in terms of the moments of the distribution. Again, time derivatives can be set up and solved using standard numerical techniques. Because the $(k + 1)$th moment depends on the lower moments, the system has to be truncated in a clever way. Again this method is very computer intensive and has not been used much.

The issues involved may become clearer when considering the average population of species i, $\langle n(i) \rangle$, which is described by equations containing terms $\langle n(i)n(j) \rangle$. This should be contrasted with Eq. (34) where the terms contain $\langle n(i) \rangle \langle n(j) \rangle \equiv n(i)n(j)$. Hence, equations have to be added to evaluate the second order moments $\langle n(i)n(j) \rangle$. Now the number of states grows exponentially with the number of species. Consider a system of only ten species in which each can have only three states (0, 1, or 2 species on the surface), the number of equations is then $3^{10} = 59\,049$ and rigorous studies of this kind have to be limited to small systems. There are ways around this, though. Only reactive species, which will have very low abundances in interstellar grain-surface chemistry, may have to be treated in a discrete way. This includes mobile species such as H, D, C, N, and O, as well as reactive radicals (e.g., HCO, O_2H, CH_3O). The concentration of abundant species can then be followed using rate equations. That boils down to replacing $\langle n(i)n(j) \rangle$ by $\langle n(i) \rangle n(j)$, where $\langle n(i) \rangle$ is evaluated using the master equation approach and $n(j)$ follows from solving the system described by Eq. (34). This system could be reduced even further by realizing that at any one time there is at most only one mobile species on the surface. That is, in practice, the accretion rate of species is so low in the ISM (typically < 1 day^{-1}) that mobile species can always find a reaction partner (or evaporate). In any case, this approach leads to hybrid methods where rate equation and master equation approaches are intermixed (Stantcheva, Shematovich, and Herbst, 2002). An automatic scheme can then be implemented whereby the method shifts from the master equation approach to the rate equation approach whenever given criteria are fulfilled on, for example, the average number of species present on the surface (Du and Parise, 2011). This method is very versatile and can take the ''discrete'' effects associated with highly mobile species as well as cascades well into account (Du, Parise, and Bergman, 2012).

Because of the difficulties in combining rate equations for gas-phase reactions with the discrete approaches for surface chemistry, some have opted to modify the rate equations in a semiempirical fashion to compensate for the inherent shortcomings of this method (Caselli, Hasegawa, and Herbst, 1998; Stantcheva, Caselli, and Herbst, 2001). Specifically, the expressions for the rate coefficients are altered to limit the probability that a reaction occurs in any given time step to at most unity. In addition, additional correction factors can be introduced to bring the results of the modified rate equation approach in agreement with those of stochastic theories for a few selected cases, which are considered representative. The resulting set of rate equations is then combined with the gas-phase rate equations and integrated using standard ordinary differential equation integrators. The advantage of this method is that it is fast and designed to combine gas and grain-surface chemistry. The disadvantage is that the system has to be validated semiempirically *a posteriori* and this will always leave inherent uncertainties. A number of studies compared results obtained with the modified rate equation approach to those from discrete methods for very limited systems (Charnley, 2001; Stantcheva, Shematovich, and Herbst, 2002; Lipshtat and Biham, 2003). The most complete of these is the study by Vasyunin *et al.* (2009). The results show substantial differences with the master equation approach when surface species are highly mobile and grain-surface chemistry is in the diffusion limit. Clearly, modified rate equations have to be used with care. Garrod (2008) introduced a variation on this theme of modified rate equations. In his approach, for rapidly migrating species, the reaction rate coefficient is taken to be the accretion rate of a species times the probability (evaluated using Poisson statistics) that the other species is present on the grain surface whenever the average number of species present on the grain is less than unity. An adjustable switching function allows a smooth transition from the rate equation to the modified rate equation system. This approach has been tested against large-scale Monte Carlo studies with encouraging results (Garrod *et al.*, 2009).

D. H_2 formation

The molecular hydrogen formation rate $R_d(H_2)$ can be derived semiempirically from UV observations of atomic and molecular hydrogen absorption lines in diffuse cloud sight lines to be

$$R(H_2) = 1\text{–}3 \times 10^{-17} nn(\mathrm{H}) \ \mathrm{cm}^{-3}\,\mathrm{s}^{-1}, \qquad (38)$$

where n is the density of H nuclei and $n(\mathrm{H})$ is the density of H atoms (Jura, 1975; Savage *et al.*, 1977). These observations refer to gas with temperatures between 50 and 100 K and dust temperatures of $\simeq 15$ K. Molecular hydrogen is also efficiently formed in photodissociation regions where the gas temperatures are in the range 300–1000 K and the dust temperature is 30–75 K (Habart *et al.*, 2004). In fact, the H_2 formation rate may be a factor of 5 higher in photodissociation regions illuminated by radiation fields about a factor $\sim 10^3$ larger than the average interstellar radiation field. Finally, the reformation of H_2 has an important influence on the structure and emission characteristics of strong

J shocks in space (Hollenbach and McKee, 1979, 1989), where the gas temperature can be some ~ 2000 K but the grain temperature is only $\simeq 15$ K. So H_2 formation under a wide range of conditions is relevant for astrophysics.

There are no efficient formation routes for H_2 in the gas phase and hence by default it is generally assumed that H_2 is formed on grain surfaces. The H_2 formation rate is then given by

$$R_d(H_2) = \tfrac{1}{2} S(T, T_d) \eta n_d \sigma_d n(H) v_H, \qquad (39)$$

where $S(T, T_d)$ is the sticking probability of a H atom with temperature T colliding with a grain of temperature T_d, η is the probability that an adsorbed H atom will migrate over the grain surface, find another H atom, and form H_2 before evaporating from the grain surface, $n_d \sigma_d$ is the total grain-surface area per unit volume, n_H is the H-atom density, and $v_H = 1.5 \times 10^4 T^{1/2}$ cm s^{-1} is the thermal speed of the H atoms. Typically, $n_d \sigma_d \simeq 10^{-21} n$ cm^{-1} and

$$R_d(H_2) \simeq 5 \times 10^{-17} \left(\frac{T}{100 \, \text{K}} \right)^{1/2} S(T, T_d) \eta(T_d)$$
$$\times n n_H \, \text{cm}^{-3} \, \text{s}^{-1}. \qquad (40)$$

For sufficiently low temperatures, S and η are ~ 1 (Hollenbach and Salpeter, 1971) and H_2 formation on interstellar grain surfaces can quantitatively explain the observed H_2 abundances.

The reaction probability has been the subject of a number of experimental and theoretical investigations. In the past, astronomical models relied mostly on the early studies by Hollenbach and Salpeter (1971). This study modeled the migration and reaction of atomic H physisorbed on ice surfaces and realized that, in space, H_2 formation is inhibited on perfect surfaces at temperatures in excess of some 13 K because an atomic H will evaporate before the next one accretes. In order to circumvent this very restrictive condition, they invoked the presence of a small number of sites with enhanced adsorption energies associated, for example, with kinks or surface defects. With reasonable (but somewhat arbitrary) assumptions, this assured efficient H_2 formation up to a critical temperature between 25 and 50 K in these models.

In the late 1990s, Vidali and co-workers (Pirronello et al., 1997, 1999) studied the formation of H_2 on olivene and amorphous carbon surfaces using TPD techniques under ultrahigh-vacuum conditions in the laboratory. Analysis and interpretation of these studies concluded that the mobility of (physisorbed) H is thermally activated in the TPD experiment and that H_2 formation on these surfaces is efficient only in a limited temperature regime (~ 5–8 K for silicates and 8–13 K for amorphous carbon, under interstellar conditions), where the lower limit indicates that H is (thought to be) immobile in physisorbed surface sites and the high limit corresponds to rapid H evaporation before recombination can occur (Katz et al., 1999). This is a very restrictive temperature range implying that H_2 formation on interstellar grain surfaces is rarely important in the interstellar medium. However, there are issues with this interpretation, specifically mobility at low T and the presence of enhanced binding sites, that are actively studied.

Given the low binding energies and barriers involved, atomic H should be highly mobile due to tunneling even at low temperatures (Cazaux and Tielens, 2002). Indeed, recent quantum mechanical evaluations of the tunneling rate and diffusion coefficient on realistic coronene-model potentials show that atomic H is essentially free to diffuse on these analogs for graphite surfaces (Bonfanti et al., 2007). The experimental TPD studies on H_2 formation on graphite and silicate surfaces have therefore been reinterpreted in terms of atomic H rapidly diffusing in physisorbed sites until being trapped in, or reacting with H trapped in, chemisorbed sites (Cazaux and Tielens, 2002, 2004). The results of these model studies imply efficient H_2 formation over a wide range of (surface) temperatures as the chemisorbed energy is $\simeq$ 0.7 eV, provided that physisorbed H can tunnel into the chemisorbed sites and react. Essentially, the chemisorbed sites act as the enhanced binding energy sites envisioned by Hollenbach and Salpeter (1971), except that they are very abundant ($\simeq 10^{15}$ cm^{-2}) even on a perfect surface. The tunneling requirement constrains the energy barrier and width of the chemisorbed barrier (Cazaux and Tielens, 2004). Experimentally and theoretically, the chemisorbed binding energy has now been estimated to be $\simeq$ 0.7 eV with an activation barrier of some $\simeq$ 0.2 eV as the C atom involved puckers out of the plane and the surface has to be reconstructed (Zecho et al., 2002; Morisset, Ferro, and Allouche, 2010). While the potential energy surface may not be accurate enough for strong conclusions to be drawn, it is unlikely that a physisorbed H atom can tunnel into the chemisorbed site at low temperatures as this involves penetration of a high barrier as well as displacement of a C atom (Sha and Jackshon, 2002). Quantum dynamic studies show indeed that sticking of gaseous H directly into chemisorbed sites is inefficient unless the kinetic energy of the incoming H atom is comparable to the energy barrier (e.g., $E_k > 0.1$–0.15 eV depending on the surface temperature) (Morisset, Ferro, and Allouche, 2010). One solution to this issue is that this barrier will be much lower at edges and kinks of a realistic surface ($\simeq$ 0.06 eV; see below). As the concentration of such sites will be small, this essentially recovers the earlier proposal by Hollenbach and Salpeter (1971). Alternatively, laboratory studies revealed that the presence of chemisorbed H present on the surface will facilitate the (chemical) adsorption of other H on neighboring sites without activation barriers (Hornekaer et al., 2006). Thus, as long as one H atom is chemisorbed, the surface coverage can become very high and chemisorbed sites may be actively involved in the formation of H_2 even at high temperatures. The energies required for sticking of the initial H atom(s) are in excess of what is expected for PDRs but are quite reasonable for interstellar shocks. The chemisorbed H would be immobile and physisorbed sites will be difficult to populate at these incoming energies. However, chemisorption and this clustering process may greatly facilitate H_2 formation in shock and PDR environments through the Ely-Rideal mechanism as the reactive cross section is substantial (~ 4–10 Å^2) (Casolo et al., 2009).

PAHs may also play an important role in the formation of H_2 in regions of low UV flux and high atomic H density. A variety of routes toward H_2 have been proposed. Under these conditions, PAHs may become "superhydrogenated" (Schutte, Tielens, and Allamandola, 1993; Le Page, Snow, and Bierbaum, 2003). Theoretical studies show that the

barrier for addition onto an outer edge site of coronene ($\simeq 0.06$ eV) (Rauls and Hornekær, 2008) is much less than chemisorption of a H atom onto the basal plane of graphite ($\simeq 0.2$ eV) (Sha and Jackshon, 2002). As for graphite (Hornekær et al., 2006), a subsequent H addition on adjacent sites is then (calculated to be) barrierless. Similarly, the barrier for addition to a PAH cation is small (Bauschlicher, 1998). Ely-Rideal reactions of gaseous H atoms with super-hydrogenated PAHs can then form H_2 even in moderately warm PDRs (Thrower et al., 2011). Curiously, in this case, the cross section estimated for the Ely-Rideal step is only 0.06 Å^2 (Mennella et al., 2012) and this difference with graphite surfaces is not understood. In any case, the importance of this process still needs to be proven. This scenario is actually open to detailed astronomical tests as superhydro-genated PAHs have a distinct spectroscopic signature present in spectra observed in shielded environments of PDRs such as the Orion Bar (Bernstein, Sandford, and Allamandola, 1996). Other scenarios have also been proposed involving dissocia-tive electron recombination of superhydrogenated PAHs (Le Page, Snow, and Bierbaum, 2009) and UV excitation (Szczepanski et al., 2011; Fu, Szczepanski, and Polfer, 2012) followed by H_2 loss.

While this route toward H_2 relies on chemisorbed H on PAHs or grains with binding energies of $E_b(H) \simeq 0.7$ eV, in principle, abstraction and addition reactions involving ali-phatic groups [$E_b(H) \simeq 3.7$ eV] or aromatic H [$E_b(H) \simeq 4.5$ eV] can open up at even higher temperatures. Laboratory studies show small ($\simeq 0.03$ Å^2) cross sections at low energies ($T = 80$–360 K) (Mennella, 2008) but curi-ously without the temperature dependence expected for the activation barrier involved ($E_a \sim 1700$ K).

A different approach to overcome the diffusion and bind-ing issues for H_2 formation was taken by Cuppen and Herbst (2005) who, upon inspection of the actual surfaces used in the experiments by the Vidali group, reemphasized the impor-tance of surface structure [cf., Hollenbach and Salpeter (1971)]. They were able to reproduce the characteristic be-havior of the TPD studies with reasonable assumptions on the surface roughness parameters (e.g., number density and en-hanced binding energy). Again the characteristic TPD curves were ascribed to a small number of enhanced binding sites that release newly formed H_2 at higher temperatures. They also modeled H_2 formation on interstellar surfaces using Monte Carlo methods and demonstrated that H_2 formation can be efficient even at high dust grain temperatures ($\simeq 50$ K), provided the surfaces are rough (Cuppen and Herbst, 2005). In this respect, while of little relevance for diffuse interstellar clouds, I note that H_2 formation on H_2O ice surfaces has been studied with TPD techniques. These studies revealed the existence of multiple absorption sites on this surface but were otherwise interpreted analogously as immobile H upon deposition which reacts and evaporates upon warm-up during TPD (Roser et al., 2002). However, there is a multitude of experimental data demonstrating that atomic H is highly mobile at low T on ice surfaces (Hornekaer et al., 2003; Matar et al., 2008; Watanabe et al., 2010; see also Sec. V.A) presumably also as a result of quantum mechanical tunneling and the H_2O-H_2 formation data have now been interpreted as evidence for highly mobile

atomic H combined with the presence of a wide distribution of physisorbed binding sites (Govers, Mattera, and Scoles, 1980; Hornekær et al., 2005; Amiaud et al., 2006) where some newly formed H_2 is trapped in high-binding-energy sites and not released until TPD starts.

The formation process of H_2 on grain surfaces may leave its signature in the excitation of interstellar H_2 (Black and van Dishoeck, 1987) and this may provide a key diagnostic. There is experimental support for the release of internally excited H_2 upon formation (Lemaire et al., 2010). However, H_2 formation typically occurs in regions where H_2 is rapidly dissociated by UV photons and then the UV pumping process to vibrationally excited levels tends to overshadow the for-mation excitation as only one in ten UV excitations leads to dissociation (and hence to reformation). In addition, a newly formed H_2 molecule on the grain surface may rapidly transfer much of its vibrational excitation to neighboring molecules (Tielens and Allamandola, 1987; Congiu et al., 2012). It is therefore no surprise that observational searches for the signature of the formation process in the H_2 rovibrational excitation of PDRs have proven to be very elusive (Tiné et al., 2003). Perhaps such observational searches should be di-rected downstream from dissociative shocks, although there too UV photons (produced by the shock) may obfuscate the formation signal.

In summary, the H_2 formation rate on grain surfaces is well determined from observations [Eq. (38)] for conditions in the diffuse ISM (e.g., $T_d \simeq 15$ K). Despite a wealth of experi-mental and theoretical studies, our understanding is incom-plete and the extrapolation to the higher temperatures characteristic for PDRs and interstellar shocks is unclear. Models have been developed that provide analytical expres-sions or tables of reaction efficiencies for use in chemical models of molecular clouds (Cazaux and Tielens, 2004; Chang, Cuppen, and Herbst, 2006). However, these models have not yet been validated against observations. Moreover, important channels such as H_2 formation on PAHs have not been fully explored. Also, over the years, much attention has been focused on graphite surfaces, partly because they are more easily modeled. However, silicates might be as relevant and they have been little unexplored beyond the early studies by the Vidali group and the characteristics of the chemisorbed sites and surface structure are unknown. Much, of course, depends also on interstellar dust properties, such as surface roughness, which are difficult to quantify. Studies on silicate surfaces exposed to energetic ion beams and with regrown oxide layers (Tielens, 2011) might be important dust analogs to explore. Such studies might be an important prelude to studies on actual stardust grains recovered from meteorites. Observationally, further studies of H_2 and its relationship to the dust and PAH properties in PDRs will be key to progress in this field.

E. The composition of ice mantles

As studies of grain mantle chemistry are still searching for accurate and yet efficient methods to evaluate gas and grain-surface chemistry simultaneously and given the rapidly expanding set of specific reaction systems studied in the laboratory, models studies are lagging in this field. A few

results will have to suffice to illustrate the various directions considered.

Keane (2002) evaluated the composition of interstellar ices using a Monte Carlo approach for grain-surface chemistry with the reaction sets originally introduced by Tielens and Hagen (1982). In this study, the grain surface and gas-phase chemistry was completely decoupled by adopting (relative) accretion rates of the (major) gas-phase species. The results showed that at low densities (e.g., high H:CO ratios in the accreting gas; $n < 10^4$ cm^{-3}) water and methanol are abundantly formed. At intermediate densities (H:CO ~ 1; $n \simeq 10^5$ cm^{-3}), water is still formed efficiently as OH formation through hydrogenation of H_2O_2 or O_3 is followed by reaction with H_2 present on the surface, releasing a new H for reaction. At high densities ($n > 10^5$ cm^{-3}), the abundance of water starts to drop and the mantle evolves toward a CO-dominated composition. In addition, comparison with observations suggested that interstellar CO_2 was mainly formed through the reaction OH + CO rather than CO + O.

Taquet, Ceccarelli, and Kahane (2012a) updated the grain-surface reaction network with the results of recent laboratory studies (Sec. V.B), adopted specific accretion rates from the gas phase, and included the effects of grain porosity. They used a rate equation approach to follow the chemistry, during the collapse of a cloud, which was validated by comparison to a Monte Carlo study for a more limited reaction set (Cuppen et al., 2009). This allowed a very extensive parameter study. These studies concluded (as well) that CH_3OH ice is formed at low densities, relatively early on in the collapse. They also found that adsorbed CO shifts from a H_2O-rich to a CH_3OH-rich environment during the evolution but there is no obvious CO-rich ice phase.

While limited in their chemical networks, early models pointed toward the high deuterium fractionation accompanying efficient hydrogenation on interstellar grain surfaces in species such as H_2CO, CH_3OH, H_2O, and NH_3 (Tielens, 1983; Charnley, Tielens, and Rodgers, 1997). Indeed, subsequent detection of high fractionation of these species in space (Turner, 1990) cleared the way for a general acceptance of the importance of grain-surface chemistry and of evaporating ices for the molecular inventory of hot cores (Ceccarelli et al., 2001; Parise et al., 2006; cf. Sec. V.F.1). The more recent experimental results are only now beginning to be explored in astronomical models. Taquet, Ceccarelli, and Kahane (2012b) studied the deuterium fractionation in this environment where the reaction set was derived from experiments (see Fig. 20). Using a simplified gas-phase network, their results showed that addition reactions (H and D converting CO into formaldehyde and methanol) alone cannot account for the observed deuterium fractionation pattern. When abstraction and addition from methanol (Sec. V.B.4) is included as well, the observed fractionation can be reproduced at very high densities ($n = 5 \times 10^6$ cm^{-3}), but this results in very low CH_3OH:CO ratios.

Cuppen et al. (2009) focused on the microscopic aspects of ice formation in the CO system: that is, they considered only hydrogenation of CO (see Fig. 19). Their study used the latest laboratory studies and (thermally driven) rates derived from Fuchs et al. (2009). They employed a Monte Carlo approach on a lattice, which allowed them to take into account the detailed morphology of the growing ice mantle; e.g., they included the effects of kinks, surface structure, and morphology of the growing ice layer. The abundance ratio in the accreting gas was initially set to $X(H)/X(CO) = 10^4/n$ but evolved with time as CO depleted onto grains. The results showed efficient methanol formation and at high densities (10^5 cm^{-3}), this led to a thin layer of ''pure CO'' covered by thick layers dominated by CH_3OH.

Finally, Du, Parise, and Bergman (2012) used the hybrid method to study ice chemistry which allowed them to adopt a large reaction set (3075 reactions among 284 gas-phase species and 56 surface species with 151 reactions). The grain-surface reaction set was based upon the analysis of the results of the Leiden laboratory group (Fuchs et al., 2009; Cuppen et al., 2010). Because they focused on explaining observations toward ρ Oph, densities were quite high, resulting in a low CH_3OH-to-CO ratio, but in these mantles the ratio of CO and CO_2 to H_2O was in good agreement with observations.

F. Grain-surface chemistry and the composition of the gas phase

1. Hot cores and corinos

Hot cores are compact (< 0.1 pc) regions of warm (> 100 K), dense ($> 10^7$ cm^{-3}) gas near massive protostars that are characterized by the presence of high abundances of hydrogenated species (Kurtz et al., 2000; Cesaroni, 2005). These regions are thought to represent one of the earliest stages in the evolution of a massive protostar. Chemically, hot cores are characterized by high abundances of saturated species, such as H_2O, NH_3, H_2CO, CH_3OH, CH_3CN, and CH_3CH_2CN (Blake et al., 1987; Wright, Plambeck, and Wilner, 1996). These hot core regions show chemical differentiation with sources dominated by oxygen-bearing molecules [e.g., the compact ridge source in the Orion Kleinman-Low (KL) nebula] and by nitrogen-bearing molecules (e.g., the hot core source in the Orion Kleinman-Low nebula). Recent interferometric studies revealed that the structure of these regions is actually much more complex with the bulk of the dust emission arising from many small and compact clumps (Friedel and Widicus Weaver, 2011). Likewise, the dichotomy in oxygen- versus nitrogen-bearing species is more complex than previously thought (Friedel and Widicus Weaver, 2012; Widicus Weaver and Friedel, 2012). In recent years, regions with similar characteristics as hot cores—but much smaller (< 100 AU) and therefore labeled hot corinos—have also been discovered around solar-type protostars (Cazaux et al., 2003; Bottinelli et al., 2004). For hot corinos, the spatial structure may also be quite complex with multiple small components contributing to the emission (Shimajiri et al., 2008).

Because of the similarity to the composition of interstellar ices, it is now generally accepted that the presence of these species in the gas phase reflects the sublimation of interstellar ices by the newly formed star when the dust reaches a temperature of ~ 100 K. The observed high abundance of deuterated species (e.g., HDCO, D_2CO, CH_2DOH, CHD_2OH, CD_3OH, CH_3OD, and NH_2D) (Ceccarelli et al., 2001; Parise et al., 2006) is also taken as evidence for the importance of ice sublimation in these regions as high deuteration is

characteristic for regions of ~ 10 K, e.g., much colder than hot cores. In this view, ices are formed at low temperatures during the cold and dense prestellar core phase of the molecular cloud, which is known to be characterized by high depletions, and, after the formation of the protostar, the sublimated gas has not yet had the time to "equilibrate" with the gas (e.g., $\tau_{chem} \sim 10^5$ yr). Sputtering in shocks may also be important in releasing these molecules into the gas phase. For a review of this key phase in the chemical evolution of regions of star formation, see Ceccarelli (2008) and Herbst and van Dishoeck (2009).

Grain-surface chemistry pathways to the simple saturated molecules (cf., Sec. V.B) and their deuterated analogs (Sec. V.B.4) characteristic of hot cores have been identified and model calculations can explain the observed abundances (Sec. V.C). Hot cores also contain a multitude of more complex species such as ethyl alcohol (CH_3C_2OH), formic acid (HCOOH), dimethyl ether (CH_3OCH_3), methyl formate (HCOOCH$_3$), methyl cyanide (CH_3CN), and ethyl cyanide (CH_3CH_2CN). The origin of these species is less obvious. Initially, as with H_2O and CH_3OH, they were thought to represent grain-surface products and putative chemical routes can be identified for species such as ethanol, dimethyl ether, and methyl formate (cf. Fig. 21) (Tielens and Hagen, 1982; Charnley and Rodgers, 2009). The absence of quantitative reaction rates and branching ratios has hampered detailed model efforts. At the same time, the near impossibility of detecting trace abundances of these species in interstellar ices severely limits observational approaches to assessing the importance of grain-surface chemistry routes.

Because almost all of the carbon is locked up in CO in dense clouds (C:CO $\sim 6 \times 10^{-3}$, Sec. IV), the grain mantle abundance of organic species containing more than one C atom is expected to be very low. The same holds for N-bearing species since most of the nitrogen is locked up in unreactive molecular nitrogen. Atomic O, on the other hand, is very much available (as it is converted into H_2O on grain surfaces). So while oxidation might be rapid, complex organic species with multiple C and/or N atoms would be difficult to form. The resulting abundance pattern of complex organic species in grain mantles would be very different from that observed in the gas phase of hot cores.

As a result, a number of different chemical routes toward molecular complexity have been proposed.

(a) *Chemistry driven by evaporating ices*: The injection of H_2O, CH_3OH, and NH_3 from the ices into the gas phase can drive a rich chemistry in these warm dense surroundings (Charnley, Tielens, and Millar, 1992; Caselli, Hasegawa, and Herbst, 1993). In these models, methanol plays a key role in driving molecular complexity because protonated methanol is readily formed and was assumed to transfer CH_4^+ groups (rather than H^+). Chemical routes toward the complex (oxide) species observed in hot cores can then be formulated. For example, the following route is available for dimethyl ether,

$$H_3^+ \xrightarrow{H_2O} H_3O^+ \xrightarrow{CH_3OH} CH_3OH_2^+ \xrightarrow{CH_3OH} CH_3OCH_4^+ \xrightarrow{e} CH_3OCH_3. \qquad (41)$$

For hot cores rich in N-bearing species, NH_3 is the precursor ice molecule which is channeled to HCN and then to CN in the gas. The reaction of cyanogen with specific hydrocarbons (also presumed to come from ices) leads then to the suite of N-bearing species observed (Charnley, Tielens, and Millar, 1992; Caselli, Hasegawa, and Herbst, 1993). The time scale for the formation of these complex organics is some 3×10^4 yr and after some 10^5 yr gas-phase chemistry will have driven all the sublimated organics to CO. So, within this model, the organic inventory provides a chemical clock with which the evolution can be timed and this derived time scale is very similar to the lifetime estimated for hot cores from considerations centered on the evolution of regions of massive star formation (Kurtz et al., 2000; Cesaroni, 2005). While this is an attractive model, recent experiments have called these chemical routes into question. First, formation of some of the key intermediaries is inhibited (Horn et al., 2004). Second, experiments have shown that dissociative electron recombination of some of these ion products leads to fragmentation rather than complex organic molecules (Geppert et al., 2006). In addition, the (small) hot corinos around low mass protostars show very similar chemical inventory as the hot cores but the inferred chemical clock is difficult to reconcile with the rapid dynamical time scales associated with these hot corinos (Ceccarelli, 2008).

(b) *Energetic processing of interstellar ices*: UV photolysis and/or ion bombardment of interstellar ices during the prestellar core phase will produce (hot) radicals, specifically H and OH, and some of these will react with other molecules while others will rattle around until they lose their excess energy and become trapped in the matrix. Upon warm-up, the trapped radicals will diffuse and can recombine with each other, forming more complex species (see Fig. 22). The more volatile products will evaporate, leaving behind a residue. An active community has extensively studied this chemistry over the years in the laboratory (Allamandola, Sandford, and Valero, 1988; Bernstein et al., 1995; Schutte and Gerakines, 1995; Gerakines, Schutte, and Ehrenfreund, 1996; Palumbo, Castorina, and Strazzulla, 1999; Gerakines, Moore, and Hudson, 2001; Strazzulla et al., 2007). Recent studies have focused on firmly identifying the chemical routes involved (Hudson et al., 2008; Öberg, Garrod et al., 2009). Astronomical models have been developed, incorporating ice photochemistry under astrophysically relevant conditions (Garrod, Weaver, and Herbst, 2008). The composition of the residues is exceedingly rich and diverse (Greenberg et al., 2000;
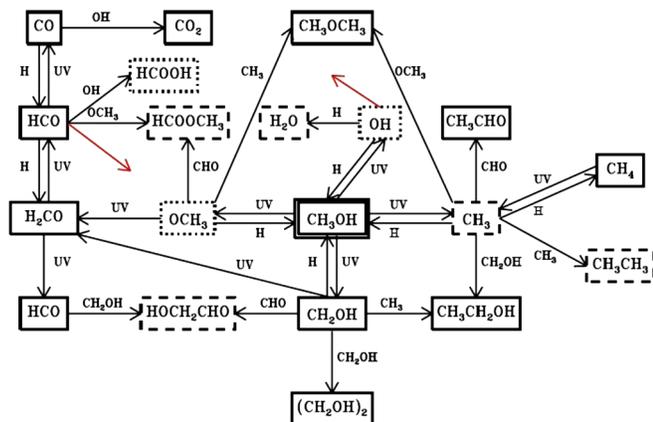
FIG. 22 (color online). UV photolysis produces radicals which can react on to form more complex organic molecules. This summarizes the products and reactions in UV photolysis of pure CH_3OH (solid boxes) or CO-CH_3OH or CH_4-CH_3OH mixtures (dashed boxes). The two colored arrows indicate that these radicals can partake in other reactions. From Öberg, Garrod *et al.*, 2009.

Dworkin *et al.*, 2004). A recent review can be found in Tielens and Allamandola (2011). These ideas are well worth pursuing further as a number of critical issues have to be examined. First, unlike grain-surface chemistry, which is dominated by kinetics, energetic processing promotes diversity and complexity. Starting with realistic interstellar ice mixtures, a variety of radicals can be produced which can recombine to a wide range of species and isomers (Allamandola, Sandford, and Valero, 1988; Bernstein *et al.*, 1995; Schutte and Gerakines, 1995). Presently, it is unclear whether this chemical diversity can be reconciled with the astronomical record that points more toward chemical specificity. Second, prolonged exposure to UV or particle radiation will lead to the production of macromolecular structures. Observationally, there is no evidence for such "organic goop" in the interstellar dust record. Third, the presence of NH_3 and H_2CO in the ices may provide an efficient polymerization route for the conversion of molecules to solid materials during warm-up (Schutte, Allamandola, and Sandford, 1993) and this complication has to be evaluated. Finally, HCO is a key, initial product of the photolysis of ices with CO but the telltale absorption signature of this molecule has never been observed, questioning the relevance of these chemical routes.

(c) *Ion-molecule chemistry in interstellar ices*: Chemical schemes based upon CH_3 transfer in ice-loaded, gaseous environments, as originally proposed by Charnley, Tielens, and Millar (1992), are very elegant and appealing but the experimental evidence argues against them (see above). However, a variant of this may be of relevance for the composition of hot cores. Specifically, it has become abundantly clear in recent years that charge can be an important aspect of interstellar ices. First, the 4.62 μm band is now generally attributed to the OCN^- ion (Demyk *et al.*, 1998). Second, any PAHs trapped in these ices can act as electron acceptors, localizing the charge and preventing

electron diffusion and recombination (Bouwman *et al.*, 2011). Likewise, trapped atoms such as Na and K can be efficient electron donors in interstellar ices. Third, recent studies on dipole alignment of molecular films (Balog *et al.*, 2009) also point toward the importance of electric fields for the evolution of interstellar ices. Accepting that interstellar ices are charged and that these charges are localized, new interesting chemical routes akin to ion-molecule gas-phase reactions but now in the solid state open up. Specifically, Fig. 23 illustrates a possible route toward dimethyl ether, based upon molecular beam experiments on methanol droplets (Selegue and List, 1994). So the scenario is as follows: typical interstellar ices containing CH_3OH and other species (e.g., H_2O) as well as traces of alkali metals are formed at low temperatures in prestellar cores. Over time, these ices are charged by visible and UV photons. Upon warm-up by a nearby protostar to ~80 K, the methanol segregates out from the water—this process is known to be important in some interstellar sight lines (Dartois *et al.*, 1999; Boogert *et al.*, 2000)—and stereochemistry in a dropletlike environment can ensue on astronomical time scales ($\sim 10^4$ yr). The resulting more weakly bound dimethyl ether molecule can then readily sublimate. While there is good experimental support for this reaction scheme in droplets, the importance of methyl transfer without fragmentation in ices is unproven and this whole scheme is highly speculative. Regardless, this discussion points toward issues that have been ignored in the past and that may actually be very important: ionization and localization of charges in ices, stereochemistry, thermal segregation of molecular mixtures, molecular solubility in water-methanol mixtures, and solid-state ion-molecule chemistry.

2. Grains and the composition of dark clouds

Accretion: The observed, pronounced depletion of molecules in the densest centers of prestellar cores (Sec. II.B.1), typically a factor of 10 for CO, is often taken as evidence for the importance of accretion of gas-phase molecules onto dust grains, forming a molecular ice mantle (cf., Sec. II.B.3). The accretion time scale is given by
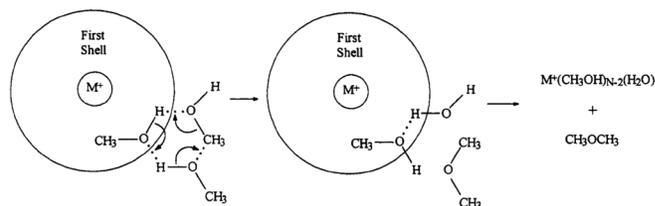

FIG. 23. Possible chemical route toward molecular complexity in methanol-rich interstellar ices. The circle around the central (alkali-metal) M^+ ion represents the first solvation shell of methanol. Methanol molecules in the second solvation shell and hydrogen bonded to the first are (stereochemically) in position to react. In this way, two methanol species are converted into dimethyl ether and water $[M^+(CH_3OH)_N \rightarrow M^+(CH_3OH)_{N-2}H_2O + CH_3OCH_3]$. From Selegue and List, 1994.

$$\tau_{\text{acc}} \simeq 3 \times 10^5 \left(\frac{10^4 \text{ cm}^{-3}}{n}\right)\left(\frac{10 \text{ K}}{T}\right)^{1/2} \text{yr}^{-1}, \qquad (42)$$

and, for dense cores, this is much shorter than the fastest, dynamical time scale, the free-fall time scale [$\tau_{\text{ff}} \simeq 4 \times 10^5 \, (10^4 \text{ cm}^{-3}/n)^{1/2}$ yr].

In contrast to CO, some species, notably N_2H^+, show a peak in their emission at the central core position. As its precursor N_2 has similar sticking and sublimation behavior to CO, this difference points toward a not well-understood chemical behavior. Analysis of the data shows that N_2 does deplete but apparently just not as much as CO. [For B68, a factor of $\sim$5 versus a factor of 100 (Maret, Bergin, and Lada, 2006).] Likely, it is a combination of a number of factors (Aikawa *et al.*, 2001), including that the main reservoir of nitrogen (N_2) is more efficiently formed in dense environments. Also, CO is the predominant destruction agent for N_2H^+ and hence the abundance of the latter increases when the former is depleted. Finally, CO may be efficiently hydrogenated into H_2CO and CH_3OH on grain surfaces, which have high binding energies to the ice, while N_2 is unreactive to atomic H and N_2 is very volatile.

Likewise, the observed high deuteration in prestellar cores is thought to reflect the extreme effects of depletion. As CO is depleted, fewer and fewer cosmic-ray-produced H_3^+ ions are destroyed through $H_3^+ + CO \rightarrow HCO^+ + H_2$. The increased abundance of H_3^+ leads then to a high abundance of H_2D^+, the precursor of DCO^+ and N_2D^+, through reactions with HD (Sec. IV.D). In fact, multiply deuterated isomers of H_3^+ become abundant. Hence, H_2D^+ and D_2H^+ are good tracers of prestellar cores (Caselli *et al.*, 2003; Vastel, Phillips, and Yoshida, 2004). Eventually, when all heavy molecules including N_2H^+ and NH_3 are frozen out, H_2D^+ and D_2H^+ are the only tracers left to determine the structure of these cores (Vastel *et al.*, 2006; Caselli *et al.*, 2008).

Ejection: Condensation of volatiles into ice mantles is counteracted by a number of processes returning grain-surface chemistry species back to the gas phase. At the edges of molecular clouds, photodesorption by penetrating ultraviolet photons from the ambient interstellar radiation field manages to keep the grain surface "clean." The thickness of the molecular cloud surface layer where grains are kept "ice free" by photodesorption can be estimated by balancing accretion and photodesorption,

$$A_v < 1.8 + \ln\left[G_o\left(\frac{Y_{\text{pd}}}{10^{-3}}\right)\left(\frac{10^4 \text{ cm}^{-3}}{n}\right)\right]. \qquad (43)$$

For water, photodesorption yields of 10^{-3} have been measured in the laboratory and calculated by molecular dynamics studies (Westley *et al.*, 1995; Andersson *et al.*, 2006; Öberg, Linnartz *et al.*, 2009; Öberg, van Dishoeck, and Linnartz, 2009; Arasa *et al.*, 2011), so grain-surface chemistry can be an important route toward new, gas-phase molecules in the surface layers of molecular clouds. In a global sense, taking accretion as the rate limiting step, for densities in excess of $n > 10^3$ cm^{-3}, grain-surface chemistry followed by photodesorption in surface layers is faster than gas-phase chemistry routes [cf., Eqs. (8) and (42)]. Of course the products are very different and such a comparison has only limited value. It should also be understood that photodesorption may well lead to fragmentation and the ejected species may not necessarily be "true" grain-surface chemistry products. Water is a point in case as photodesorption is initiated by absorption into a dissociative state. The OH and H fragments may recombine on their way to the surface to reform H_2O but H (formed in deeper layers) may also kick out another H_2O molecule. Typically, the injected OH:H_2O ratio is 1.4 at low temperatures (Andersson *et al.*, 2006; Arasa *et al.*, 2011). Inspired by observations with the submillimeter wave astronomy satellite (SWAS), detailed models have been developed for gaseous H_2O and these place water formation on grain surfaces followed by photodesorption into the gas phase (and then photodissociation to OH and O) and hence localize gaseous H_2O in molecular cloud surface layers (Hollenbach *et al.*, 2009). In these model calculations, adopting the high OH:H_2O ratio in the desorbed products indicated by experiments and theory provides a better fit to observations of translucent clouds.

As for H_2O, photodesorption of CO_2 and CH_3OH is initiated by fragmentation at yields of 10^{-3} with products CO and O and, likely, CH_3O (and H) and CH_3 (and OH) (Öberg, 2009; Öberg, van Dishoeck, and Linnartz, 2009). The UV photodesorption of CO, on the other hand, is initiated by absorption into bound states and has a measured yield which is an order of magnitude higher than H_2O when averaged over the interstellar radiation field between 912 and 1800 Å (Muñoz Caro *et al.*, 2010; Fayolle *et al.*, 2011). Unlike H_2O and OH, the effects of photodesorption on the abundances of these other species and the resulting chemistry in the gas phase has not been studied in detail.

Inside dense clouds, UV photons produced by cosmic rays can photodesorb molecules. Balancing accretion and desorption, we have for the gas-phase abundance of species i, $X_{g,i}$,

$$X_{g,i} \simeq 5 \times 10^{-8}\left(\frac{Y_{\text{pd}}}{10^{-3}}\right)\theta_i\left(\frac{10^4 \text{ cm}^{-3}}{n}\right), \qquad (44)$$

where θ_i is the surface concentration of species i (or its precursor). Hence, even deep inside dense clouds, grain-surface chemistry can contribute to the composition of the gas phase. Of course, rapid gas-phase reactions such as protonation and dissociative electron recombination can affect these abundance estimates. In this respect, a recent study of the prestellar core L1544 reveals a weak water line with an inverse P Cygni profile (Caselli *et al.*, 2012). Modeling reveals the fact that the absorption is due to the appreciable column density of water associated with the molecular cloud surface discussed above. However, the emission component is due to a low level of gaseous H_2O in the dense central core maintained by, for example, photodesorption due to the cosmic-ray-induced UV radiation field and velocity shifted due to the contraction of the core (Caselli *et al.*, 2012).

Grain-surface chemistry products may also be ejected into the gas phase upon formation as some of the excess energy can go into translational motion of the molecule in the physisorbed potential. In general, a species will be formed in a highly vibrationally and/or rotationally excited state. Coupling of this energy to the translational energy channel will be hampered for vibrational energy by the large energy gap while transfer of energy in the translational energy channel to the phonon bath of the grain will be rapid. There

are some experimental data on energy transfer within low-temperature matrices and this has been discussed in an astrophysical setting by Tielens and Allamandola (1987). However, these issues are amenable to direct laboratory measurements rather than extrapolations from energy transfer studies and that should be a high priority. For H_2 formation, this is now being done (Lemaire *et al.*, 2010).

Finally, impacts by 10–100 MeV/nucleon heavy cosmic rays will deposit energy at a rate of $4 \times 10^{11} (MeV/E)$ eV/cm and heat an ice mantle to temperatures of 50–200 K. This can lead to evaporation of volatile ice mantle species (Bringa and Johnson, 2004; Shen *et al.*, 2004). Taking a typical Fe cosmic-ray intensity, $\mathcal{N}_{CR}$ of 10^{-4} particles $cm^{-2} s^{-1} sr^{-1}$, the time scale for a CR hit is

$$\tau_{CR} = \pi a^2 4\pi \mathcal{N}_{CR} \simeq 8 \times 10^4 \left(\frac{1000 \text{ Å}}{a}\right)^2 \text{ yr.} \qquad (45)$$

The initial energy deposition leads to a thermal spike which can lead to appreciable ejection of species, including species that are not that volatile (e.g., H_2O but also large molecules) (Johnson *et al.*, 1991). There is also a "late" release of volatile species as the grain cools down, predominantly through sublimation (Bringa and Johnson, 2004). Additionally, UV photolysis of ice grains may have produced stored radicals inside the ice. Upon warm-up of the ice, these radicals may become mobile and recombine. The released chemical energy may exceed the deposited cosmic-ray energy and in laboratory experiments "explosive" desorption events have been observed (D'Hendecourt *et al.*, 1982).

Ice mantle species can also be returned to the gas phase through sputtering in fast shocks and there is ample evidence for this, e.g., the outflow in L1157 (Codella *et al.*, 2010). The warm postshock gas can also drive an interesting chemistry and lead, in particular, to high abundances of H_2O and this has to be taken into account in the analysis.

Observationally, there is evidence for the importance of the injection of grain-surface products into the gas phase in dense and quiescent molecular cloud cores. Hydrogen peroxide (H_2O_2) as well as the hydroperoxyl radical (HO_2) have been detected toward the source, ρ Oph A, with similar abundances of $\simeq 10^{-10}$ (Du, Parise, and Bergman, 2012; Parise, Bergman, and Du, 2012). There is no obvious gas-phase reaction route toward H_2O_2 while it is a main intermediary in the H_2O formation routes on grain surfaces (see Fig. 19; Sec. V.B.2). Models including gas and grain-surface chemistry predict HO_2:H_2O_2 ratios of $\simeq 3$ where both species are formed on the grain surface and it is (rather arbitrarily) assumed that 1% of all reactions on the grain-surface reactions result in ejection (Parise, Bergman, and Du, 2012). The hydroperoxyl radical could also be a product of a photo-desorption process where adsorbed H_2O_2 is photodissociated and the "hot" product is ejected. It is not clear what the branching ratio HO_2:H_2O_2 is of this process but for water ice, the HO:H_2O ratio is $\simeq 1.4$ in photodesorption experiments (Andersson *et al.*, 2006; Öberg, Linnartz *et al.*, 2009; Arasa *et al.*, 2011). The radical abundance in interstellar ices is expected to be very low. Hence, it is unlikely that these species measure a bulk sublimation process such as cosmic-ray-driven desorption rather than a surface process such as molecular formation or photodesorption. While the adopted

values are uncertain, the key point is that these species are difficult to form in the gas phase but are key intermediaries on grain surfaces (Parise, Bergman, and Du, 2012). Further experimental studies can elucidate the actual ejection mechanism and this may provide deep insight into the interaction of grains and gas in the ISM.

3. Grains and the ortho-para ratio of molecules

Some molecules can exist in two distinct states, depending on the spin of the nucleus: the para state when the spins are antiparallel and the ortho state when they are parallel. Because of the symmetry of the wave function, the para states are associated with the even rotational levels and the ortho states with the odd levels. Rotational transitions between ortho and para states require a simultaneous transition of the nuclear spins of the molecule. The radiative lifetime for decay from the ortho to the para state is therefore long. The energy difference between these two states can be quite large compared to interstellar temperatures (i.e., for H_2 about 170 K and for H_2O about 55 K). The ortho and para species are in essence distinct chemical species and this energy difference can have a profound influence on the chemistry involved. Elegant experiments have demonstrated this, for example, for the H_2-H_3^+ system [cf., Hugo, Asvany, and Schlemmer (2009)] and this may play a role in, for example, initiating gas-phase nitrogen chemistry (Sec. IV.C).

Over the years, the ortho-para ratio has been developed into a new tool to study chemical reaction routes in the ISM. Early observational studies focused on formaldehyde (Kahane *et al.*, 1984), which has only a very small energy difference (15 K), and as the observations suffered from beam dilution, interpretation was not easy. With HIFI/Herschel, systematic studies of H_2O in space have become possible and H_2O has a much larger ortho-para energy difference. The first results of these studies show that, while foreground sources show the high temperature ortho-para ratio, H_2O in the gas clouds associated with the expanding molecular ring[7] has an ortho-para ratio consistent with the local gas and dust temperature (Lis *et al.*, 2010). Ammonia provides an interesting probe of the processes involved in the ortho-para conversion as the NH_3 inversion levels provide a direct measure of the kinetic gas temperature. Observations of the W43 cloud revealed that the ortho-para ratio indicates a much lower temperature than the observed rotational temperature and the kinetic temperature of the gas which can be derived from it (Nishitani *et al.*, 2012). Ortho-para ratios have been measured for a number of gaseous species (H_2O, NH_3, CH_4) in the coma of comets. The measured ortho-para ratios are typically lower than the high temperature limits and also less than the temperature at which some of these species sublimate when the comet approaches the Sun (Crovisier, 1998; Kawakita, Russo, and Furusho, 2006; Mumma and Charnley, 2011). Often this has been interpreted as evidence of the formation temperature of the ices where it is tacitly assumed that the ortho-para ratio is preserved over 4.55×10^9 yr.

---

[7]The expanding molecular ring is a dynamical feature in the distribution of molecular gas in the inner 200 pc of the Milky Way (Morris and Serabyn, 1996).

An early discussion on the role of ices in setting the ortho-para ratio of interstellar molecules can be found in Tielens and Allamandola (1987). In view of the large reaction heat available upon formation and the considerable rearrangement of the hydrogen nuclei involved in most reactions, most molecules will form in the high-temperature limit where the ortho-para ratio is set by the statistical weights of the nuclear spin states. In ice, interaction of the nuclear spins of neighboring molecules will cause an equilibration of the ortho-para ratio, typically on a day's time scale. The presence of paramagnetic impurities or lattice defects will cause an even faster ortho-para transformation time scale. In either case, the inhomogeneous magnetic-dipole field generated by the nuclear spin of a neighboring molecule or the unpaired electron of a paramagnetic impurity or lattice defect couples to the proton magnetic moment and causes a transformation between the spin states (Wigner, 1933). As a difference with gas-phase collisions, surfaces act to enlarge the interaction time scale with the local molecular environment.

Experiments on the ortho-para conversion of H_2 date back some 80 yr (Farkas and Sachsse, 1933). In recent years, driven in part by the new observational results on the ortho-para ratio in molecular clouds and in comets, a number of dedicated experiments have been performed addressing the conversion in and on ices. For H_2, rapid ($\simeq 1$ hr) nuclear spin conversion has been measured for ices with traces of O_2 present (Watanabe et al., 2010; Chehrouri et al., 2011). Similarly, the evolution of the rotational population of H_2 trapped in Ar and Xe has been followed in situ and in time through their rovibrational transitions and the results show that the matrix converts the ortho-para ratio on the order of hours (Abouaf-Marguin et al., 2007, 2009). A quantum mechanical study also concludes that the spin conversion of H_2O in an ice environment by magnetic dipolar interactions and spin-spin couplings is efficient (Buntkowsky et al., 2008). Thermal desorption of H_2O at 150 K from amorphous solid water ice surfaces deposited at 8 K finds the high-temperature limit for the ortho-para ratio in the evaporated molecules. Photodesorption of H_2O from this ice at 8 K also results in a high-temperature ortho-para ratio (Hama et al., 2011) suggesting that most of the desorbed H_2O results from photodissociation and subsequent reformation rather than "knock-on" ejection.

Thus, experiments and theory show that the ortho-para ratio of molecules from evaporated ices does not reflect their temperature at formation (or condensation). Rather, on an astronomically very short time scale, the ortho-para ratio equilibrates to the value set by the matrix temperature. This implies that, for thermally sublimating ices, the ortho-para ratio will then be the high-temperature limit as sublimation temperatures are quite high and the time scales of evaporating grains in the Solar System are measured in days and in molecular clouds in tens of thousands of years. The ortho-para ratio in molecules sputtered from ices by energetic ions is an unexplored area of research. While interstellar ices may be very cold and characterized by low ortho-para ratios, the ionization along the penetrating ion path will create electric fields that may facilitate the conversion process as the sputtered molecule makes it to the surface. So, in this case as well, high-temperature ortho-to-para ratios might be expected but this is to be confirmed by experiments.

In light of these experiments, the origin of the low ortho-para ratio measured for comets is puzzling. Experiments and theory agree that this is not a relic of the Solar System formation some 4.55×10^9 yr ago. Rather, it must reflect the evaporation process. Possibly it indicates that the spin states of H_2O molecules in ice crystals are not equal to the spin states of isolated H_2O molecules in the gas phase (Buntkowsky et al., 2008). Alternatively, the binding energy of ortho and para forms to the ice surface may differ (Dulieu, 2011). Experimental studies show that ortho H_2 and D_2 are bound slightly more strongly (by 2.6 and 1.4 meV) to an amorphous ice surface than the para forms of these molecules because the nonspherical ortho wave function interacts with the asymmetric part of the adsorption potential (Hixson et al., 1992; Buch and Devlin, 1993; Amiaud et al., 2008). This difference in the adsorption energy will directly affect the ortho-para ratio of the sublimating molecules; of course, in steady sublimation, only if the sublimation time scale is long compared to the ortho-para conversion time scale. For amorphous solid water, the conversion time scale is $\simeq 10^2$ min (Hixson et al., 1992) and is short compared to the sublimation time scale in the ISM and comets. For H_2, the 2.6 meV difference then translates into a ortho-para ratio difference of a factor of 20 at 10 K. Of course, for H_2 the residence time has to be long enough for the conversion to occur and hence the temperature cannot be too high. Thus, this effect on the ortho-para conversion on grain surfaces is likely not very important for photodissociation regions. In conclusion, the ortho-para ratio of sublimating ices reflects the details of the sublimation process and the interaction of species with the surface. As the aspects (comet morphology, surface structure, and temperature profile) involved in sublimation are rather difficult to study through other means, the ortho-para ratio may provide deep insight into the structure and evolution of comets.

Finally, it should be mentioned that ion-molecule reactions can reset the ortho-para ratio in the gas phase. One key reaction in this is the proton exchange reaction with H_3^+. Adopting the typical Langevin rate for this (10^{-9} cm^3 s^{-1}), assuming that dissociative electron recombination is fast, and a H_3^+ abundance of 10^{-8} yields a time scale $3 \times 10^9/n$ yr. This should be compared to the accretion time scale on dust grains, $\simeq 10^9/n$ yr. This process would drive the ortho-para ratio to a high-temperature ratio again.

VI. PAHS AND INTERSTELLAR CHEMISTRY

This section reviews the role of PAHs in the chemistry of the ISM. It begins with a review of the chemistry involved in the formation of PAH molecules in the high-density and high-temperature environment of stellar outflows (Sec. VI.A). The formation of fullerenes in stellar outflows is also examined (Sec. VI.B). This is followed by a review of the photochemistry of PAHs in the ISM, including the resulting fragmentation to small hydrocarbon species and isomerization to fullerenes (Sec. VI.C). PAHs are readily attacked by small radicals in the hot environment of protoplanetary disks (Sec. VI.D) and processed by energetic ions in strong shock waves (Sec. VI.E). These destruction processes may be counteracted by formation and chemical growth of PAHs in cold and dense molecular clouds (Sec. VI.F). This section

ends with a short discussion on the interrelationship of PAHs, fullerenes, and diamondoids in space (Sec. VI.G).

A. PAHs and soot formation in stellar ejecta

We start here with the ejecta of old, "dying" stars starting in the photosphere with typical temperatures and pressures of 2500 K and 10^{-6} atm and a chemistry largely in thermodynamic equilibrium. Stellar pulsations drive shock waves which travel through the photosphere, lifting material to great heights above the stellar surface, and heating and dissociating molecules present. These molecules can then reform in the adiabatically cooling gas behind the shock front. In this extended molecular layer, chemical nucleation of nanoparticles is initiated. These nanoparticles grow through chemical processes while simultaneously being accelerated by radiation pressure. The gas is momentum coupled to these nanograins and a slow (a few to 30 km/s) stellar wind [mass loss rate, $\dot{M} \sim (10^{-7}-10^{-4})M_\odot/\text{yr}$] ensues. During a short phase ($\simeq 10^4–10^6$ yr), the star returns most of its mass back to the interstellar medium enriched by the nucleosynthesis products from its interior.

The molecular composition of these outflows depends strongly on the C:O abundance ratio. Initially, C:O starts at less than 1 but nucleosynthesis in the deep interiors coupled with mixing can change this ratio to >1. In the former, oxide species dominate (H_2O, SiO, TiO, ...) in the photosphere and the dust is in the form of simple oxides and/or silicates. In the latter, the excess C forms C_2H_2, HCN in the photosphere, and soot condenses out in the ejecta. Large PAH molecules can form as molecular building blocks or intermediaries in the soot condensation process. In the outer layers, penetrating FUV photons can ionize and photodissociate molecules produced at the base of the flow. This gives rise to a rich neutral-neutral and ion-molecule chemistry and, for C-rich outflows, species such as HC_3N, C_4H, ... are routinely observed. A recent review of simple gaseous molecules and their chemistry in stellar ejecta is presented in Ziurys (2006). The formation of PAHs in stellar ejecta has recently been reviewed from a chemical perspective by Cherchneff (2011), while experimental studies on soot formation have been reviewed by Jäger, Mutschke, and Henning (2011).

1. PAH chemistry in sooting stellar ejecta

Based upon the rich soot formation literature in terrestrial settings, the chemistry involved in stardust formation was best developed for C-rich ejecta (Frenklach and Feigelson, 1989; Cherchneff, Barker, and Tielens, 1992; Cherchneff, 2012). As for soot (Frenklach et al., 1985), the condensation process is thought to be initiated with the closure of the first ring followed by chemical growth of this benzene ring to large PAHs through reactions with the main feedstock C_2H_2. The first step can start with the reaction of two propargyl radicals C_3H_3 to form the phenyl radical C_6H_5 or, for example, with the reaction of 1-buten-3-ynyl (C_4H_3) radical with acetylene which can also lead to phenyl (Cherchneff, 2011). The starting radicals are formed through simple reactions from acetylene. Through rapid hydrogen addition and abstraction reactions, phenyl will establish a steady state with benzene. Phenyl can react with acetylene to form

phenylacetylene (C_8H_6, a benzene molecule with one H replaced by C_2H). Abstraction reactions with atomic H can create a new radical site which is very reactive with acetylene and forms the naphtyl radical. The radical site will attack the triple bond in the vinyl group and this closes the second ring to the naphthalyl radical. The process of H abstraction (with radical formation) and carbon (acetylene) addition (the HACA process) can be repeated to add more and more aromatic rings to the growing PAH (Frenklach et al., 1985; Cherchneff, 2011). The details of the carbon condensation route are then set by kinetics. Pericondensed, highly compact PAHs (pyrene, coronene, ovalene, ...) are highly favored in these condensation routes due to their maximum resonance energy and minimal stress energy (Stein, 1978).

Analysis of this system shows that there is a (temperature) window of opportunity for rapid PAH growth between 900 and 1100 K (Frenklach and Feigelson, 1989; Cherchneff, Barker, and Tielens, 1992). For temperatures above 1100 K, the key reactions (H abstraction and C addition) are reversible. At 1100 K, the C addition becomes irreversible but H abstraction is still in fast equilibrium. So, chemical growth can be rapid. At temperatures below 900 K, H abstraction freezes out kinetically as well and further growth is inhibited.

The efficiency of the PAH formation process in stellar outflows (fraction of C_2H_2 converted into PAHs) is then set by the density and time spent in the zone with this temperature range. Initial studies by Frenklach and Feigelson (1989) adopted a very slow (and unrealistic) flow velocity and, for that reason, obtained high yields. Cherchneff, Barker, and Tielens (1992) adopted a steady wind profile for the ejecta and a parcel of gas spends only a limited amount of time in the PAH formation region. Resulting PAH yields were therefore very modest (5×10^{-5}). Thus while the chemistry is well understood, models did not seem to be able to make it work and the field was stagnant for a long time until Cherchneff (2012) recognized the importance of including a realistic description of the outflow process. This study is the most complete both in chemistry and in physical description of the ejecta. Specifically, Cherchneff (2012) included the strong shock waves driven by stellar pulsations that traverse the photosphere and create a surrounding, extended molecular layer. This model provides a good description of the global dynamics and flow of the ejecta through the PAH-growth temperature range. The shocks heat and compress the gas, breaking down molecules, which then reform when the gas cools down adiabatically as the parcel of gas expands and then falls back to almost the same location in the photosphere. So, while the gas has high velocities, the actual flow velocity is very slow and the gas cycles many times through the right temperature range. With this much more realistic model for AGB ejecta, calculated yields are $\sim 10^{-1}$. Coalescence of these PAHs into larger molecular structures and coagulation onto growing dust grains are key to further evolution (Cherchneff, 2011; Jäger, Mutschke, and Henning, 2011). It is clear that, with the combination of detailed chemical kinetics with realistic astronomical models for the stellar ejecta of AGB stars (Cherchneff, 2012), PAH formation in AGB ejecta is now beginning to be understood at a level that will allow for the first time confident incorporation into models for the stellar winds and the evolution of stars on the AGB.

2. Observations of PAHs in stellar ejecta

There is very limited direct observational support for the formation of PAHs in the outflow from C-rich AGB stars. Indirect, the infrared spectra of such objects reveal rovibrational transitions of C_2H_2 (the main feedstock for PAH and soot formation) in the photosphere and its depletion in the ejecta (Keady, Hall, and Ridgway, 1988) as well as abundant carbonaceous dust (cf., the spectrum of IRC + 10216 in Fig. 24). There is no sign of PAHs in the spectra. The absence of the PAH infrared emission features is generally ascribed to a lack of ultraviolet photons in their cool ($\simeq$ 2000–3000 K) stellar spectra. This is corroborated by the infrared spectra of a few C-rich AGB stars with blue stellar companions that show weak PAH emission features (Buss, Tielens, and Snow, 1991; Speck and Barlow, 1997; Boersma, Hony, and Tielens, 2006), but it is conceivable that the irradiation with UV photons from the companion has influenced the chemistry. As the central stellar object evolves toward the blue and the ejected material coasts away at 10–30 km/s, weak PAH features develop on the strong dust continuum (see Fig. 24).
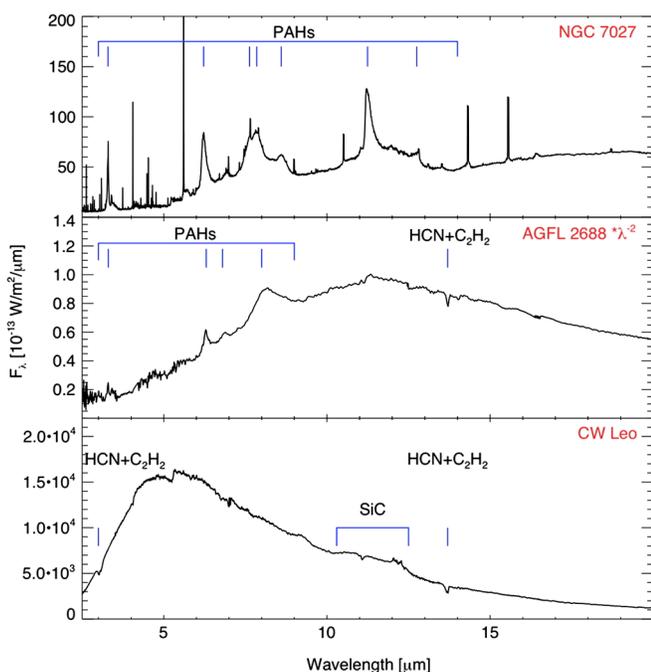

FIG. 24 (color online). Infrared spectra of three successive stages in the evolution of low-mass stars obtained with the short-wavelength spectrometer on the infrared space observatory. Bottom panel: The archetypical asymptotic giant branch (AGB) object IRC + 10216 reveals the presence of strong C_2H_2 (and HCN) rovibrational absorption bands as well as a midinfrared amorphous carbon dust continuum and a weak SiC dust emission feature. Middle panel: The infrared spectrum of the post-AGB object CRL 2688 (aka the egg nebula) is dominated by a strong amorphous carbon dust continuum with weak PAH emission features. Rovibrational absorption bands due to HCN and C_2H_2 are also visible. Note that, for comparison, the flux scale has been multiplied by λ^2. Top panel: The midinfrared spectrum of the planetary nebula NGC 7027 is dominated by strong PAH emission features. The narrow lines are HI recombination and collisionally excited lines of ions, originating in the central, ionized gas region. From Hony, 2002.

The source GL 2688 has an F-supergiant spectrum[8] and has some UV photons available to pump the PAHs. When the central object is a white dwarf and the shell has clearly expanded away, the PAH emission features dominate the midinfrared spectra (see Fig. 24). The central star of NGC 7027 has an effective temperature of some 200 000 K.

While this and comparable data provide strong evidence for the injection of PAHs by C-rich stellar objects and the roles of PAHs in the sooting process of C stars are well modeled, there are still major questions. In particular, it may well be that, during the AGB phase, all of the PAHs formed are incorporated into growing soot grains (Jäger et al., 2009). PAH moieties in these soot grains can then be released into the gas phase when graphitic grains collide with each other at relative velocities in excess of 1 km/s and shatter into small fragments either in the AGB outflows or in the shocks driven by stellar jets during the post-AGB phase. For carbon soot grains, PAHs are likely the dominant fragmentation products (Tielens et al., 1994; Jones, Tielens, and Hollenbach, 1996). In this view, grain-grain collisions can be an important source of PAHs in the ISM as well, as supernova ejecta drive strong shocks through the interstellar gas (Jones, Tielens, and Hollenbach, 1996). The increasingly strong ultraviolet radiation field as well as penetrating FUV photons from the interstellar radiation field as the envelope thins during the post-AGB phase can also process gaseous PAHs (Sec. VI.C) driving the PAH family to the most stable species. The so-called 21 μm post-AGB objects provide evidence for the importance of this processing. These post-AGB objects are surrounded by a shell of dust and gas coasting away from the central F-supergiant star. Spectra of these objects show, relatively speaking, evidence for more aliphatic sidegroups in the PAH molecular structure (at the $\simeq$ 10% level relative to the aromatic component) than any other class of sources. Spatially resolved, near-infrared spectroscopy reveals that the aliphatic-to-aromatic ratio decreases with distance from the star (Goto et al., 2003), presumably because the penetrating interstellar radiation field preferentially drives off the aliphatic groups (Tielens, 2005) or perhaps even converts them into aromatic structures.

B. Fullerene formation in stellar ejecta

Well before the identification of C_{60} and C_{70} in planetary nebulae and in the ISM (Cami et al., 2010; Sellgren et al., 2010) (Sec. II.D), the formation of fullerene species in stellar ejecta was considered plausible for RCrB[9] and population I WC[10] Wolf-Rayet stars. These objects are C rich and highly

---

[8]Supergiant is a spectroscopic designation for a low gravity photosphere and it should be understood that this is really a low mass star.

[9]RCrB stars are low mass, cool supergiants of spectral type F to K surrounded by extensive cool dust shells. These rare objects are hydrogen deficient and carbon rich that undergo, irregularly, large drops in optical brightness as the star "puffs" a little sooting cloud along the line of sight to the Earth.

[10]WC Wolf-Rayet stars are evolved massive stars, which are losing copious amounts of mass ($10^{-5} M_\odot$/yr) in a fast (2000 km/s) wind. This wind has ejected the unprocessed H envelope of these stars, uncovering the core which is enriched in helium burning products.

H depleted. In view of the efficient formation of fullerenes (and soot) in the vaporized carbon rods (Krätschmer *et al.*, 1990), this association is reasonable. The chemical kinetics of the growth of small carbon chains, rings, clusters, and cages has been considered for the ejecta of WC stars (Cherchneff *et al.*, 2000). The results show that efficient formation of carbon clusters requires much higher densities than expected in steady outflows. Since then, it has become clear that dust formation in these environments is localized in the interacting wind zone of the WC primary with the Of companions (Tuthill *et al.*, 2008). Over the intervening years, chemical pathways toward fullerenes have been an active area of research [see, for example, Irle *et al.* (2003) and Zheng, Irle, and Morokuma (2005)]. Hence, it may be time to revisit this issue.

Despite early claims (Cami *et al.*, 2010), the ejecta of PNe with spectra that are dominated by fullerenes are not H depleted. This is not much of an issue though. While early laboratory studies indicated that H-free plasmas are required for efficient fullerene formation, more recent laboratory experiments on soot formation reveal that the yield of fullerenes in flames can be as high as 20% of the soot (Howard *et al.*, 1991, 1992). Experiments reveal a peak in the fullerene formation rate around 2100 K (Pope and Howard, 1996). The route toward fullerenes in flames may involve direct reactions with acetylene and go through corannulene (Pope, Marr, and Howard, 1993) or, alternatively, proceed through highly catacondensed PAHs—PAHs with high H:C ratios (Bachmann, Wiese, and Homann, 1996). Astrophysical studies on soot formation produce soot with fullerenelike structures at high temperatures (~ 3500 K) (Jäger *et al.*, 2008). Thus, possibly, the few, specific planetary nebulae with spectra dominated by fullerenes are characterized by chemistry in their ejecta (during the AGB phase?) through this high-temperature, fullerene route while most AGB precursors of planetary nebula make soot through the regular, low temperature, PAH route (Jäger *et al.*, 2009). The importance of these chemical routes toward fullerenes and soot have not yet been evaluated for conditions relevant for AGB ejecta.

C. Photochemistry of interstellar PAHs

A limited number of experiments have studied the photochemistry of PAHs (Gotkis *et al.*, 1993; Jochims *et al.*, 1994; Jochims, Baumgärtel, and Leach, 1999; Joblin, 2003). These studies show that, at low internal energies, PAHs will predominantly lose H atoms and can efficiently be stripped of all H. At high internal energies, loss of C can start to play a role as well. These experiments have been interpreted in terms of the kinetic parameters involved in the unimolecular dissociation of highly vibrationally excited PAH molecules (Le Page, Snow, and Bierbaum, 2001, 2003; Tielens, 2005). Unfortunately, because of experimental limitations, the focus has been on small catacondensed PAHs which are readily photoprocessed and the extrapolation toward large astrophysically relevant species is not straightforward. In particular, bond energies do not provide a good description of the unimolecular rates. Nevertheless, a semiquantitative model has emerged whereby large interstellar PAHs are first fully stripped of H atoms. Upon further photolysis, the resulting graphene sheet will then start to lose C atoms, evolving toward smaller and smaller flats, rings, and carbon-chain radicals (see Fig. 25).
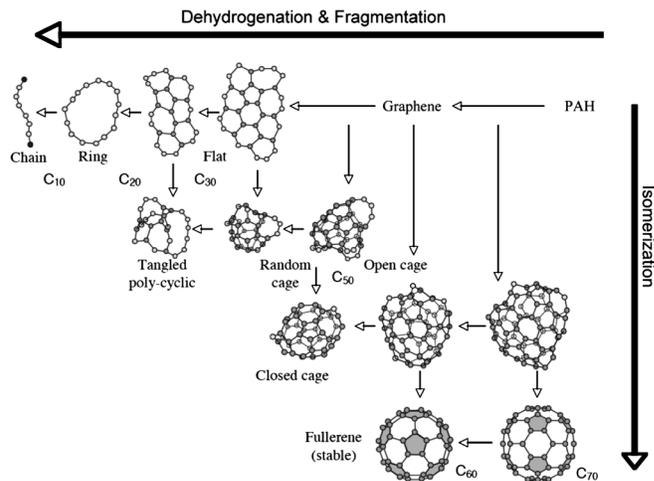

FIG. 25. Schematic representation of top-down interstellar carbon chemistry. The chemical evolution of PAHs in the interstellar medium under the influence of UV photons combines the effects of dehydrogenation and fragmentation with those of isomerization. Fully hydrogenated PAHs, injected by stars into the ISM, are at the top right side. Near bright stars, UV photolysis will preferentially lead to complete H loss (e.g., the "weakest link") and the formation of graphene. Further fragmentation may lead to the formation of flats, rings, and chains. However, this process competes with isomerization to various types of stable intermediaries such as cages and fullerenes.

This fragmentation process competes with isomerization (upon photoabsorption) toward cages and fullerenes. In particular, quantum chemical calculations show that atoms at the zigzag edges of graphene are more labile than those in the armchair structure (Chuvilin *et al.*, 2010). Hence, the former are preferentially lost, leading to the formation of reconstructed edges bearing pentagons, and these pentagons will induce curvature, leading possibly even to closure in the form of C_{60} (Girit *et al.*, 2009; Koskinen, Malola, and Hånakkinen, 2009).

Photolysis of interstellar PAHs is thus thought to be initiated by H loss. However, this process can be balanced by reactions with abundant H. The evolution of the system can then be described by a parameter ψ, describing the balance between these two processes,

$$\psi = \frac{k_H n_H}{k_{UV} p_{dis}(N_c, E)} \simeq 0.2 \frac{n_H}{N_c G_0 p_{dis}(N_c, E)}, \qquad (46)$$

with k_H the reaction rate for dehydrogenated PAHs with atomic H [measured to be $\simeq 10^{-10}$ cm^3 s^{-1} for a number of small PAHs (Snow *et al.*, 1998)], k_{UV} the UV photon absorption rate ($\simeq 8 \times 10^{-10} N_c G_0$ s^{-1}), and p_{dis} the dissociation probability. Infrared radiative cooling, at a rate $k_{ir}(E)$, is the dominant competition for fragmentation and p_{dis} can be written as

$$p_{dis} = \frac{k(E)}{k_{IR}(E) + k(E)}. \qquad (47)$$

The infrared cooling rate is obtained by summing over the emission in all modes [Eq. (4)]. The unimolecular dissociation rate $k(E)$ can be evaluated by considering the mode leading to dissociation in contact with a heat bath at an effective temperature T_e, viz.,

$$k(E) = k_0(T_e) \exp[-E_0/kT_e], \qquad (48)$$

where E_0 is the binding energy of the fragment (Klots, 1989; Tielens, 2005). The preexponential factor k_0 depends on the interaction potential and is set by the entropy change associated with the transition state. The effective temperature T_e is, to first order, given by

$$T_e = T_m - \frac{E_0}{2C_m} = T_m\left(1 - 0.2\frac{E_0}{E}\right), \qquad (49)$$

where the second term is a finite heat bath correction. Limited experiments on a few small PAHs have been used to derive the parameters describing the unimolecular decomposition of PAHs (Jochims et al., 1994; Jochims, Baumgärtel, and Leach, 1999). The results show that the unimolecular dissociation rate (and thus p_{dis}) is a strong function of the internal energy and PAH size (Tielens, 2005). The hydrogen coverage of interstellar PAHs is a sensitive function of ψ and a small increase of ψ can change PAHs from fully hydrogenated to a fully stripped graphene sheet (Le Page, Snow, and Bierbaum, 2003; Tielens, 2005; Berné and Tielens, 2012). Because of the strong dependence on PAH size, for given physical conditions (n_H/G_0), there is a critical PAH size. PAHs smaller than this critical size will be rapidly stripped of their H's, converted into graphene, and then further fragmented into smaller hydrocarbons or isomerized into cages and fullerenes (see Fig. 25).

There is observational evidence for the importance of PAH photolysis in the ISM. The emission of PAHs drops precipitously in regions of ionized gas (Tielens et al., 1993) and this has been generally interpreted as a rapid destruction of the PAHs by the energetic photons (~ 25 eV) rampant in this environment. Indeed, the PAH emission features are generally taken as a tracer of the neutral gas surrounding such HII regions (Hollenbach and Tielens, 1999) and it has been speculated that the destruction of PAHs in these environments is at the origin of the small hydrocarbon radicals observed near the transition from neutral to ionized gas (Pety et al., 2005). Recently, indirect evidence for the importance of isomerization in space was uncovered. Figure 26 summarizes observations of the PAH, fullerene, and dust emission in the reflection nebula NGC 7023 obtained by instruments on the Spitzer Space Telescope and the Herschel Space Observatory. This multitude of data can be analyzed to derive the abundances of the PAHs and C_{60} relative to that of the dust (Sec. II.C). The results show that the PAH abundance decreases from about 10^{-1} to 10^{-2} of the elemental C when approaching the star. In contrast, the C_{60} abundance increases from about 10^{-5} to 10^{-4} of the elemental C close to the star. This different spatial behavior is directly evident in the spectra when comparing the relative strengths of the PAH and C_{60} bands (see Fig. 26). The density and temperature are too low and the UV field too strong in this nebula to build up C_{60} directly through reactions from C atoms with small hydrocarbon radicals. Rather, this is in agreement with the photochemistry outlined above. Indeed, analysis shows that for the conditions in this nebula, 70-C-atom PAHs will become prone to H stripping and C loss can be initiated (Berné and Tielens, 2012). So, it is quite feasible that, while most of the PAHs are destroyed, some of them are converted to C_{60} through this process. The C_{60} formed this way is much more stable to fragmentation than PAHs and can survive very close to the star. So, in this view, the changing C_{60}:PAH ratio
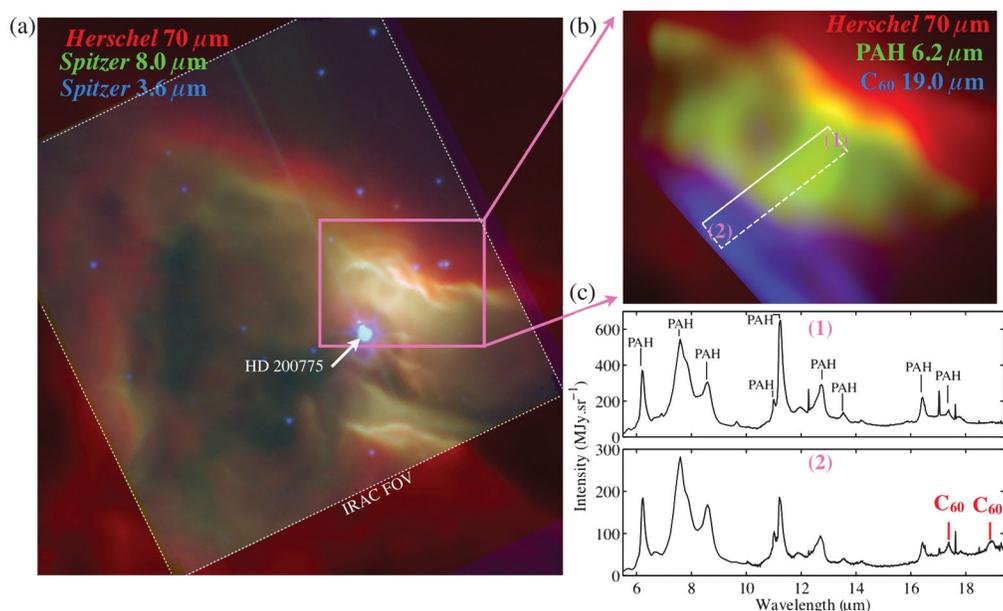

FIG. 26 (color). (a) False color image of the NGC 7023 reflection nebula. Red: Emission by large ($\simeq 1000$ Å) dust grains in radiative equilibrium with the stellar light as traced by PACS and Herschel. Green: The emission of the 7.7 μm PAH CC mode observed with IRAC and Spitzer. Blue: The emission of the 3.3 μm PAH CH mode observed with IRAC and Spitzer. The position of the intermediate-mass young star HD 200775 illuminating the nebula is indicated. (b) Color coded image of the spatial distribution of different compounds in NGC 7023: Red is the dust emission of dust. Green and blue show the emission integrated in the 6.2 μm C-C band of PAHs and in the 18.9 μm C_{60} band observed with infrared spectrograph (Spitzer). The white rectangle shows the region on which the extraction of the PAH and C_{60} abundance was performed. (c) Spitzer IRS midinfrared spectra taken at positions (1) (upper panel) and (2) (lower panel) in (b). The distances from the star at positions (1) and (2) are 35'' and 15'', respectively. The bands of PAHs and C_{60} are labeled in the spectra.

in the ISM is a signature of the UV photolysis of PAHs and observational searches for other fragmentation products (e.g., acetylene, small chains, and hydrocarbon radicals) may elucidate the chemical routes involved in top-down chemistry.

D. PAHs and hot chemistry

PAHs can also be chemically processed by, e.g., H and OH radicals in warm gas in the inner disk and early accretion phases of planet-forming disks around young stellar objects (Kress, Tielens, and Frenklach, 2010). Figure 27 shows the calculated chemical time scale for PAH loss as a function of the temperature of the gas. The adopted pressure is typical for models of protoplanetary disks but the results are not very sensitive to this. PAHs are stable when the dynamical time scale of the system is shorter than this chemical time scale and typically this is the case for temperatures less than 1000 K (Kress, Tielens, and Frenklach, 2010). As this figure indicates, PAHs will be quickly destroyed ($< 10^6$ yr) in the inner regions (< 5 AU) of protoplanetary disks. The processes that created the chondrules in the Solar System likely
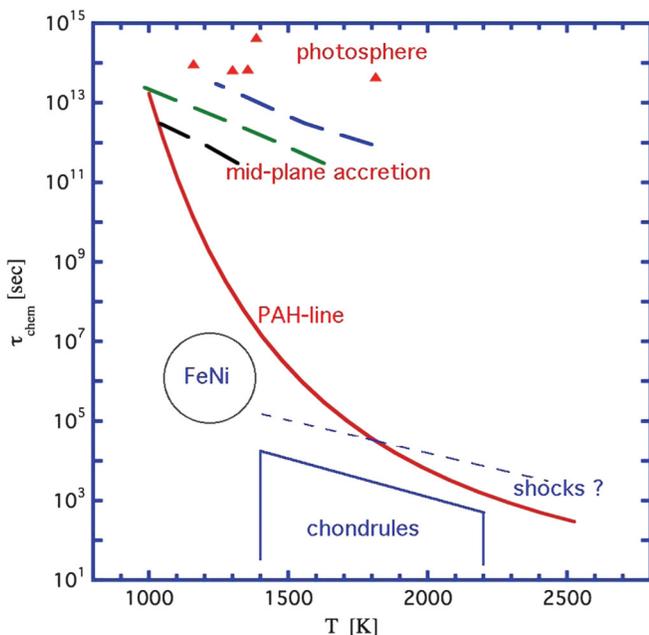

FIG. 27 (color online). Chemical time scale for the breakdown of PAHs through chemical attack by H and OH radicals as a function of the temperature of the gas (Kress, Tielens, and Frenklach, 2010). At a given temperature, PAHs will be stable for time scales below the line marked "PAH line." The colored dashed lines indicate calculated temperatures in the midplane at 1, 2, and 5 AU (between 10^4 and 10^6 yr) for a typical model for the evolution of the early solar nebula (Bell *et al.*, 1997). The box labeled "chondrules" gives the temperature-time regime experienced by chondrules in meteorites as derived from their texture (Connolly *et al.*, 2006). The line labeled "shocks" is an indication that the processes producing chondrules may lead to more extreme conditions without leaving traces in the meteorites. The circle indicates typical conditions derived from analysis of meteoritic FeNi (Meibom *et al.*, 2000). The triangles mark the temperatures derived from *K*-band CO observations (Najita, Carr, and Mathieu, 2003) of a few T-Tauri stars for which accurate isochrone ages have been determined (Bertout, Siess, and Cabrit, 2007).

also drove an interesting chemistry characterized by higher temperatures but shorter time scales. Finally, we note that the gas in the photosphere of the inner disk is also very warm but the PAHs themselves are not (except immediately after UV photon absorption). Hence whether this radical chemistry can play a role in the disk photosphere will need to be assessed.

Small hydrocarbon released by the destruction of PAHs (e.g., C_2H_2) will be partly oxidized to CO (and CO_2) and partly channeled to CH_4 and this is an effective way to drive the CH_4:CO ratio to values more appropriate of "chemical equilibrium" at the temperatures and pressures of the disks. Small, catacondensed PAHs are more susceptible to attack by radicals than larger, pericondensed PAHs, resulting in faster chemical time scales for the former as compared to the latter. Temperatures and pressures are very conducive to chemical growth of PAHs as well and a fraction of the C_2H_2 released by the radical attack on catacondensed PAHs will flow along these routes, growing pericondensed PAHs to ever larger sizes. However, eventually, even the more stable PAHs will typically be destroyed by the radicals. Finally we mention that if the diffusion time scale in the disk is much faster than the oxidation time scale, the hydrocarbons produced this way (the modified PAHs, CH_4, C_2H_2, and their radicals) will spread throughout the disk and be available for a rich organic chemistry.

E. PAH processing by energetic ions

In the interstellar medium, PAH molecules can be processed by energetic ions in shocks, in the hot but tenuous gasses of supernova remnants, and in cosmic rays. Each of these is characterized by very different ion energies ranging from 50 eV/amu in interstellar shocks, ~ 1 keV in supernova remnants, to 100 MeV/nucleon in cosmic rays. In view of the astrophysical interest, dedicated experimental programs have been started and first results published on a few simple PAHs and PAH clusters (Holm *et al.*, 2010; Postma *et al.*, 2010; Reitsma *et al.*, 2012). The results show that interaction of keV ions with PAHs is dominated by charge exchange and electronic stopping and leads to extensive fragmentation into small hydrocarbon ions as well as formation of up to triply charged parent ions. He^{2+} is found to be more effective in destruction than H^+ due to two-electron processes. Elegant experiments involving H^- formation have been used to directly probe the internal energy and potential energy surface involved in the fragmentation (Reistma *et al.*, 2012). Besides H, H_2, and C_2H_2, the loss of $C_3H_3^+$ was also observed, highlighting the importance of isomerization. The cluster studies reveal surprisingly that molecular fragmentation may be just as strong for clusters as monomers interacting with highly charged ions (Holm *et al.*, 2010). These first results illustrate the importance for astrophysics of systematic studies of PAH fragmentation by energetic ions and a characterization of the fragments and their spectroscopic fingerprints.

Detailed models for the processing of PAHs by energetic ions have been developed and applied to astrophysically relevant environments (Micelotta, Jones, and Tielens, 2010a, 2010b, 2011). The results depend strongly on the (adopted) lower limit to the cosmic-ray energy spectrum as well as on the barriers involved in the fragmentation channels which have been estimated based upon UV dissociation studies on small catacondensed PAHs. The results indicate

lifetimes of $\sim 100 \times 10^6$ yr in the ISM. This is much shorter than the injection time scale of PAHs into the ISM by stars ($\simeq 2 \times 10^9$ yr) and implies a rapid formation time scale of PAHs in the ISM. As cosmic-ray fragmentation results in the loss of a few carbon atoms at a time, chemical growth as outlined in Sec. VI.F might be effective to counteract destruction. However, shocks tend to destroy PAHs completely. Hence, this destruction process needs to be counteracted by fresh injection. Possibly this could indicate the importance of shattering in carbonaceous grain-grain collisions in space (Jones, Tielens, and Hollenbach, 1996).

F. Formation of PAHs in molecular clouds

Following the tentative discovery of benzene in the post-AGB objects (Cernicharo *et al.*, 2001; Bernard-Salas *et al.*, 2006), existing models for carbon chemistry (Sec. IV.F) have been extended to study the formation of this first aromatic ring, benzene in circumstellar and interstellar environments. Benzene formation is initiated through reactions of $C_2H_2^+$ with C_2H_2 to $C_4H_3^+$, which then reacts with C_2H_2 leading to closure of the first ring (McEwan *et al.*, 1999). Calculated benzene abundances are always very limited, reaching 10^{-9} at early times but quickly dropping to $\sim 10^{-14}$ at $t > 1$ Myr (McEwan *et al.*, 1999) and build-up of the first aromatic ring is unlikely to be an efficient route toward PAHs in dense cold molecular clouds.

A more promising avenue might be chemical growth of preexisting PAHs in the ISM. A recent combined crossed-beam and theoretical study has shown that naphthalene can be formed in the gas phase via a barrierless and exoergic reaction between the phenyl radical (C_6H_5) and vinylacetylene ($CH_2{=}CH{-}C{\equiv}CH$) involving a van der Waals complex and submerged barrier in the entrance channel (Parker *et al.*, 2012). Likely, this is just one example of a class of rapid reactions between PAH radicals and hydrocarbons. As partially dehydrogenated PAHs could well be abundant in the PDR surfaces of molecular clouds (cf., Sec. VI.C), this opens up channels for PAH growth in the ISM provided the right "feedstock" is available. In that respect, it should be recognized that the breakdown of small PAHs in these zones will provide a reservoir of acetylene as well as small hydrocarbon radicals. These could be further broken down to atomic form but, given the reaction routes outlined above, they may also react with larger PAHs present (cf., Sec. VI.D).

Based upon the ion-molecule chemistry routes outlined above, the formation of PAHs has also been studied for conditions relevant for stellar ejecta in post-AGB winds. These models predict high benzene abundances ($\sim 10^{-6}$) if the gas is C rich, warm ($T \sim 250$ K), dense ($n \sim 10^9$ cm^{-3}), and has a high ionization rate ($\zeta \sim 6 \times 10^{-15}$ s^{-1}) (Woods *et al.*, 2003). These conditions are very restrictive and may not be widely applicable.

G. The interrelationship of PAHs, fullerenes, and diamondoids in space

Thermodynamically, graphite is the preferred state of bulk carbon at low pressures ($\simeq 10$–30 GPa, depending on temperature). High pressures favor diamonds. At very high pressures (> 1000 GPa), carbon may exist preferably in a metallic phase. For nanosized grains, however, stabilities are reversed (Barnard, 2005). Essentially, at the nanoscale, surface contributions to the energy become important and, for an equal number of carbon atoms, the surface-to-volume ratio is lower for diamond structures than for graphenes. The location of the crossover depends on the "molecular" structures considered and the details of the theory employed and is in the range of 10–50 Å (Badziag *et al.*, 1990; Winter and Ree, 1998; Barnard, 2005). At very small sizes ($\lesssim 20$ Å), other carbon forms such as fullerenes and onionlike carbon are thought to be dominant as these forms eliminate surface effects and (dangling) bonds completely at the expense of a small excess amount of strain energy (Barnard, Russo, and Snook, 2003). For even smaller sizes, carbon chains ($< C$ atoms), one-dimensional rings, and flats are favored (Jones, 1999). In this zoo called nanocarbon clusters, a large number of mixed phases can also coexist, including bucky diamonds consisting of diamond cores surrounded by fullerene surface layers, which to the level of accuracy of calculations are equally stable (Barnard, 2005).

In a highly nonequilibrium environment such as space, kinetic effects rather than thermodynamics will however dominate the abundance of carbon species. In the ejecta from carbon-rich asymptotic giant branch stars, PAHs are expected to be the key molecular intermediaries in the conversion of acetylene into (highly graphitic) soot at relevant temperatures and pressures (cf., Sec. VI.A.1) (Frenklach and Feigelson, 1989; Cherchneff, Barker, and Tielens, 1992; Jäger *et al.*, 2009; Cherchneff, 2012). At higher temperatures, the chemical route toward soot involves fullerenelike structures (Pope, Marr, and Howard, 1993; Jäger *et al.*, 2008). In space, fullerenes may also be formed directly in highly carbon-rich and/or hydrogen-poor ejecta such as WC and RCrB stars where dangling bonds may carry a high energy penalty (Sec. VI.B).

Alternatively, it has been suggested that the fullerenes in planetary nebulae are produced by high-velocity, vaporizing collisions among carbonaceous grains (García-Hernández, Kameswara Rao, and Lambert, 2011). Very high-velocity collisions would completely vaporize these grains (Tielens *et al.*, 1994) and chemistry in the cooling, expanding carbon-rich, H-depleted plasma might lead toward fullerenes through processes akin to those occurring in laser vaporization of graphite rods (Kroto *et al.*, 1985). However, at the nanoscale size of interstellar grains, the plumes generated by an impact expand and cool very rapidly and building up of C_{60} from small units might well be inhibited.

In the ISM, observations show that the fullerene abundance increases close to an illuminating star in the photodissociation region, NGC 7023, while the PAH abundance decreases (Berné and Tielens, 2012). The low pressures and temperatures and the high UV fields will inhibit direct gas-phase formation of fullerenes in these environments. Hence, a model has been suggested that forms fullerenes through dehydrogenation of PAHs to form graphene which can fragment further or isomerize toward fullerenes (Sec. VI.C) (Berné and Tielens, 2012) and there are experimental studies supporting the key steps involved—complete PAH dehydrogenation, pentagon formation, and pentagon mobility (albeit it not under the same conditions). The observations of NGC 7023 suggest that this process is not very efficient in

the ISM and does not go to completion even close to the illuminating star. Hence, this is not likely to be the major route toward fullerenes in planetary nebulae.

The planetary nebulae with clear fullerene emission features in their spectra also show the broad 11.3 and $\simeq 30$ μm bands due to SiC and MgS dust grains [cf., the spectra in Cami *et al.* (2010), Bernard-Salas *et al.* (2012), and García-Hernández *et al.* (2012)]. In addition, there is a broad feature between 6 and 9 μm (likely associated with aromatic CC stretches) and a strongly rising dust continuum likely due to amorphous carbon dust. There is no direct evidence for aliphatic groups in these spectra associated either with the molecular component or with the dust. Nevertheless, hydrogenated amorphous carbon grains are sometimes observed in post–asymptotic-giant-branch objects and Micelotta *et al.* (2012) speculated that fullerenes can form through photochemically processing of hydrogenated amorphous carbon nanograins in these planetary nebulae. The starting structures adopted in this study are rather arbitrary and the chemical pathways by necessity very specific. DFT calculations on possible intermediaries might be helpful in delineating the chemical routes and stable fragments. In the interstellar regions such as NGC 7023, the aliphatic component associated with nanostructures is very small ($< 2\%$ of the C) and this route is not likely to be important.

In terrestrial settings, diamondoids are formed under high pressure and temperature in oil deposits. Diamondoids have also been identified in detonation soot and again high temperature, high pressure chemical routes may be indicated. Diamondoids grow through the addition of four carbon atoms, replacing three hydrogen atoms on the starting diamondoid and thus closing the next cage. This is analogous to diamond formation in chemical vapor deposition studies where methyl groups replace a hydrogen on a hydrogen-passivated diamond surface. While this typically produces diamond films, under very specific conditions, nanodiamond films can also be produced. There is experimental evidence that hydrogen is necessary for the growth of diamond nanoparticles to stabilize their surfaces (Raty *et al.*, 2003; Birrell *et al.*, 2006). In space, diamondoids are observed in meteorites and in the inner $\simeq$ 10 AU of some (e.g., two) protoplanetary disks. There is some evidence from the study of solar system materials that most of the diamonds are formed locally and are not inherited from the interstellar medium (Dai *et al.*, 2003). The only occasional presence of CH bonds associated with nanodiamondoids in disks around young stars indicates that the conditions for diamondoid formation in space are very specific and are likely also available only temporarily. In the inner, warm, accretion disk around a newly forming star, CO can be converted into CH_4 and perhaps through x rays or UV photons, methyl radicals can be produced. If a simple diamondoid could chemically "nucleate" then chemical growth might be rapid. Theoretical studies suggest then that, as these diamondoids approach a size of $\simeq 20$ Å, bare, reconstructed diamond surface are energetically preferred over hydrogenated surfaces, thereby stopping further growth (Raty and Galli, 2003). Indeed, a narrow size range around 10–20 Å seems to be a general characteristic of diamondoids irrespective of their formation mechanism and the physical conditions involved. Such nanodiamonds will thus consist of a diamond core surrounded by a few surface layers of sp^2 and sp^3 bonded carbons in onionlike carbon shells and nanosized graphite platelets. Such a core-surface structure has been observed for meteoritic diamonds (Bake *et al.*, 1988) and detonation diamonds (Aleksenskii *et al.*, 1999). The nanodiamonds observed in the disks around HD 97048 and Elias 1 would then be a sign of currently active hydrocarbon chemistry, leading toward diamondoids and diamondoids might also be present in other disks but, in the absence of CH modes, not emitting in the CH stretching region (Jones *et al.*, 2004b). The only IR signature may then be a band at 7.8 μm and it would be prominent as all the energy absorbed by a reconstructed diamondoid will have to be emitted through this mode (Jones *et al.*, 2004b).

From this brief survey, it is clear that the interrelationship of interstellar PAHs, fullerenes, diamondoids, and nanograins is of key importance to understand the chemical evolution of large carbonaceous molecules in space.

VII. THE MOLECULAR INVENTORY OF REGIONS OF PLANET FORMATION

One key goal of astrochemistry is to understand the organic inventory of regions of star and planet formation, in particular, in the habitable zone and the processes that play a role therein. Here we briefly review some relevant observations and their implications of the warm gas in protoplanetary disks associated with T Tauri and Herbig AeBe stars (Sec. VII.A). This is followed by a discussion on the chemical history of cometary ices (Sec. VII.B) and meteorites (Sec. VII.C) in the Solar System in light of the interstellar processes discussed previously.

A. Chemical inventory of the warm, inner regions of protoplanetary disks

Infrared studies revealed an interesting array of abundant molecules in the warm gas of protoplanetary disks and hot cores including CH_4, OH, H_2O, CO, CO_2, C_2H_2, HCN, and HNCO (Najita, Carr, and Mathieu, 2003; Lahuis *et al.*, 2007; Knez *et al.*, 2009). The chemistry of these regions was recently reviewed by Bast *et al.* (2013). Some of these species are readily made on grain surfaces and may be released into the gas phase as ice grains approach the young stellar object (Herbst and van Dishoeck, 2009). However, C_2H_2 and HCN are not typical surface chemistry products; in fact, hydrogen readily attacks the triple bonds of these species on cold grain surfaces. The observed abundances of these species are much higher in these regions than in prestellar cores, so they are unlikely to be the products of gas-phase chemistry in the prestellar core phase that were stored in ice mantles until the hot core phase. Acetylene might be produced by the breakdown of PAHs (Sec. VI.D) in the inner disk followed by rapid diffusion throughout the disk (Kress, Tielens, and Frenklach, 2010). Most likely, though, these species reflect the opening up of reaction channels in the warm gas as x rays and UV photons heat and photodissociate molecular gas in the photosphere of protoplanetary disks (Bast *et al.*, 2013). Photodissociation and ionization break carbon and nitrogen out of their main reservoirs and that initiates a rich chemistry (Najita, Ádámkovics, and Glassgold, 2011). In contrast to the

diffuse ISM (Secs. IV.B and IV.C), in the warm photospheric gas, reactions of atomic C with H_2 will lead to CH_4 and C_2H_2, while reactions of N with intermediate hydrocarbon radicals, CH and CH_2, will produce HCN (see Fig. 15) (Agúndez, Cernicharo, and Goicoechea, 2008). Likewise, N can be rapidly channeled to NH_3 in this warm gas through reactions with H_2 (see Fig. 16).

B. Comets and interstellar ices

Comets are generally thought to contain a pristine record of the prestellar core and/or the quiescent outskirts of the protosolar nebula, and models based upon aggregation of interstellar ice grains have long been in vogue (Greenberg, 1998). However, it is now clear that some solid components (crystalline silicates, calcium-aluminum-inclusion fragments) in comets may well have formed in the inner solar nebula and then diffused outward (Nakamura et al., 2008; Zolensky et al., 2008; MacPherson and Boss, 2011). The chemical inventory of comets provides another window into the early phases of the assemblage of the Solar System and can be used to address this issue. In addition, the organic inventory of comets is of interest since some 10% of the volatile budget may have been delivered by comets during the late bombardment and these molecules are of particular relevance to jump start life on the early Earth. Comets as they approach the Sun will start to sublimate and the molecular composition of the resulting coma can be studied through the rotational spectra in the submillimeter and the fluorescence bands in the visible and near IR. Compilations and references to these studies can be found in Bockelée-Morvan et al. (2000), Crovisier et al. (2004), and Mumma and Charnley (2011).

The chemical inventory of comets is very rich and diverse (see Fig. 28) and we recognize interstellar-ice-like and grain-surface-chemistry-like (Sec. V.E) species, hot-corino-like complex organic molecules (Sec. V.F.1), and disk-photosphere and hot-chemistry-like species (Sec. VII.A). Each of these very different reservoirs, from very different

spatial locations in the solar nebula, and their characteristic chemical processes seem to have contributed to the cometary composition. This heterogeneity implies extensive spatial mixing of the solar nebula. This conclusion is in line with evidence on cometary dust grain components.

On a global scale, abundances in comets of a variety of species are comparable to those in interstellar or circumstellar environments (see Fig. 28), pointing toward a shared chemical origin. However, there are some differences in detail. For the simple ice species, abundances of CO and CO_2 are very similar while H_2CO and CH_3OH (all relative to H_2O) are somewhat more abundant than in typical interstellar ices, indicating a higher atomic H over CO ratio in the accreting gas. This is indicative of formation in a low density environment with a high H:CO ratio and that is incompatible with formation in the solar nebula. Rather it points to a direct inheritance from the prestellar core phase.

Species such as methanol, formaldehyde, formic acid, methyl formate, and formamide are present in comets at abundances quite similar to those in hot corinos (see Fig. 28) (Bockelée-Morvan et al., 2000). However, the deuterium fractionation of these species is typically much less in comets than in hot corinos (see Fig. 28). Thus while the agreement in chemical composition of these species supports a model for comets in terms of aggregated interstellar ice grains, the much lower deuterium fractionation suggests "reequilibration" at much higher temperatures, probably in the inner solar nebula close to the snow line. But the physical conditions there will be very different (much higher densities, temperatures, and lower H:CO ratios in the gas phase) and one would expect that that favors different chemical routes (Sec. V.F.1). For one, hydrogenation would be much less prevalent. Likely, these molecules would undergo a complex sublimation-distillation process whereby interstellar ice grains evaporate when they approach the snow line ($\simeq 4$ AU for the Solar System); the gasses partly equilibrate their deuterium fractionation signature in the warm gas but this would have to happen without affecting their
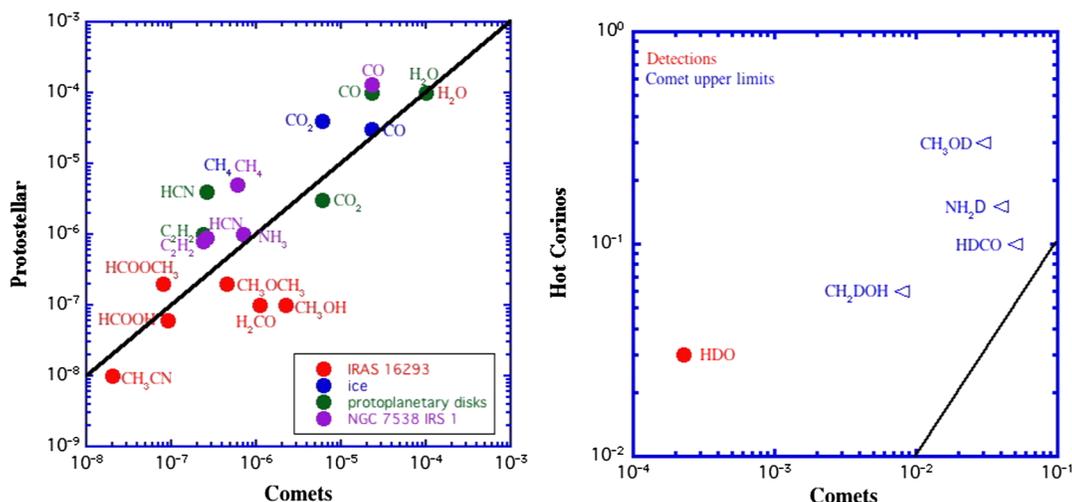

FIG. 28 (color online).   Left: A comparison of the chemical composition of Solar System comets with that measured for regions of low-mass star formation, including the hot corino in IRAS 16293+5050, the hot core in NGC 7538 IRS1, ices in dark clouds, and the photosperes of protoplanetary disks (e.g., IRAS 16293-2422). Right: A comparison of the deuterium fractionations in comets with that measured for regions of low mass star formation. See text for details.

chemical signature. In my view, these two signatures, complex organic inventory and deuterium fractionation, of comets still need to be reconciled.

The observed high abundance of simple hydrocarbons in comets (see Fig. 28) is not an ice chemistry or hot corino signature but rather reflects hot chemistry in the inner nebula. Two models [gas-phase chemistry in hot disk photosphere driven by UV photons or x rays (Sec. VII.A) and photochemical or radical breakdown of large PAHs (Secs, VI.C and VI.D)] have been developed but still need to be evaluated for the cometary organic inventory. In any case, the presence of these species also supports this conclusion of extensive mixing of material in protoplanetary disks (Sec. VII.A).

C. Chemical inventory of meteorites

Carbonaceous meteorites are among the most primitive objects of the Solar System. They exhibit significant carbon contents mostly occurring as insoluble organic matter. The macromolecular structure of this material resembles that of terrestrial kerogen[11] with polycyclic aromatic and heterocyclic aromatic macromolecules with peripheral functional groups such as OH and COOH bridged by alkyl chains and ether linkages (Pizzarello, Cooper, and Flynn, 2006). In addition, carbonaceous meteorites contain numerous soluble organic compounds. Many of these have familiar biochemical counterparts [amino acids, fatty acids, purines, pyrimidines, and sugars (Cronin and Chang, 1993; Botta and Bada, 2002)] but the soluble organic inventory is very rich and includes alcohols, aldehydes, amides, amines, monocarboxylic and dicarboxylic acids, aliphatic and aromatic hydrocarbons, heterocyclic aromatics, hydroxy acids, ketones, phosphonic and sulfonic acids, sulfides, and ethers. Concentrations of the major representatives of these classes vary widely from less than 10 ppm (amines) to tens of ppm (amino acids) to hundreds of ppm (carboxylic acids). The total soluble fraction can be as extreme as 0.3 (e.g., Murchison) in CM[12] carbonaceous meteorites.

In contrast to the Earth's biosphere, meteoritic biomolecules are a diverse and random mixture and this lack of specificity points toward an origin in abiotic processes. Both the soluble and insoluble organic components of meteorites show an anomalous isotopic composition in H, C, and N. In particular, the enrichment in D is evidence for formation at the low temperature characteristics for the cold interiors of dense clouds rather than the warm nebular gas available in the asteroidal formation zone. Hence, it is generally accepted that the initial reservoir was inherited from the molecular cloud from which the Solar System formed and/or the outskirts of the solar nebula and transported to the asteroid belt through ice grains. However, this prestellar origin is overlaid by multiple chemical processes that occurred at various stages during the collapse phase, nebular transport, incorporation into Solar System bodies, and on the meteoritic parent body.

Unraveling this complex chemical history has proven to be a daunting task. A number of general processes have been implicated with varying level of detail and success in explaining characteristic features of the organic record in meteorites. These include Strecker synthesis for amino acids and energetic processing by UV photons and/or energetic ions.

Specifically, the coexistence of soluble organics with clay minerals suggests active chemistry during aqueous (and thermal) alteration of the parent body, such as hydrolysis of nitriles and saturation of double bonds. In particular, Strecker synthesis of amino acids from ketones with ammonia and hydrocyanic acid likely played an important role during this phase (Peltzer and Bada, 1978). Similar processes are thought to have played a role on the early Earth as well (Miller and Urey, 1959). The molecular precursors (H_2CO, NH_3, HCN) are present in interstellar clouds and whether the observed interstellar abundances and isotopic fractionations can plausibly account for the meteoritic abundances is amenable to quantitive study. Similar detailed reaction pathways have been discussed for other soluble organics in an aqueous parent-body environment [cf., Pizzarello, Cooper, and Flynn (2006), and references therein]. Alternatively, some of the organics may have been formed by energetic processing of simple precursor ices and specific experiments have been performed and reaction pathways identified—involving CO_2 in addition to alkyl amine radicals—in support of this hypothesis [cf., Hudson *et al.* (2007)].

The relationship of the other important carbon reservoir in interstellar clouds, PAHs, to the organic inventory of meteorites is unclear. Often, interstellar PAHs are linked to the insoluble macromolecular organic material in meteorites, which consists of condensed aromatic units connected by aliphatic and other chains and with various functional groups attached. However, the aromatic units in meteoritic material are a few rings in size, much smaller than the typical size of interstellar PAHs. Secondary processing by liquid water on the meteorite parent body strongly influences the final molecular architecture of meteoritic macromolecular materials and that has not been fully explored in this context yet. In view of the heterogeneity of this material and the high abundance of nonaromatic moieties and heteroatoms, my guess would be that interstellar PAHs are not involved. Instead, the elemental and isotopic composition of the insoluble organic material in meteorites points toward the energetic processing, probably by energetic ions, of a heterogenous mixture in the form of simple organic ices. The lack of large PAHs in the meteoritic organic record could reflect processing and extensive mixing in the inner solar nebula. However, some large interstellar PAHs should have been brought in to the parent body with the Strecker molecular precursors and the (processed) organic ices unless interstellar PAHs did not participate in ice formation, coagulation, and settling in the solar nebula.

It is clear that we do not yet have a clear grasp of the relative importance of different possible reaction pathways. The Stardust mission has sampled and the Rosetta mission will sample cometary reservoirs and the comparison with meteoritic and interplanetary dust particle organic inventories will hopefully allow us to further disentangle the different chemical origins involved.

---

[11]Organic material occurring in oil shales and derived from living organisms such as algae and other low plant forms (Durand, 1980).

[12]Depending on their composition, carbonaceous meteorites are subdivided into different classes, which is thought to reflect the parent body from which the meteorite was derived. The CM class is characterized by a rich array of organic compounds.

VIII. MOLECULAR TOOLS

This section reviews three examples of the role of molecules in the study of the interstellar medium of galaxies. First, gas-phase molecular formation routes are driven by cosmic-ray ionization and hence molecular observations can be used to probe the distribution of cosmic rays in the Milky Way and other galaxies (Sec. VIII.A). Second, the excitation of molecules is very sensitive to the physical conditions and hence molecules can be used by astronomers as sensitive thermometers and barometers for a variety of circumstellar, interstellar, and nuclear environments (Sec. VIII.B). Third, the high spectral resolution of heterodyne techniques in the (sub) millimeter wavelength region can separate the frequency shifts between isotopologs due to small changes in the moments of inertia. Hence, rotational spectroscopy provides a unique tool to study the enrichment of the elemental evolution of the galaxy (Sec. VIII.C).

A. Molecules tracing cosmic rays

High-energy ($\gtrsim 10$ MeV/nucleon) particles are an important component of the interstellar medium, contributing appreciably to the overall energy density and pressure budget of interstellar gas. Cosmic rays consist mainly of relativistic protons with energies between 10 MeV and 10 GeV, 10% helium, and heavier elements and electrons at about the 1% level. The relative abundances of the elements in the cosmic rays is nonsolar, attesting to the importance of spallation production of light elements and an origin either in material of stellar (likely SN) composition or in sputtered interstellar grains. The interaction of energetic (1–10 GeV) cosmic-ray protons with interstellar gas gives rise to gamma rays with $E_\gamma \gtrsim 50$ MeV through π^0-meson decay emission. Likewise, the interaction of energetic (<1 GeV) electrons with interstellar gas gives rise to gamma rays through bremsstrahlung and inverse Compton scattering. Gamma-ray observations, in combination with interstellar gas surveys, can therefore be used to measure the distribution of cosmic rays (and gas) in the Galaxy (Grenier, Casandjian, and Terrier, 2005). Cosmic rays are tied to the galactic magnetic field and confined to a disk of radius 12 kpc with a thickness of ~2 kpc. Cosmic rays seem to draw their energy from supernovae with an efficiency of about 10% of the kinetic energy of the ejecta. The pressure due to cosmic rays provides support against gravity for the gas in the ISM. Ionization by cosmic rays is an important heating source of gas in dense clouds which are shielded from stellar photons. The low level of ionization produced by cosmic rays also couples the (predominantly) neutral gas to the magnetic field. Hence, cosmic rays influence the star formation process as they provide both thermal and magnetic support against gravity.

Low energy ($\simeq 10$–100 MeV) cosmic rays are important for the heating and ionization of interstellar gas. Unfortunately, for energies below 1 GeV/nucleon, the cosmic-ray flux is difficult to measure within the heliosphere due to strong modulation by the solar wind. The low energy interstellar cosmic-ray flux can, however, be measured through molecular observations (Sec. IV.H). These indirect measurements imply a primary cosmic-ray ionization rate in the diffuse ISM of $\zeta_{CR} \simeq 2 \times 10^{-16}$ (H atom)$^{-1}$ s^{-1} (McCall et al., 2003; Le Petit,

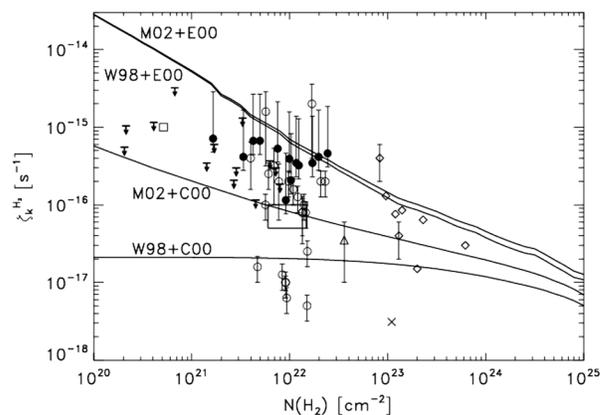

FIG. 29. The cosmic-ray ionization rate as a function of the shielding column of H$_2$ (Padovani, Galli, and Glassgold, 2009). The curves are models with different extrapolations for the low energy cosmic-ray ion (M02, W98) and electron (E00, C00) fluxes. The observational data have been determined from molecular observations and are summarized in Padovani, Galli, and Glassgold (2009).

Roueff, and Herbst, 2004). Inside dense clouds, the cosmic-ray ionization rate is measured to be much smaller [$\zeta_{CR} \simeq 3 \times 10^{-17}$ (H atom)$^{-1}$ s^{-1}] (Caselli, Walmsley, Terzieva, and Herbst, 1998; van der Tak and van Dishoeck, 2000; Hezareh et al., 2008). As cosmic rays penetrate molecular clouds, their energy drops due to ionization of gas. As low energy cosmic rays are constantly replenished by the slowing down of more energetic cosmic rays, this drop is characterized by a power-law behavior rather than exponential attenuation (see Fig. 29) (Padovani, Galli, and Glassgold, 2009). The parameters describing this power law strongly depend on the adopted initial spectrum. The much higher ionization rate observed in diffuse clouds as compared to dense clouds implies that the cosmic-ray spectrum keeps rising below 100 MeV/nucleon. This comparison also seems to suggest that ionization by energetic electrons might be important. The penetration of cosmic rays into molecular cloud cores can also be affected by magnetic fields through magnetic focusing and mirroring effects (Cesarsky and Volk, 1978; Padoan and Scalo, 2005; Padovani and Galli, 2011). Mirroring is particularly relevant for dense cores and reduces the cosmic-ray ionization rate by a factor depending on the core's mass-to-flux ratio. For reasonable values this factor is $\simeq 3$ (Padovani and Galli, 2011).

Cosmic rays with energies below $\simeq 10^{15}$ eV/nucleon are thought to be accelerated by supernova remnants. While there is no direct evidence for this, this would imply localized regions of much higher cosmic-ray ionization rates near associations of massive stars. Observations with the Fermi Gamma Ray Space Telescope suggest much higher cosmic-ray fluxes for clouds near supernova remnants (Thompson, Baldini, and Uchiyama, 2012). Model studies show that, depending on the minimum energy of the cosmic rays produced by supernova remnants, molecular clouds associated with supernova remnants will experience an ionization rate which can be many orders of magnitude higher than the average rate in molecular clouds (Becker et al., 2011; Schuppan et al., 2012). Observations of H$_3^+$ along sight lines through molecular cloud material associated with the supernova remnant, IC 443, imply ionization rates of $\simeq 2 \times 10^{-15}$

considerably above rates for other directions (Indriolo *et al.*, 2010). Likewise, observations of HCO^+ and DCO^+ toward the W51C, another supernova remnant interacting with a molecular cloud, imply cosmic-ray ionization rates a factor of 100 larger than typical for molecular clouds (Ceccarelli *et al.*, 2011). These studies exemplify the power of molecular studies for studying the acceleration and propagation of cosmic rays in the interstellar medium and Atacama Large Millimeter and Submillimeter Array (ALMA) will be able to fully open up this field of "cosmic-ray" studies in galaxies.

B. Molecules measuring physical conditions

The multitude of rotational lines due to a myriad of molecular species, each with their own characteristic critical density and excitation energy, provide a powerful tool to study the physical properties of molecular clouds. Figure 30 provides an overview of often used molecular diagnostics. Rotational lines of CO probe regions with densities of $\simeq 3 \times 10^3 \, J^3 \, cm^{-3}$ and temperatures of $\simeq 3 \, J^2$. Thus, the 1-0 and 2-1 transitions are well suited for the study of general molecular clouds. The mid-J CO transitions, such as $J = 7\text{-}6$, are sensitive to lukewarm gas near young stellar objects or in photodissociation regions, while 14-13 and higher transitions generally trace warm gas associated with shocks. CO rovibrational emission in the fundamental (4.6 μm) or overtone region (2.3 μm) of the spectrum originates from dense, hot gas near a star or in a planet-forming disk. Because of the larger dipole moment, rotational lines of trace species such as CS, HCN, and HCO^+ have higher critical densities than CO and thus probe dense cores in molecular clouds. Molecular hydrogen has only electric-quadrupole transitions and its low-J rotational transitions are readily excited in low-density gas. However, the large energy spacing of H_2 requires high temperatures. Near-IR, rovibrational transitions of H_2 are indicative of warm (~ 1000K), dense ($\sim 10^4 \, cm^{-3}$) gas in shocks (or UV-pumped gas). The metastable and nonmetastable inversion lines of NH_3 are excited in medium density gas (10^4–$10^6 \, cm^{-3}$), while the far-IR rotational transitions of hydrides such as H_2O probe warm and denser (10^6–$10^9 \, cm^{-3}$) gas.
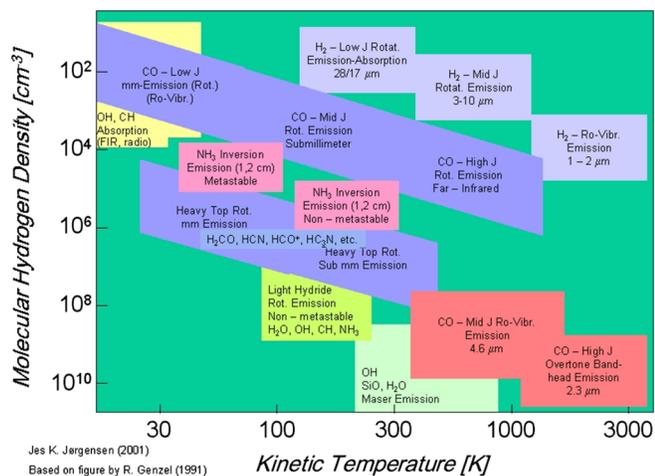

FIG. 30 (color online). An overview of the molecular lines and the range of physical conditions in molecular clouds for which they are effective probes. Adapted from Genzel, 1991 and provided by Jess Jorgenson.
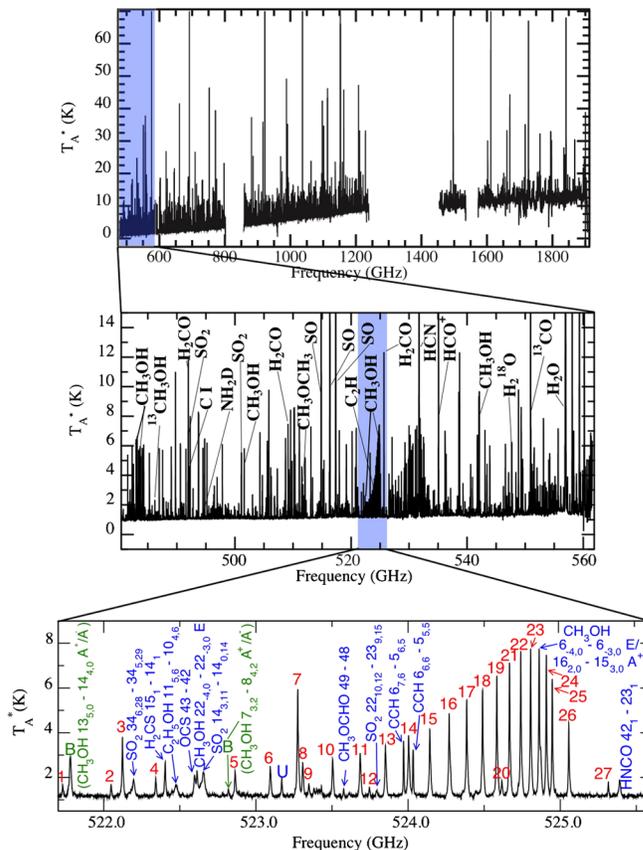

FIG. 31 (color online). HIFI spectral survey of the Orion KL region. Top panel: The complete spectral scan (490 GHz to 1.9 THz) reveals the rich line forest. There are some 10^5 lines in this spectrum. Middle panel: A zoom in on the 490–530 GHz spectral range with some of the stronger lines identified. Bottom panel: The 522.5–525.5 GHz range shows velocity-resolved lines. The numbered lines are CH_3OH lines used in the analysis of the temperature structure of the region. Figure courtesy of Ted Bergin and the HIFI/HEXOS Key Program.

Spectral surveys provide a convenient way to use molecules as thermometers and barometers of the emitting gas. With the advent of broadband heterodyne receivers, large-scale spectral surveys covering a wide spectral range have come within reach. This has been one of the strong points of the HIFI instrument onboard the Herschel Space Observatory. As an example, Fig. 31 shows the rich spectrum of the region of massive star formation in Orion obtained by HIFI/Herschel (Bergin *et al.*, 2010). At the lower frequencies, this survey is essentially line confusion limited and there are an estimated 10^5 lines in this spectrum. At the high spectral resolution ($R = 5 \times 10^5$, $\Delta v \simeq 0.5$ km/s), the lines are resolved and this allows us to distinguish the different spatial components present in the beam. Within a subband, the lines are internally well calibrated and thus allow a detailed and reliable analysis and this makes line surveys such an excellent tool to determine the physical conditions.

1. Methanol as a probe

Methanol provides an excellent example of the use of molecules as a density and temperature probe. Torsional motion associated with the internal rotation of the methyl

group with respect to the OH bond can couple to other degrees of freedom and, as a result, the abundant methanol molecule has numerous and often very strong rotational transitions spanning the range from the far infrared to the millimeter range. Methanol is therefore commonly considered a "weed" molecule that has to be rigorously "rooted out" when searching for molecular complexity. However, by the same token, methanol is also a powerful probe of the physical conditions in the gas and the structure of the region. In their study of the KL nebula, the HIFI-HEXOS team selected some 40 CH_3OH lines from the 400 lines present in HIFI bands 1a and 4b that are isolated and hence readily and reliably interpreted. Kama *et al.* (2010) and the HIFI-CHESS team made a similar study of the intermediate mass protostars OMC 2 FIR 4. These CH_3OH lines are confined within a small frequency range but cover a wide range in upper-state energy with minimal line blending. These lines originate from the compact ridge, one of the two hot core sources present in the beam. Assuming optically thin emission, observed line intensities can be transformed into column densities in the upper level,

$$N_u = \frac{1.94 \times 10^3}{A_{ul}} \left(\frac{T_B \Delta v}{\text{K km s}^{-1}}\right)\left(\frac{\nu_{ul}}{\text{GHz}}\right)^2 \text{ cm}^{-2}, \qquad (50)$$

with T_B, ν_{ul}, A_{ul}, and Δv the brightness temperature, frequency, Einstein A transition probability, and line width of the transition, respectively. The rotational diagram, plotting derived column densities divided by the statistical weight as a function of upper level energy, provides a powerful tool for the analysis of line data (Goldsmith and Langer, 1999). In local thermodynamic equilibrium, level populations are given by

$$\frac{N_u}{N_{\text{mol}}} = \frac{g_u \exp[-E_u/kT_x]}{\Phi(T_x)}, \qquad (51)$$

with T_x the excitation temperature, and N_{mol} the abundance, and the data for Orion KL are shown in Fig. 32 (Wang *et al.*, 2011). Because the partition function Φ is not very sensitive to the temperature, in LTE the level populations will span up a straight line with a slope given by the excitation temperature and the intercept provides the total column density of the molecule.

There are various pitfalls in the use of this diagram. Particular care has to be taken when the emission is optically thick, the molecule is subthermally excited, and/or the region has temperature and density gradients (Goldsmith and Langer, 1999). Also at low densities, high-lying levels can be suprathermally excited, giving rise to positive curvature in rotational diagrams which is easily mistaken for the presence of multiple temperature components (Leung, 1978; Neufeld, 2012). Yet the ease of use has made this diagram a first step in any analysis of the physical conditions of molecular regions. The rotation diagram method delivers good results for dense regions such as Orion KL. In general, though, the assumptions of LTE and low opacity may not be met for a range of lines. In such cases, the statistical equilibrium equations describing the level populations, including the effects of collisions and radiative transfer, have to be solved numerically (see Sec. VIII.B.2).
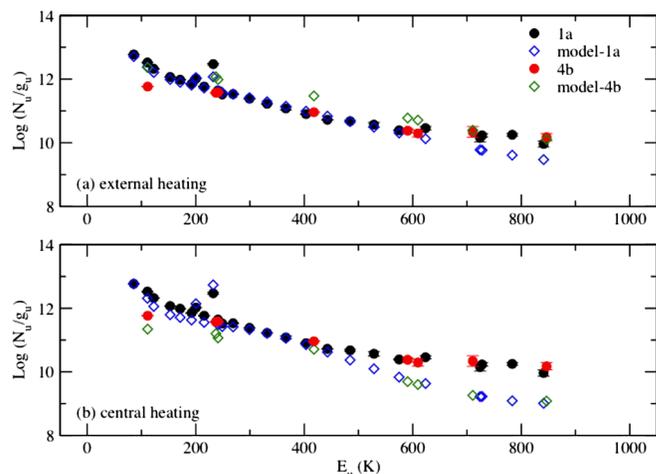
FIG. 32 (color online). The rotational diagram derived column densities divided by the statistical weight as a function of upper level energy. Here this is illustrated for the CH_3OH lines in HIFI bands 1a and 4b (see Fig. 31). Optically thin lines characterized by a single excitation temperature would produce a straight line with a slope given by the temperature and an intercept proportional to the total column density. The results are compared to model calculations for a clump heated from the inside (bottom) and from the exterior (top). Model calculated line intensities have been treated in the same way as the observations to produce this diagram. From Wang *et al.*, 2011.

For the HIFI survey of the compact ridge, detailed model calculations are compared to the observations in the rotational diagram, where the model intensities have been treated in the same way as the observational data (see Fig. 32). There has been a long-standing debate whether the compact ridge (and the hot core) in Orion are externally heated by a nearby protostar as the very narrow linewidth and high temperature and column density are inconsistent with normal, centrally heated star-forming cores (Blake *et al.*, 1987; Kaufman, Hollenbach, and Tielens, 1998). An external heating source is strongly supported by the HIFI methanol study (see Fig. 32) as the data show a much better agreement with an externally heated clump than with an internal heat source (Wang *et al.*, 2011). As revealed by interferometric studies, a similar situation pertains to the prototypical hot core, the Orion hot core, which is located nearby and also seems to be heated from the outside (Zapata, Schmid-Burgk, and Menten, 2011).

2. Molecular data

The unbiased spectral surveys undertaken by the HIFI key programs have returned $\sim 10^5$ spectral lines for sources such as Orion KL and the galactic center (see Fig. 31). The large bandwidths and high sensitivities of ALMA guarantee that essentially all sources will show many lines from many molecules at every observation. Note also that the ALMA interferometer will have more than 10 times higher angular resolution than Herschel or ground-based single dish telescopes and will resolve the line emission regions of many sources, producing three-dimensional data cubes (with radial velocity as the third dimension). Analysis of this overwhelming data set presents a daunting task. Many of these lines are due to a few abundant simple molecules associated with hot

cores, notably CH_3OH, or shocks (e.g., SO_2). Astronomers will have to turn into gardeners and carefully remove these weeds without affecting the weak emission lines due to less abundant, but potentially very important, chemical diagnostic flowers. Of course, really the weeds give as much insight as the flowers (Sec. VIII.B) and should be carefully handled. This analysis requires dedicated programs on laboratory measurements and theoretical calculations of molecular line frequencies. Once available, because so many lines over such a wide spectral range are measured, an iterative process can be started that corrects the observed spectra with estimated line intensities of these weeds. This will require collisional excitation data that improve on column density estimates of excited levels derived from rotational diagram analysis (Sec. VIII.B). These collisional rates will have to be calculated using quantum chemical methods to determine the potential energy surfaces in the interaction for astrophysically relevant species with the predominant collision partners, atomic or molecular hydrogen and helium. These calculations have to be validated with experimental studies on (selected) state-to-state excitations.

All of these data, spectroscopy and molecular excitation rates, then have to be made available to the community through open access databases. For spectroscopy the Cologne database for molecular spectroscopy (CDMS, http://www.astro.uni-koeln.de/cdms/), the Jet Propulsion Laboratory (JPL) catalog (http://spec.jpl.nasa.gov/), and user-friendly splatalogue (http://splatalogue.net/) are geared toward radio and (sub)millimeter rotational transitions. Molecular excitation data are available through the Observatoire de Paris rovibrational collisional excitation database BASECOL (http://basecol.obspm.fr/) and the Leiden Atomic and Molcular database (LAMDA; http://home.strw.leidenuniv.nl/~moldata/). The RATRAN radiative transfer program is accessible through http://home.strw.leidenuniv.nl/~moldata/radex.html.

One challenging aspect to these efforts is that, while these areas serve great needs for the astronomical community, research on frequencies or oscillator strength of molecular transitions is not forefront science within molecular physics. Likewise, investigating chemical reactions involving astronomically relevant species is not central to modern chemistry. Funding support for activities in these areas is therefore not high priority within these communities. As a result, international agencies such as the European Southern Observatory or at the European Union level through the Framework Program will have to take the lead in organizing, coordinating, and funding these scientific activities.

As no single institute or even country covers all of the relevant physics and chemistry expertise inhouse, this process requires an international self-organization of the field. This has started already in Europe, initially supported by the European Union through its Marie Curie Program. Several countries have also organized astrochemistry networks, notably France in terms of the Physique Chimie du Milieu Interstellaire (PCMI) program of the Centre National de la Recherche Scientifique (CNRS), The Netherlands with the Dutch Astrochemistry Network of the Netherlands Organisation for Scientific Research (NWO), and in Germany through the Physics of the Interstellar Medium Priority Program of the German Research Foundation (DFG). The Virtual Atomic and Molecular Data Center (VAMDC; http://www.vamdc.org/) provides e-infrastructure for the exchange of atomic and molecular data. Increased cooperation between these different efforts at the transnational level will be instrumental in guiding this research and allowing us to draw the full scientific benefit of the large investments in telescope and instrumentation hardware of modern ground-based, airborne, and space-based observatories. Unfortunately, at present, there is no good funding mechanism for a sustained, multinational program.

C. Isotope studies

Isotopes are generally formed by distinct nucleosynthetic processes that operate efficiently under very different conditions and therefore they originate from very different stars. For example, interstellar ^{12}C is mainly produced by the triple alpha process and injected into the interstellar medium by intermediate mass asymptotic giant branch stars. Asymptotic giant branch stars can also be an important source of ^{13}C but likely this isotope has a large contribution from thermonuclear runaway processes during a nova explosion (Tielens, 1990). For the oxygen isotopes, ^{16}O is produced mainly during He and Ne burning in massive stars and injected into the interstellar medium during core-collapse (type II) supernova explosions. The origin of the two other isotopes (^{17}O and ^{18}O) is less clear as cool bottom processing and hot bottom burning may influence the isotopic ratios produced during nucleosynthesis on the asymptotic giant branch and these processes are not well understood. Explosive hydrogen burning in nova readily produces ^{17}O. ^{17}O may also have an important contribution from intermediate-mass giant stars while ^{18}O may be produced by very massive stars during the Wolf-Rayet phase (Henkel and Mauersberger, 1993).

Molecular isotope studies of stellar ejecta and of isotope gradients in the galaxy provide a window to the processes that are key to understanding the evolution of the elemental enrichment of the interstellar medium by stars, including stellar nucleosynthesis as well as dispersal and mixing into the interstellar medium. Such studies are presently in their infancy but ALMA will truly open up the universe to detailed studies of the distribution of isotopes. In the past, galactic elemental abundance gradients have been searched for using, e.g., CO and its isotopes (Wouterloot et al., 2008), but those studies are hampered by the high optical depth in the main isotope and detailed (and uncertain) radiative transfer models are required in the interpretation. While these studies show that the galactic center may have a low ^{18}O:^{17}O ratio, the scatter in the individual measurements is as large as any putative gradient (Wouterloot et al., 2008). For species such as CN, the hyperfine components can be used to assess the effects of optical depth directly and this has, for example, been used in a study of the C-isotope ratios in the ejecta of asymptotic giant branch stars (Milam, Woolf, and Ziurys, 2009) and the C- and N-isotope ratios in the interstellar medium (Adande and Ziurys, 2012).

The effects of chemical processes in the ISM have to be recognized and accounted for in studies of the elemental enrichment (cf., Sec. IV.E). It can then be advantageous to

select species that are formed through "high temperature" processes such as CH^+ (cf., Sec. IV.I.4) to probe the true isotopic composition of interstellar gas (Ritchey, Federman, and Lambert, 2011). Of course, this probes only the gaseous isotope ratio of interstellar medium. As isotopes may well originate from distinct stellar sources [cf., Anders and Zinner (1993), Amari (2010), and Nittler and Gaidos (2012)] and these may be characterized by very different dust condensation efficiencies, gas-phase molecules may not reflect the true isotopic composition of the interstellar medium. Such isotopic sequestering may also affect the isotopic abundance ratio measured in warm regions as different stardust compounds may be released at different rates by chemical processing (cf., Sec. VI.D). This effect could also have had some effect on the carbon and oxygen isotopes in Solar System materials. Mostly, observed variations in the isotopic composition of, e.g., C and N in different Solar System bodies are, however, attributed to the effects of chemical processing at low temperatures albeit that the chemical pathways are very much unclear (Aleon, 2010; Matrajt *et al.*, 2012; Wirström *et al.*, 2012). Fractionation of oxygen isotopes in Solar System bodies (meteoritic components such as calcium-aluminum-rich inclusions, planets, solar wind) are particularly interesting as they represent mixing between an ^{16}O-rich and an ^{16}O-poor reservoir. This has long been interpreted as evidence for pollution of the solar nebula by ejecta from a nearby supernova, an event which is also thought to be responsible for the presence of life ^{26}Al in the solar nebula (Cameron and Truran, 1977; MacPherson *et al.*, 2005). However, more recently a chemical origin has grown in popularity for these O-isotope variations. In this, O-isotope variations are attributed to CO-isotope-selective dissociation (cf., Sec. IV.E) in the upper layers of the disk photosphere which leads to an enrichment of the heavier isotopes in the gas phase. This oxygen may then rapidly be converted into ^{16}O-poor water available for reaction with oxide grains. Simple models have been developed in which this process is quite efficient in the outer solar nebula and this material can then be transported inward for reactions with solids in the planet-forming regions of the disk (Young, 2007). Of course, there are many processes involved which are poorly or not at all understood but the chemical aspects of it are open to direct testing. In particular, the effects of CO self-shielding can be probed in diffuse clouds (Sec. IV.E) (Visser, van Dishoeck, and Black, 2009). Infrared rovibrational absorption line studies can also study CO-isotope fractionation in some fortuitously well-oriented protoplanetary disks around young stellar objects and, while such studies are difficult to interpret uniquely, first results are encouraging (Smith *et al.*, 2009). With ALMA it may also become possible to directly test the general relevance of the "SN-pollution" scenario in detail as well as by searching, for example, for isotopic variations in aluminum or more generally for any SN-specific isotopes in protoplanetary disks.

Finally, it should be noted that analysis of individual stardust grains, isolated from meteorites, can provide direct insight in the nucleosynthetic processes of stars and the elemental enrichment of the interstellar medium for those elements that participate in the dust formation process or that are trapped in the stardust birth site by, e.g., ion implantation

(Anders and Zinner, 1993; Amari, 2010; Nittler and Gaidos, 2012).

IX. EPILOGUE

This review highlights the progress made, observationally and theoretically, in understanding the organic inventory, the origin and evolution, and the role of molecules in the ISM of galaxies over the past 20 years. We now know that molecules are everywhere, the organic inventory is very diverse, and molecules play an important role in many processes that drive the evolution of the interstellar medium. Eddington lamented, after the discovery of the first diatomic molecules, that "atoms are physics but molecules are chemistry." As a physicist, he regretted the loss of innocence when simple physical formulas have to give way to the complex chemical solutions of a molecular universe. However, the multitude of rotational, vibrational, and electronic transitions of molecules provide unique opportunities to probe the Universe in much greater detail than ever before and we have just started to explore this.

With the Herschel Space Telescope still gathering data, the Atacama Large Millimeter Array (ALMA), and also the newly expanded Karl G. Jansky Very Large Array (JVLA) starting up, the Stratospheric Observatory For Infrared Astronomy (SOFIA) taking off, and the James Webb Space Telescope (JWST) mission on the horizon, the future for molecular astrophysics looks bright. Over the next decade we can expect to make great strides in addressing the three grand challenges of molecular astrophysics: (1) What is the organic inventory of space, in particular, in regions of star and planet formation and how does that relate to the prebiotic origin of life, (2) what is the role of molecules in the evolution of the universe, (3) how can we use molecules to study the Universe? Specifically, the HIFI/Herschel data on simple hydrides can be mined for the initiating steps in gas-phase chemistry. ALMA will provide an unprecedented wealth of molecular data that can be used to probe the physical conditions in regions of star formation. In addition, ALMA can be expected to address the interaction of gas and grains both in hot cores and hot corinos near protostars where ice mantle products evaporate and initiate a rich chemistry and in prestellar cores where accretion takes place and nonthermal evaporation mechanisms feedback to the gas-phase molecular inventory. SOFIA is specifically geared toward probing the evolution of PAHs in space and determining their role in the physics and chemistry of photodissociation regions near massive stars. This will be an essential step in understanding in a quantitative way the dominant heating of interstellar gas and the role of PAHs in the ionization balance. Both of these are key to understanding the interaction of massive stars with their environment and the global evolution of the interstellar medium of galaxies. JWST has the spatial resolution to probe the chemical evolution of these species in protoplanetary disks on the 10 AU scale. In addition, with our insights on the role of PAHs in the ISM developed through SOFIA, such JWST observations give us great insight into the physical structure of, in particular, the disk photosphere. SOFIA and JWST will also form a great tandem in addressing the organic inventory in the habitable zone of terrestrial planet formation around nearby young stars. SOFIA can probe the spatial distribution at the AU level of simple but key molecules,

C_2H_2, CH_4, NH_3, HCN, and H_2O through high spectral resolution, while JWST will have the spatial resolution to do this on a 10 AU scale. And perhaps, we might even dream of solving the 80-year-old riddle of the diffuse interstellar bands as we start to better understand the complex pathways of interstellar chemistry. My hunch is that the DIB carriers are lurking somewhere in the trickle-down chemical pathways. I am convinced that would open up new and unexplored views on the organic inventory of space and the processes that play a role therein. In contrast to Eddington, in many ways, I would say that with molecules the Universe is only now truly opening up.

ACKNOWLEDGMENTS

REFERENCES

Abouaf-Marguin, K., A. M. Vasserot, C. Pardanaud, and X. Michaut, 2007, Chem. Phys. Lett. **447**, 232.

Abouaf-Marguin, L., A. M. Vasserot, C. Pardanaud, and X. Michaut, 2009, Chem. Phys. Lett. **480**, 82.

Adams, N. G., et al., 1991, J. Chem. Phys. **94**, 4852.

Adande, G. R., and L. M. Ziurys, 2012, Astrophys. J. **744**, 194.

Agúndez, M., J. Cernicharo, and J. R. Goicoechea, 2008, Astron. Astrophys. **483**, 831.

Aikawa, Y., et al., 2001, Astrophys. J. **552**, 639.

Aleksenskii, A. E., et al., 1999, Phys. Solid State **41**, 668.

Aleon, J., 2010, Astrophys. J. **722**, 1342.

Al-Halabi, A., and E. F. van Dishoeck, 2007, Mon. Not. R. Astron. Soc. **382**, 1648.

Allamandola, L. J., D. M. Hudgins, C. W. Bauschlicher, Jr., and S. R. Langhoff, 1999, Astron. Astrophys. **352**, 659.

Allamandola, L. J., S. A. Sandford, and G. J. Valero, 1988, Icarus **76**, 225.

Allamandola, L. J., A. G. G. M. Tielens, and J. R. Barker, 1989, Astrophys. J. Suppl. Ser. **71**, 733.

Amari, S., 2010, in *The 10th International Symposium on Origin of Matter and Evolution of Galaxies*, AIP Conf. Proc. No. 1269 (AIP, New York), p. 27.

Amiaud, L., et al., 2006, J. Chem. Phys. **124**, 094702.

Amiaud, L., et al., 2008, Phys. Rev. Lett. **100**, 056101.

Anders, E., and E. Zinner, 1993, Meteoritics **28**, 420.

Andersson, S., A. Al-Halabi, G. J. Kroes, and E. F. van Dishoeck, 2006, J. Chem. Phys. **124**, 064715.

Apkarian, V. A., and N. Schwentner, 1999, Chem. Rev. **99**, 1481.

Arasa, C., S. Andersson, H. Cuppen, G. J. van Dishoeck, and G. J. Kroes, 2011, J. Chem. Phys. **134**, 164503.

Armus, L., et al., 2007, Astrophys. J. **656**, 148.

Atkinson, R., et al., 2004, Atmos. Chem. Phys. **4**, 1461.

Bachmann, M., W. Wiese, and K.-H. Homann, 1996, *Twenty-Sixth Symposium on Combustion* (Combustion Institute, Pittsburgh), p. 2259.

Badziag, P., W. S. Verwoerd, W. P. Ellis, and N. R. Greiner, 1990, Nature (London) **343**, 244.

Bake, D. F., et al., 1988, Nature (London) **332**, 611.

Bally, J., and W. D. Langer, 1982, Astrophys. J. **255**, 143.

Balog, R., P. Cicman, N. C. Jones, and D. Field, 2009, Phys. Rev. Lett. **102**, 073003.

Barker, J. R., L. J. Allamandola, and A. G. G. M. Tielens, 1987, Astrophys. J. **315**, L61.

Barnard, A. S., 2005, Diamonds & Related Mat. **15**, 285.

Barnard, A. S., S. P. Russo, and I. K. Snook, 2003, J. Chem. Phys. **118**, 5094.

Bast, J., F. Lahuis, E. F. van Dishoeck, and A. G. G. M. Tielens, 2013, Astron. Astrophys. **551**, A118.

Bauschlicher, C. W., 1998, Astrophys. J. **509**, L125.

Bauschlicher, Jr., C. W., E. Peeters, and L. J. Allamandola, 2008, Astrophys. J. **678**, 316.

Bauschlicher, Jr., C. W., E. Peeters, and L. J. Allamandola, 2009, Astrophys. J. **697**, 311.

Becker, J. K., J. H. Black, M. Safarzadeh, and F. Schuppan, 2011, Astrophys. J. Lett. **739**, L43.

Bell, K. R., P. M. Cassen, H. H. Klahr, and T. Henning, 1997, Astrophys. J. **486**, 372.

Benderskii, A. V., and C. A. Wight, 1996, J. Chem. Phys. **104**, 85.

Bergin, E. A., J. Alves, T. Huard, and C. J. Lada, 2002, Astrophys. J. **570**, L101.

Bergin, E. A., D. R. Ciardi, C. J. Lada, J. Alves, and E. A. Lada, 2001, Astrophys. J. **557**, 209.

Bergin, E. A., and M. Tafalla, 2007, Annu. Rev. Astron. Astrophys. **45**, 339.

Bergin, E. A., et al., 2005, Astrophys. J. **627**, L33.

Bergin, E. A., et al., 2010, Astron. Astrophys. **521**, L20.

Bernard-Salas, J., et al., 2012, Astrophys. J. **757**, 41.

Bernard-Salas, J., et al., 2006, Astrophys. J. **652**, L29.

Berné, O., and A. G. G. M. Tielens, 2012, Proc. Natl. Acad. Sci. U.S.A. **109**, 401.

Berné, O., et al., 2007, Astron. Astrophys. **469**, 575.

Bernstein, M. P., S. A. Sandford, and L. J. Allamandola, 1996, Astrophys. J. **472**, L127.

Bernstein, M. P., S. A. Sandford, L. J. Allamandola, S. Chang, and M. A. Scharberg, 1995, Astrophys. J. **454**, 327.

Bertie, J. E., and J. P. Devlin, 1983, J. Chem. Phys. **78**, 6203.

Bertout, C., L. Siess, and S. Cabrit, 2007, Astron. Astrophys. **473**, L21.

Biennier, L., F. Salama, L. Allamandola, and J. Scherer, 2003, J. Chem. Phys. **118**, 7863.

Bierbaum, V. M., 2011, Proc. Int. Astron. Union **7**, 383 [*The Molecular Universe*, Proceedings of the IAU Symposium 280, Vol. 7 (Cambridge University Press, Cambridge, England, 2011), p. 383].

Biham, O., I. Furman, V. Pirronello, and G. Vidali, 2001, Astrophys. J. **553**, 595.

Birrell, J., J. E. Gerbi, O. A. Auciello, and J. A. Carlisle, 2006, J. Phys. Condens. Matter **18**, S1771.

Black, J. H., and E. F. van Dishoeck, 1987, Astrophys. J. **322**, 412.

Blake, G. A., E. C. Sutton, C. R. Masson, and T. G. Phillips, 1987, Astrophys. J. **315**, 621.

Bockelée-Morvan, D., *et al.*, 2000, Astron. Astrophys. **353**, 1101.

Boersma, C., L. J. Allamandola, and R. Rubin, 2012, Astrophys. J. (in press).

Boersma, C., S. Hony, and A. G. G. M. Tielens, 2006, Astron. Astrophys. **447**, 213.

Boersma, C., *et al.*, 2009a, Astron. Astrophys. **502**, 175.

Boersma, C., *et al.*, 2009b, Astrophys. J. **690**, 1208.

Boersma, C., *et al.*, 2010, Astron. Astrophys. **511**, A32.

Bohme, D. K., 1992, Chem. Rev. **92**, 1487.

Bonfanti, M., R. Martinazzo, G. F. Tantardini, and A. Ponti, 2007, J. Phys. Chem. C **111**, 5825.

Boogert, A. C. A., and P. Ehrenfreund, 2004, in *Astrophysics of Dust*, ASP Conference Series (Astronomical Society of the Pacific, San Francisco), Vol. 309, p. 547.

Boogert, A. C. A., A. G. G. M. Tielens, C. Ceccarelli, A. M. S. Boonman, E. F. van Dishoeck, J. V. Keane, D. C. B. Whittet, and T. de Graauw, 2000, Astron. Astrophys. **360**, 683.

Boogert, A. C. A., *et al.*, 2000, Astron. Astrophys. **353**, 349.

Boogert, A. C. A., *et al.*, 2008, Astrophys. J. **678**, 985.

Botta, O., and J. L. Bada, 2002, Surv. Geophys. **23**, 411.

Bottinelli, S., *et al.*, 2004, Astrophys. J. **617**, L69.

Bouwman, J., *et al.*, 2011, Astron. Astrophys. **529**, A46.

Braunstein, M., and J. W. Duff, 2000, J. Chem. Phys. **112**, 2736.

Bréchignac, P., and T. Pino, 1999, Astron. Astrophys. **343**, L49.

Bringa, E. M., and R. E. Johnson, 2004, Astrophys. J. **603**, 159.

Buch, V., and J. P. Devlin, 1993, J. Chem. Phys. **98**, 4195.

Buntkowsky, G., *et al.*, 2008, Z. Phys. Chem. **222**, 1049.

Buss, Jr., R. H., A. G. G. M. Tielens, and T. P. Snow, 1991, Astrophys. J. **372**, 281.

Cameron, A. G. W., and J. W. Truran, 1977, Icarus **30**, 447.

Cami, J., J. Bernard-Salas, E. Peeters, and S. E. Malek, 2010, Science **329**, 1180.

Cami, J., F. Salama, J. Jiménez-Vicente, G. A. Galazutdinov, and J. Krełowski, 2004, Astrophys. J. **611**, L113.

Cami, J., P. Sonnentrucker, P. Ehrenfreund, and B. H. Foing, 1997, Astron. Astrophys. **326**, 822.

Cardelli, J. A., D. M. Meyer, M. Jura, and B. D. Savage, 1996, Astrophys. J. **467**, 334.

Caselli, P., T. I. Hasegawa, and E. Herbst, 1993, Astrophys. J. **408**, 548.

Caselli, P., T. I. Hasegawa, and E. Herbst, 1998, Astrophys. J. **495**, 309.

Caselli, P., F. van der Tak, C. Ceccarelli, and A Bacmann, 2003, Astron. Astrophys. **403**, L37.

Caselli, P., C. M. Walmsley, M. Tafalla, L. Dore, and P. C. Myers, 1999, Astrophys. J. **523**, L165.

Caselli, P., C. M. Walmsley, R. Terzieva, and E. Herbst, 1998, Astrophys. J. **499**, 234.

Caselli, P., *et al.*, 2008, Astron. Astrophys. **492**, 703.

Caselli, P., *et al.*, 2010, Astron. Astrophys. **521**, L29.

Caselli, P., *et al.*, 2012, Astrophys. J. Lett. **759**, L37.

Casolo, S., R. Martininazzo, M. Bonfanti, and G. F. Tantardini, 2009, J. Phys. Chem. A **113**, 14 545.

Cazaux, S., and A. G. G. M. Tielens, 2002, Astrophys. J. **575**, L29.

Cazaux, S., and A. G. G. M. Tielens, 2004, Astrophys. J. **604**, 222.

Cazaux, S., *et al.*, 2003, Astrophys. J. **593**, L51.

Ceccarelli, C., 2008, Proc. Int. Astron. Union **4**, 79 [*Organic Matter in Space*, Proceedings of the IAU Symposium 251, Vol. 4 (Cambridge University Press, Cambridge, England, 2008), p. 79].

Ceccarelli, C., L. Loinard, A. Castets, A. G. G. M. Tielens, E. Caux, B. Lefloch, and C. Vastel, 2001, Astron. Astrophys. **372**, 998.

Ceccarelli, C., *et al.*, 2011, Astrophys. J. Lett. **740**, L4.

Cernicharo, J., and R. Bachiller, 2011, *The Molecular Universe*, Proceedings of the IAU Symposium 280 (Cambridge University Press, Cambridge, England).

Cernicharo, J., *et al.*, 2001, Astrophys. J. **546**, L123.

Cesaroni, R., 2005, Proc. Int. Astron. Union **1**, 59 [*Massive Star Birth: A Crossroads of Astrophysics*, Proceedings of the IAU Symposium 227, Vol. 1 (Cambridge University Press, Cambridge, England, 2005), p. 59].

Cesarsky, C. J., and H. J. Volk, 1978, Astron. Astrophys. **70**, 367.

Chang, Q., H. M. Cuppen, and E. Herbst, 2006, Astron. Astrophys. **458**, 497.

Charnley, S. B., 1998, Astrophys. J. **509**, L121.

Charnley, S. B., 2001, Astrophys. J. **562**, L99.

Charnley, S. B., A. G. G. M. Tielens, and T. J. Millar, 1992, Astrophys. J. **399**, L71.

Charnley, S. B., A. G. G. M. Tielens, and S. D. Rodgers, 1997, Astrophys. J. **482**, L203.

Charnley, S. B., and S. B. Rodgers, 2009, *Bioastronomy 2007: Molecules, Microbes and Extraterrestrial Life* (Astronomical Society of the Pacific, San Francisco), Vol. 420, p. 29.

Chehrouri, M., *et al.*, 2011, Phys. Chem. Chem. Phys. **13**, 2172.

Cherchneff, I., 2011, EAS Publications Series **46**, 177.

Cherchneff, I., 2012, arXiv:1111.6809.

Cherchneff, I., J. R. Barker, and A. G. G. M. Tielens, 1992, Astrophys. J. **401**, 269.

Cherchneff, I., Y. H. Le Teuff, P. M. Williams, and A. G. G. M. Tielens, 2000, Astron. Astrophys. **357**, 572.

Chiar, J. E., P. A. Gerakines, D. C. B. Whittet, Y. J. Pendleton, A. G. G. M. Tielens, A. J. Adamson, and A. C. A. Boogert, 1998, Astrophys. J. **498**, 716.

Chlewicki, G., *et al.*, 1987, Astron. Astrophys. **173**, 131.

Chuvilin, A., U. Kaiser, E. Bichoutskaia, N. A. Besley, and A. N. Khlobystov, 2010, Nat. Chem. **2**, 450.

Codella, C., *et al.*, 2010, Astron. Astrophys. **518**, L112.

Collier, W. B., G. Ritzhaupt, and J. P. Devlin, 1984, J. Phys. Chem. **88**, 363.

Congiu, E., *et al.*, 2012, Astrophys. J. Lett. **750**, L12.

Connolly, H. C., S. J. Desch, R. D. Ash, and R. H. Jones, 2006, in *Meteorites and the Early Solar System II* (University of Arizona Press, Tucson), p. 383.

Cook, D. J., and R. J. Saykally, 1998, Astrophys. J. **493**, 793.

Cronin, J. R., and S. Chang, 1993, in *The Chemistry of Lifes Origin*, edited by J. M. Greenberg, C. X. Mendoza-Gmez, and V. Pirronello (Kluwer, Dordrecht), p. 209.

Crovisier, J., 1998, Faraday Discuss. **109**, 437.

Crovisier, J., *et al.*, 2004, Astron. Astrophys. **418**, 1141.

Cuppen, H., and E. Herbst, 2005, Mon. Not. R. Astron. Soc. **361**, 565.

Cuppen, H. M., and E. Herbst, 2007, Astrophys. J. **668**, 294.

Cuppen, H. M., S. Ioppolo, C. Romanzin, and H. Linnartz, 2010, Phys. Chem. Chem. Phys. **12**, 12 077.

Cuppen, H. M., E. F. van Dishoeck, E. Herbst, and A. G. G. M. Tielens, 2009, Astron. Astrophys. **508**, 275.

Dai, Z. R., *et al.*, 2003, Lun. Plan. Sci. **34**, 1121.

Dalgarno, A., and R. A. McCray, 1973, Astrophys. J. **181**, 95.

Dame, T. M., *et al.*, 1987, Astrophys. J. **322**, 706.

Danilychev, A. V., and V. A. Apkarian, 1993, J. Chem. Phys. **99**, 8617.

Dartois, E., K. Demyk, L. d'Hendecourt, and P. Ehrenfreund, 1999, Astron. Astrophys. **351**, 1066.

Demyk, K., *et al.*, 1998, Astron. Astrophys. **339**, 553.

Desert, F.-X., F. Boulanger, and J. L. Puget, 1990, Astron. Astrophys. **237**, 215.

D'Hendecourt, L. B., L. J. Allamandola, F. Baas, and J. M. Greenberg, 1982, Astron. Astrophys. **109**, L12.

Dickey, J. M., and R. W. Garwood, 1989, Astrophys. J. **341**, 201.

di Francesco, J., et al., 2007, *Protostars and Planets V*, edited by B. Reipurth, D. Jewitt, and K. Keil (University of Arizona Press, Tucson), p. 17.

Dislaire, V., et al., 2012, Astron. Astrophys. **537**, A20.

Douglas, A. E., 1977, Nature (London) **269**, 130.

Du, F., and B. Parise, 2011, Astron. Astrophys. **530**, A131.

Du, F., B. Parise, and P. Bergman, 2012, Astron. Astrophys. **538**, A91.

Du, F., B. Parise, and A. G. G. M. Tielens, 2012 (unpublished).

Dulieu, F., 2011, Proc. Int. Astron. Union **7**, 405 [*The Molecular Universe*, Proceedings of the IAU Symposium 280, Vol. 7 (Cambridge University Press, Cambridge, England, 2011), p. 405].

Dulieu, F., et al., 2010, Astron. Astrophys. **512**, A30.

Durand, B., 1980, *Kerogen: Insoluble Organic Matter from Sedimentary Rocks* (Editions Technip, Paris).

Dworkin, J. P., J. Seb Gillette, M. P. Bernstein, S. A. Sandford, L. J. Allamandola, J. E. Elsila, D. Ryan McGlothlin, and R. N. Zare, 2004, Adv. Space Res. **33**, 67.

Egan, M. P., et al., 1998, Astrophys. J. **494**, L199.

Ehrenfreund, P., J. Cami, E. Dartois, and B. H. Foing, 1997, Astron. Astrophys. **317**, L28.

Ehrenfreund, P., E. Dartois, K. Demyk, and L. D'Hendecourt, 1998, Astron. Astrophys. **339**, L17.

Ehrenfreund, P., and B. H. Foing, 1996, Astron. Astrophys. **307**, L25.

Eichelberger, B., T. P. Snow, C. Barckholz, and V. Bierbaum, 2007, Astrophys. J. **667**, 1283.

Elitzur, M., and W. D. Watson, 1978, Astrophys. J. **222**, L141.

Farkas, L., and H. Sachsse, 1933, Z. Phys. Chem. Abt B **23**, 1.

Fayolle, E. C., et al., 2011, Astrophys. J. Lett. **739**, L36.

Federman, S. R., 1982, Astrophys. J. **257**, 125.

Federman, S. R., et al., 1994, Astrophys. J. **424**, 772.

Felenbok, P., and E. Roueff, 1996, Astrophys. J. **465**, L57.

Felker, P. M., and A. H. Zewail, 1983, Chem. Phys. Lett. **102**, 113.

Flower, D. R., G. Pineau des Forêts, and C. M. Walmsley, 2006, Astron. Astrophys. **449**, 621.

Foing, B. H., and P. Ehrenfreund, 1994, Nature (London) **369**, 296.

Fontani, F., et al., 2012, Mon. Not. R. Astron. Soc. **423**, 2342.

Fontani, F., et al., 2011, Astron. Astrophys. **529**, L7.

Fournier, J., J. Deson, C. Vermeil, and G. C. Pimentel, 1979, J. Chem. Phys. **70**, 5726.

Frenklach, M., D. W. Clary, W. C. Gardiner, and S. E. Stein, 1985, in *Twentieth Symposium (International) on Combustion* (The Combustion Institute, Pittsburgh), p. 887.

Frenklach, M., and E. D. Feigelson, 1989, Astrophys. J. **341**, 372.

Friedel, D. N., and S. L. Widicus Weaver, 2011, Astrophys. J. **742**, 64.

Friedel, D. N., and S. L. Widicus Weaver, 2012, Astrophys. J. Suppl. Ser. **201**, 17.

Friedman, S. D., et al., 2011, Astrophys. J. **727**, 33.

Fu, Y., J. Szczepanski, and N. C. Polfer, 2012, Astrophys. J. **744**, 61.

Fuchs, G. W., et al., 2009, Astron. Astrophys. **505**, 629.

Fulare, J., M. Jacobi, and J. P. Maier, 1993, Chem. Phys. Lett. **211**, 227.

Fulare, J., D. Lessen, P. Freivogel, and J. P. Maier, 1993, Nature (London) **366**, 439.

Furuya, K., Y. Aikawa, N. Sakai, and S. Yamamoto, 2011, Astrophys. J. **731**, 38.

Galazutdinov, G. A., F. A. Musaev, A. V. Bondar, and J. Krełowski, 2003, Mon. Not. R. Astron. Soc. **345**, 365.

Galliano, F., S. C. Madden, A. G. G. M. Tielens, E. Peeters, and A. P. Jones, 2008, Astrophys. J. **679**, 310.

García-Hernández, D. A., N. Kameswara Rao, and D. L. Lambert, 2011, Astrophys. J. **729**, 126.

García-Hernández, D. A., et al., 2012, Astrophys. J. **760**, 107.

Garrod, R. T., 2008, Astron. Astrophys. **491**, 239.

Garrod, R. T., A. I. Vasyunin, D. A. Semenov, D. S. Wiebe, and Th. Henning, 2009, Astrophys. J. **700**, L43.

Garrod, R. T., S. L. W. Weaver, and E. Herbst, 2008, Astrophys. J. **682**, 283.

Geballe, T. R., F. Najarro, D. F. Figer, B. W. Schlegelmilch, and D. de La Fuente, 2011, Nature (London) **479**, 200.

Genzel, R., 1991, in *The Physics of Star Formation and Early Stellar Evolution*, edited by C. J. Lada and N. D. Kylafis (Kluwer, Dordrecht), p. 155.

Geppert, W. D., et al., 2004, Astrophys. J. **609**, 459.

Geppert, W., et al., 2006, Faraday Discuss. **133**, 177.

Gerakines, P. A., M. H. Moore, and R. L. Hudson, 2001, J. Geophys. Res. **106**, 33 381.

Gerakines, P. A., W. A. Schutte, and P. Ehrenfreund, 1996, Astron. Astrophys. **312**, 289.

Gerakines, P. A., et al., 1999, Astrophys. J. **522**, 357.

Gerin, M., et al., 2010a, Astron. Astrophys. **518**, L110.

Gerin, M., et al., 2010b, Astron. Astrophys. **521**, L16.

Gerin, M., et al., 2012, Proc. Roy. Soc. (to be published).

Gibb, E. L., D. C. B. Whittet, A. C. A. Boogert, and A. G. G. M. Tielens, 2004, Astrophys. J. Suppl. Ser. **151**, 35.

Gibb, E. L., et al., 2000, Astrophys. J. **536**, 347.

Gielen, C., J. Cami, J. Bouwman, E. Peeters, and M. Min, 2011, Astron. Astrophys. **536**, A54.

Girit, C., et al., 2009, Science **323**, 1705.

Godard, B., E. Falgarone, and G. Pineau Des Forêts, 2009, Astron. Astrophys. **495**, 847.

Goldsmith, P. F., and W. D. Langer, 1999, Astrophys. J. **517**, 209.

Goldsmith, P. F., et al., 2008, Astrophys. J. **680**, 428.

Gonzalez, C. A., T. C. Allison, and F. Louis, 2001, J. Phys. Chem. A **105**, 11 034.

Gotkis, Y., et al., 1993, J. Phys. Chem. **97**, 12 282.

Goto, M., et al., 2003, Astrophys. J. **589**, 419.

Goumans, T. P. M., 2012 (private communication).

Goumans, T. P. M., S. Andersson, 2010, Mon. Not. R. Astron. Soc. **406**, 2213.

Goumans, T. P. M., J. Kästner, 2011, J. Phys. Chem. A **115**, 10 767.

Govers, T., L. Mattera, and G. Scoles, 1980, J. Chem. Phys. **72**, 5446.

Gredel, R., S. Lepp, A. Dalgarno, and E. Herbst, 1989, Astrophys. J. **347**, 289.

Gredel, R., E. F. van Dishoeck, and J. H. Black, 1993, Astron. Astrophys. **269**, 477.

Gredel, R., et al., 2011, Astron. Astrophys. **530**, A26.

Greenberg, J. M., 1998, Astron. Astrophys. **330**, 375.

Greenberg, J. M., et al., 2000, Astrophys. J. **531**, L71.

Grenier, I. A., J.-M. Casandjian, and R. Terrier, 2005, Science **307**, 1292.

Grim, R. J. A., and L. B. D'Hendecourt, 1986, Astron. Astrophys. **167**, 161.

Guillois, O., G. Ledoux, and C. Reynaud, 1999, Astrophys. J. **521**, L133.

Gumenchuk, 2007, Ph.D. (Tech University Munich).

Güthe, F., M. Tulej, M. V. Pachkov, and J. P. Maier, 2001, Astrophys. J. **555**, 466.

Habart, E., F. Boulanger, L. Verstraete, C. M. Walmsley, and G. Pineau des Forêts, 2004, Astron. Astrophys. **414**, 531.

Hama, T., N. Watanabe, A. Kouchi, and M. Yokoyama, 2011, Astrophys. J. Lett. **738**, L15.

Hasegawa, T. L., E. Herbst, and C. M. Leung, 1992, Astrophys. J. Suppl. Ser. **82**, 167.

Henkel, C., and R. Mauersberger, 1993, Astron. Astrophys. **274**, 730.

Herbig, G. H., 1995, Annu. Rev. Astron. Astrophys. **33**, 19.

Herbst, E, and E. F. van Dishoeck, 2009, Annu. Rev. Astron. Astrophys. **47**, 427.

Herbst, E., 1981, Nature (London) **289**, 656.

Herbst, E., 2005, ESA Special Publication **577**, 205.

Herbst, E., 2009, *Submillimeter Astrophysics and Technology: A Symposium Honoring Thomas G. Phillips* (Astronomical Society Pacific, San Francisco), Vol. 417, p. 153.

Herbst, E., and W. Klemperer, 1973, Astrophys. J. **185**, 505.

Herbst, E., and V. I. Shematovich, 2003, Astrophys. Space Sci. **285**, 725.

Hezareh, T., M. Houde, C. McCoey, C. Vastel, and R. Peng, 2008, Astrophys. J. **684**, 1221.

Hidaka, H., M. Watanabe, A. Kouchi, and N. Watanabe, 2009, Astrophys. J. **702**, 291.

Hidaka, H., *et al.*, 2004, Astrophys. J. **614**, 1124.

Hily-Blant, P., *et al.*, 2010, Astron. Astrophys. **521**, L52.

Hirahara, Y., *et al.*, 1992, Astrophys. J. **394**, 539.

Hiraoka, K., *et al.*, 1998, Astrophys. J. **498**, 710.

Hirota, T., M. Ohishi, and S. Yamamoto, 2009, Astrophys. J. **699**, 585.

Hirota, T., T. Sakai, N. Sakai, and S. Yamamoto, 2011, Astrophys. J. **736**, 4.

Hixson, H. G., *et al.*, 1992, J. Chem. Phys. **97**, 753.

Hobbs, L. M., *et al.*, 2009, Astrophys. J. **705**, 32.

Hollenbach, D., M. J. Kaufman, E. A. Bergin, and G. J. Melnick, 2009, Astrophys. J. **690**, 1497.

Hollenbach, D., M. J. Kaufman, D. Neufeld, M. Wolfire, and J. R. Goicoechea, 2012, Astrophys. J. **754**, 105.

Hollenbach, D., and C. F. McKee, 1979, Astrophys. J. Suppl. Ser. **41**, 555.

Hollenbach, D., and C. F. McKee, 1989, Astrophys. J. **342**, 306.

Hollenbach, D. J., and A. G. G. M. Tielens, 1999, Rev. Mod. Phys. **71**, 173.

Hollenbach, D. J., and E. E. Salpeter, 1971, Astrophys. J. **163**, 155.

Holm, A. I. S., *et al.*, 2010, Phys. Rev. Lett. **105**, 213401.

Hony, S., 2002, Ph.D. (University of Amsterdam).

Hony, S., C. Van Kerckhoven, E. Peeters, A. G. G. M. Tielens, D. M. Hudgins, and L. J. Allamandola, 2001, Astron. Astrophys. **370**, 1030.

Horn, A., *et al.*, 2004, Astrophys. J. **611**, 605.

Hornekaer, L., A. Baurichter, V. V. Petrunin, D. Field, and A. C. Luntz, 2005, Proc. Int. Astron. Union **1**, 337 [*Astrochemistry: Recent Successes and Current Challenges*, Proceedings of the IAU Symposium 231, Vol. 1 (Cambridge University Press, Cambridge, England, 2005), p. 337].

Hornekaer, L., *et al.*, 2003, Science **302**, 1943.

Hornekaer, L., *et al.*, 2005, J. Chem. Phys. **122**, 124701.

Hornekaer, L., *et al.*, 2006, Phys. Rev. Lett. **97**, 186102.

Howard, J. B., *et al.*, 1992, Carbon **30**, 1183.

Howard, J. B., *et al.*, 1991, Nature (London) **352**, 139.

Hudgins, D. M., C. W. Bauschlicher, Jr., and L. J. Allamandola, 2005, Astrophys. J. **632**, 316.

Hudson, R. L., *et al.*, 2007, in "*Bioastronomy 2007: Molecules, Microbes, and Extraterrestrial Life*", edited by K. J. Meech *et al.* (ASP, San Francisco), Vol. 420, p. 157.

Hudson, R. L., *et al.*, 2008, in *The Solar System Beyond Neptune*, edited by M. A. Barucci, H. Boehnhardt, D. P. Cruikshank, and A. Morbidelli (University of Arizona Press, Tucson), p. 507.

Hugo, E., O. Asvany, and S. Schlemmer, 2009, J. Chem. Phys. **130**, 164302.

Indriolo, N., *et al.*, 2010, Astrophys. J. **724**, 1357.

Ioppolo, S., *et al.*, 2008, Astrophys. J. **686**, 1474.

Ioppolo, S., Y. van Boheemen, H. M. Cuppen, E. F. van Dishoeck, and H. Linnartz, 2011, Mon. Not. R. Astron. Soc. **413**, 2281.

Irle, S., G. Zheng, M. Elstner, and K. Morokuma, 2003, Nano Lett. **3**, 1657.

Jäger, C., F. Huisken, H. Mutschke, I. L. Jansa, and T. Henning, 2009, Astrophys. J. **696**, 706.

Jäger, C., H. Mutschke, and T. Henning, 2011, EAS Publications Series **52**, 245.

Jäger, C., H. Mutschke, T. Henning, and F. Huisken, 2008, Astrophys. J. **689**, 249.

Joblin, C., 2003, Semaine de l'Astrophysique Francaise Report No. SF2A-2003, p. 175.

Joblin, C., D. Toublanc, P. Boissel, and A. G. G. M. Tielens, 2002, Mol. Phys. **100**, 3595.

Jochims, H. W., H. Baumgärtel, and S. Leach, 1999, Astrophys. J. **512**, 500.

Jochims, H. W., E. Ruhl, H. Baumgartel, S. Tobita, and S. Leach, 1994, Astrophys. J. **420**, 307.

Johnson, R. E., B. Donn, V. Pirronello, and B. Sundqvist, 1991, Astrophys. J. **379**, L75.

Jones, A. P., A. G. G. M. Tielens, and D. J. Hollenbach, 1996, Astrophys. J. **469**, 740.

Jones, A. P., *et al.*, 2004a, Astron. Astrophys. **416**, 235.

Jones, A. P., *et al.*, 2004b, in *Astrophysics of Dust*, edited by A. N. Witt *et al.* (Astrophysical Society Pacific, San Francisco), Vol. 309, p. 589.

Jones, O. P., 1999, J. Chem. Phys. **110**, 5189.

Joulain, K., E. Falgarone, G. Pineau des Forets, and D. Flower, 1998, Astron. Astrophys. **340**, 241.

Jura, M., 1975, Astrophys. J. **197**, 575.

Kahane, C., *et al.*, 1984, Astron. Astrophys. **137**, 211.

Kaifu, N., *et al.*, 2004, Publ. Astron. Soc. Jpn. **56**, 69.

Kama, M., *et al.*, 2010, Astron. Astrophys. **521**, L39.

Katz, N., I. Furman, O. Biham, V. Pirronello, and G. Vidali, 1999, Astrophys. J. **522**, 305.

Kaufman, M. J., D. J. Hollenbach, and A. G. G. M. Tielens, 1998, Astrophys. J. **497**, 276.

Kawakita, H., *et al.*, 2006, Astrophys. J. **643**, 1337.

Keady, J. J., D. N. B. Hall, and S. T. Ridgway, 1988, Astrophys. J. **326**, 832.

Keane, J., 2002, Ph.D. (University of Groningen).

Keller, L. D., *et al.*, 2008, Astrophys. J. **684**, 411.

Kiviniemi, T, *et al.*, 2004, J. Chem. Phys. **121**, 1839.

Klots, C. E., 1989, J. Chem. Phys. **93**, 1176.

Knauth, D. C., B.-G. Andersson, S. R. McCandliss, and H. Warren Moos, 2004, Nature (London) **429**, 636.

Knez, C., J. H. Lacy, N. J. Evans II, E. F. van Dishoeck, and M. J. Richter, 2009, Astrophys. J. **696**, 471.

Kokkin, D. L., *et al.*, 2008, Astrophys. J. **681**, L49.

Koskinen, P., S. Malola, and H. Hånakkinen, 2009, Phys. Rev. B **80**, 073401.

Krätschmer, W., L. D. Lamb, K. Fostiropoulos, and D. R. Huffman, 1990, Nature (London) **347**, 354.

Krelowski, J., and G. A. H. Walker, 1987, Astrophys. J. **312**, 860.

Krełowski, J., G. Galazutdinov, and R. Kołos, 2011, Astrophys. J. **735**, 124.

Krełowski, J., *et al.*, 1999, Astron. Astrophys. **347**, 235.

Krełowski, J., *et al.*, 2010, Astrophys. J. Lett. **714**, L64.

Kress, M. E., A. G. G. M. Tielens, and M. Frenklach, 2010, Adv. Space Res. **46**, 44.

Kroto, H. W., J. R. Heath, S. C. Obrien, R. F. Curl, and R. E. Smalley, 1985, Nature (London) **318**, 162.

Kurtz, S., R. Cesaroni, E. Churchwell, P. Hofner, and C. M. Walmsley, 2000, *Protostars and Planets* (University of Arizona Press, Tucson), Vol. 4, p. 299.

Kuzmin, M. V., and A. A. Stuchebrukhov, 1985, Chem. Phys. Lett. **119**, 556.

Kwok, S., and Y. Zhang, 2011, Nature (London) **479**, 80.

Lahuis, F., *et al.*, 2007, Astrophys. J. **659**, 296.

Langhoff, S., 1996, J. Phys. Chem. **100**, 2819.

Larsson, M., W. D. Geppert, and G. Nyman, 2012, Rep. Prog. Phys. **75**, 066901.

Lattelais, M., F. Pauzat, Y. Ellinger, and C. Ceccarelli, 2009, Astrophys. J. **696**, L133.

Leach, S., 1987, in *Polycyclic Aromatic Hydrocarbons and Astrophysics*, edited by A. Léger, L. d'Hendecourt, and N. Boccara (Reidel, Dordrecht), p. 89.

Le Bourlot, J., 1991, Astron. Astrophys. **242**, 235.

Lee, S. T., T. S. Reighart, and S. V. Olesik, 1996, Fluid Phase Equilib. **122**, 223.

Leger, A., L. D'Hendecourt, and D. Defourneau, 1989, Astron. Astrophys. **216**, 148.

Lemaire, J. L., *et al.*, 2010, Astrophys. J. Lett. **725**, L156.

Le Page, V., T. P. Snow, and V. M. Bierbaum, 2001, Astrophys. J. Suppl. Ser. **132**, 233.

Le Page, V., T. P. Snow, and V. M. Bierbaum, 2003, Astrophys. J. **584**, 316.

Le Page, V., T. P. Snow, and V. M. Bierbaum, 2009, Astrophys. J. **704**, 274.

Le Petit, F., E. Roueff, and E. Herbst, 2004, Astron. Astrophys. **417**, 993.

Lepp, S., and A. Dalgarno, 1988, Astrophys. J. **324**, 553.

Leung, C. M., 1978, Astrophys. J. **225**, 427.

Leung, C. M., E. Herbst, and W. F. Huebner, 1984, Astrophys. J. Suppl. Ser. **56**, 231.

Lewis, R. S., T. Ming, J. F. Wacker, E. Anders, and E. Steel, 1987, Nature (London) **326**, 160.

Linnartz, H., *et al.*, 2010, Astron. Astrophys. **511**, L3.

Lipshtat, A., and O. Biham, 2003, Astron. Astrophys. **400**, 585.

Lis, D., G. A. Blake, E. Herbst, 2006, in *Astrochemistry: Recent Successes and Current Challenges*, Proceedings of the IAU Symposium 231 (Cambridge University Press, Cambridge, England).

Lis, D. C., *et al.*, 2010, Astron. Astrophys. **521**, L26.

Liseau, R., *et al.*, 2012, Astron. Astrophys. **541**, A73.

Liszt, H., and R. Lucas, 2001, Astron. Astrophys. **370**, 576.

Liszt, H., and R. Lucas, 2002, Astron. Astrophys. **391**, 693.

Liszt, H., R. Lucas, and J. Pety, 2005, Proc. Int. Astron. Union **1**, 187 [*Astrochemistry: Recent Successes and Current Challenges*, Proceedings of the IAU Symposium 231, Vol. 1 (Cambridge University Press, Cambridge, England, 2005), p. 187].

Liszt, H. S., J. Pety, and R. Lucas, 2008, Astron. Astrophys. **486**, 493.

Liszt, H. S., and L. M. Ziurys, 2012, Astrophys. J. **747**, 55.

Lohmar, I., J. Krug, and O. Biham, 2009, Astron. Astrophys. **504**, L5.

Lucas, R., and H. S. Liszt, 2002, Astron. Astrophys. **384**, 1054.

Luine, J. A., and G. H. Dunn, 1985, Astrophys. J. **299**, L67.

Lutz, D., *et al.*, 2007, Astrophys. J. **661**, L25.

Mac Low, M.-M., and R. S. Klessen, 2004, Rev. Mod. Phys. **76**, 125.

MacPherson, G. J., and A. Boss, 2011, Proc. Natl. Acad. Sci. U.S.A. **108**, 19 152.

MacPherson, G. J., S. B. Simon, A. M. Davis, L. Grossman, and A. N. Krot, 2005, *Chondrites and the Protoplanetary Disk* (Astronomical Society Pacific, San Francisco), Vol. 341, p. 225.

Madden, S. C., A. Poglitsch, N. Geis, G. J. Stacey, and C. H. Townes, 1997, Astrophys. J. **483**, 200.

Maezawa, H., *et al.*, 1999, Astrophys. J. **524**, L129.

Maier, J. P., 1994, Nature (London) **370**, 423.

Maier, J. P., N. M. Lakin, G. A. H. Walker, and D. A. Bohlender, 2001, Astrophys. J. **553**, 267.

Maier, J. P., G. A. H. Walker, and D. A. Bohlender, 2004, Astrophys. J. **602**, 286.

Maier, J. P., *et al.*, 2011a, Astrophys. J. Lett. **729**, L20.

Maier, J. P., *et al.*, 2011b, Astrophys. J. **726**, 41.

Malloci, G., C. Joblin, and G. Mulas, 2007, Chem. Phys. **332**, 353.

Maret, S., E. A. Bergin, and C. J. Lada, 2006, Nature (London) **442**, 425.

Matar, E., *et al.*, 2008, Astron. Astrophys. **492**, L17.

Matrajt, G., S. Messenger, D. Bronwlee, and D. Joswiak, 2012, Meteorit. Planet. Sci. **47**, 525.

Mattila, K., D. Lemke, L. K. Haikala, R. J. Laureijs, A. Leger, K. Lehtinen, C. Leinert, and P. G. Mezger, 1996, Astron. Astrophys. **315**, L353.

McCall, B. J., T. R. Geballe, K. H. Hinkle, and T. Oka, 1998, Science **279**, 1910.

McCall, B. J., T. Oka, J. Thorburn, L. M. Hobbs, and D. G. York, 2002, Astrophys. J. **567**, L145.

McCall, B. J., J. Thorburn, L. M. Hobbs, T. Oka, and D. G. York, 2001, Astrophys. J. **559**, L49.

McCall, B. J., *et al.*, 2003, Nature (London) **422**, 500.

McCall, B. J., *et al.*, 2010, Astrophys. J. **708**, 1628.

McCarthy, M. C., C. A. Gottlieb, H. Gupta, and P. Thaddeus, 2006, Astrophys. J. **652**, L141.

McDowell, M. R. C., 1961, The Observatory **81**, 240 [http://www.ulo.ucl.ac.uk/obsmag/].

McEwan, M. J., *et al.*, 1999, Astrophys. J. **513**, 287.

Meibom, A., S. J. Desch, A. N. Krot, J. N. Cuzzi, M. I. Petaev, L. Wilson, and K. Keil, 2000, Science **288**, 839.

Menéndez, J., and J. B. Page, 2000, in *Light Scattering in Solids VIII* (Springer, Berlin), Vol. 27.

Mennella, V., 2008, Astrophys. J. **684**, L25.

Mennella, V., L. Hornekaer, J. Thrower, and M. Accolla, 2012, Astrophys. J. Lett. **745**, L2.

Merrill, P. W., 1934, Publ. Astron. Soc. Pac. **46**, 206.

Meyer, D. M., and K. C. Roth, 1991, Astrophys. J. **376**, L49.

Micelotta, E. R., *et al.*, 2012, Astrophys. J. **761**, 35.

Micelotta, E. R., A. P. Jones, and A. G. G. M. Tielens, 2010a, Astron. Astrophys. **510**, A36.

Micelotta, E. R., A. P. Jones, and A. G. G. M. Tielens, 2010b, Astron. Astrophys. **510**, A37.

Micelotta, E. R., A. P. Jones, and A. G. G. M. Tielens, 2011, Astron. Astrophys. **526**, A52.

Milam, S. N., C. Savage, M. A. Brewster, L. M. Ziurys, and S. Wyckoff, 2005, Astrophys. J. **634**, 1126.

Milam, S. N., N. J. Woolf, and L. M. Ziurys, 2009, Astrophys. J. **690**, 837.

Miller, S. L., and H. C. Urey, 1959, Science **130**, 245.

Miyauchi, N., *et al.*, 2008, Chem. Phys. Lett. **456**, 27.

Mokrane, H., *et al.*, 2009, Astrophys. J. **705**, L195.

Morisset, S., Y. Ferro, and A. Allouche, 2010, J. Chem. Phys. **133**, 044508.

Morris, M., and E. Serabyn, 1996, Annu. Rev. Astron. Astrophys. **34**, 645.

Moutou, C., J. Krełowski, L. D'Hendecourt, and J. Jamroszczak, 1999, Astron. Astrophys. **351**, 680.

Mumma, M.J., and S.B. Charnley, 2011, Annu. Rev. Astron. Astrophys. **49**, 471.

Muñoz Caro, G.M., *et al.*, 2010, Astron. Astrophys. **522**, A108.

Murray, B.J., 2003, Ph.D. (University of East Anglia).

Nagaoka, A., N. Watanabe, and A. Kouchi, 2007, J. Phys. Chem. A **111**, 3016.

Najita, J., J.S. Carr, and R.D. Mathieu, 2003, Astrophys. J. **589**, 931.

Najita, J.R., M. Ádámkovics, and A.E. Glassgold, 2011, Astrophys. J. **743**, 147.

Nakamura, T., *et al.*, 2008, Science **321**, 1664.

Neufeld, D.A., 2012, Astrophys. J. **749**, 125.

Neufeld, D.A., and M.G. Wolfire, 2009, Astrophys. J. **706**, 1594.

Neufeld, D.A., *et al.*, 2010a, Astron. Astrophys. **518**, L108.

Neufeld, D.A., *et al.*, 2010b, Astron. Astrophys. **521**, L10.

Nguyen, T.L., J.F. Stanton, and J.R. Barker, 2011, J. Phys. Chem. A **115**, 5118.

Nishitani, H., *et al.*, 2012, Publ. Astron. Soc. Jpn. **64**, 30.

Nittler, L.R., and E. Gaidos, 2012, Meteorit. Planet. Sci. **47**, 2031.

Oba, Y., N. Watanabe, A. Kouchi, T. Hama, and V. Pirronello, 2010, Astrophys. J. Lett. **712**, L174.

Oba, Y., *et al.*, 2012, Astrophys. J. **749**, 67.

Öberg, K.I., 2009, Ph.D. thesis (Leiden University).

Öberg, K.I., R.T. Garrod, E.F. van Dishoeck, and H. Linnartz, 2009, Astron. Astrophys. **504**, 891.

Öberg, K.I., H. Linnartz, R. Visser, and E.F. van Dishoeck, 2009, Astrophys. J. **693**, 1209.

Öberg, K.I., E.F. van Dishoeck, and H. Linnartz, 2009, Astron. Astrophys. **496**, 281.

Oka, T., and E. Epp, 2004, Astrophys. J. **613**, 349.

Oka, T., *et al.*, 2003, Astrophys. J. **582**, 823.

Oomens, J., 2011, EAS Publications Series **46**, 61.

Padoan, P., and J. Scalo, 2005, Astrophys. J. **624**, L97.

Padovani, M., and D. Galli, 2011, Astron. Astrophys. **530**, A109.

Padovani, M., D. Galli, and A.E. Glassgold, 2009, Astron. Astrophys. **501**, 619.

Pagani, L., E. Roueff, and P. Lesaffre, 2011, Astrophys. J. Lett. **739**, L35.

Pagani, L., *et al.*, 2009, Astron. Astrophys. **494**, 623.

Palumbo, M.E., A.C. Castorina, and G. Strazzulla, 1999, Astron. Astrophys. **342**, 551.

Pan, L., and P. Padoan, 2009, Astrophys. J. **692**, 594.

Parise, B., *et al.*, 2011, Astron. Astrophys. **526**, A31.

Parise, B., P. Bergman, and F. Du, 2012, Astron. Astrophys. **541**, L11.

Parise, B., C. Ceccarelli, A.G.G.M. Tielens, A. Castets, E. Caux, B. Lefloch, and S. Maret, 2006, Astron. Astrophys. **453**, 949.

Parise, B., *et al.*, 2005, Astron. Astrophys. **431**, 547.

Parker, D.S.N., *et al.*, 2012, Proc. Natl. Acad. Sci. U.S.A. **109**, 53.

Pech, C., C. Joblin, and P. Boissel, 2002, Astron. Astrophys. **388**, 639.

Peebles, P.J.E., and R.H. Dicke, 1968, Astrophys. J. **154**, 891.

Peeters, E., S. Hony, C. Van Kerckhoven, A.G.G.M. Tielens, L.J. Allamandola, D.M. Hudgins, and C.W. Bauschlicher, 2002, Astron. Astrophys. **390**, 1089.

Peeters, E., *et al.*, 2004, Astrophys. J. **604**, 252.

Peltzer, E.T., and J.L. Bada, 1978, Nature (London) **272**, 443.

Perault, M., *et al.*, 1996, Astron. Astrophys. **315**, L165.

Perets, H.B., *et al.*, 2005, Astrophys. J. **627**, 850.

Persson, C.M., *et al.*, 2010, Astron. Astrophys. **521**, L45.

Persson, C.M., *et al.*, 2012, Astron. Astrophys. **543**, A145.

Petrie, S., and E. Herbst, 1997, Astrophys. J. **491**, 210.

Pety, J., D. Teyssier, D. Fossé, M. Gerin, E. Roueff, A. Abergel, E. Habart, and J. Cernicharo, 2005, Astron. Astrophys. **435**, 885.

Pillai, T., F. Wyrowski, S.J. Carey, and K.M. Menten, 2006, Astron. Astrophys. **450**, 569.

Pineda, J.L., *et al.*, 2010, Astrophys. J. **721**, 686.

Pino, T., *et al.*, 2008, Astron. Astrophys. **490**, 665.

Pino, T., *et al.*, 2011, EAS Publications Series **46**, 355.

Pirali, O., M. Vervloet, J.E. Dahl, R.M.K. Carlson, A.G.G.M. Tielens, and J. Oomens, 2007, Astrophys. J. **661**, 919.

Pirronello, V., O. Biham, C. Liu, L. Shen, and G. Vidali, 1997, Astrophys. J. **483**, L131.

Pirronello, V., C. Liu, J. Roser, and G. Vidali, 1999, Astron. Astrophys. **344**, 681.

Pizzarello, S., G.W. Cooper, G.J. Flynn, 2006, in *Meteorites and the Early Solar System II*, edited by D. Lauretta and H. McSween (Arizona Press, Tucson), p. 625.

Pontoppidan, K.M., *et al.*, 2003, Astron. Astrophys. **408**, 981.

Pontoppidan, K.M., *et al.*, 2008, Astrophys. J. **678**, 1005.

Pope, C.J., and J.B. Howard, 1996, Tetrahedron **52**, 5161.

Pope, C.J., J.A. Marr, and J.B. Howard, 1993, J. Phys. Chem. **97**, 11 001.

Postma, J., S. Bari, R. Hoekstra, A.G.G.M. Tielens, and T. Schlathölter, 2010, Astrophys. J. **708**, 435.

Prasad, S.S., and S.P. Tarafdar, 1983, Astrophys. J. **267**, 603.

Puget, J.L., and A. Leger, 1989, Annu. Rev. Astron. Astrophys. **27**, 161.

Rachford, B.L., *et al.*, 2002, Astrophys. J. **577**, 221.

Rapacioli, M., C. Joblin, and P. Boissel, 2005, Astron. Astrophys. **429**, 193.

Ratajczak, A., E. Quirico, A. Faure, B. Schnitt, and C. Ceccarelli, 2009, Astron. Astrophys. **496**, L21.

Rathborne, J.M., J.M. Jackson, and R. Simon, 2006, Astrophys. J. **641**, 389.

Raty, J.-Y., and G. Galli, 2003, Nat. Mater. **2**, 792.

Raty, J.-Y., G. Galli, C. Bostedt, T.W. van Buuren, and L.J. Terminello, 2003, Phys. Rev. Lett. **90**, 037401.

Rauls, E., and L. Hornekær, 2008, Astrophys. J. **679**, 531.

Raut, U., and R.A. Baragiola, 2011, Astrophys. J. Lett. **737**, L14.

Reitsma, G., *et al.*, 2012, J. Phys. B **45**, 215201.

Requena-Torres, M.A., J. Martín-Pintado, S. Martín, and M.R. Morris, 2008, Astrophys. J. **672**, 352.

Ricca, A., C. Bauschlicher, C. Boersma, A.G.G.M. Tielens, and L.J. Allamandola, 2012, Astrophys. J. **754**, 75.

Ricca, A., C.W. Bauschlicher, Jr., A.L. Mattioda, C. Boersma, and L.J. Allamandola, 2010, Astrophys. J. **709**, 42.

Ritchey, A.M., S.R. Federman, and D.L. Lambert, 2011, Astrophys. J. **728**, 36.

Roberts, H., E. Herbst, and T.J. Millar, 2003, Astrophys. J. **591**, L41.

Roberts, H., and T.J. Millar, 2000, Astron. Astrophys. **361**, 388.

Roberts, H., and T.J. Millar, 2007, Astron. Astrophys. **471**, 849.

Robinson, J., 2006, *The History of Winemaking* (Oxford University Press, New York).

Roser, J.E., G. Manicò, V. Pirronello, and G. Vidali, 2002, Astrophys. J. **581**, 276.

Roser, J.E., G. Vidali, G. Manicò, and V. Pirronello, 2001, Astrophys. J. **555**, L61.

Rouan, D., A. Leger, A. Omont, and M. Giard, 1992, Astron. Astrophys. **253**, 498.

Sakai, N., O. Saruwatari, T. Sakai, S. Takano, and S. Yamamoto, 2010, Astron. Astrophys. **512**, A31.

Sakai, N., *et al.*, 2007, Astrophys. J. **663**, 1174.

Sakai, N., *et al.*, 2010, Astrophys. J. Lett. **718**, L49.

Salama, F., *et al.*, 2011, Astrophys. J. **728**, 154.

Sarre, P. J., J. R. Miles, and S. M. Scarrott, 1995, Science **269**, 674.

Sarre, P. J., *et al.*, 1995, Mon. Not. R. Astron. Soc. **277**, L41.

Sassara, A., G. Zerza, M. Chergui, and S. Leach, 2001, Astrophys. J. Suppl. Ser. **135**, 263.

Savage, B. D., J. F. Drake, W. Budich, and R. C. Bohlin, 1977, Astrophys. J. **216**, 291.

Scarrott, S. M., S. Watkin, J. R. Miles, and P. J. Sarre, 1992, Mon. Not. R. Astron. Soc. **255**, 11P.

Schrimpf, A., *et al.*, 1996, J. Phys. Condens. Matter **8**, 3677.

Schuppan, F., J. K. Becker, J. H. Black, and S. Casanova, 2012, Astron. Astrophys. **541**, A126.

Schutte, W. A., L. J. Allamandola, and S. A. Sandford, 1993, Icarus **104**, 118.

Schutte, W. A., and P. A. Gerakines, 1995, Planet. Space Sci. **43**, 1253.

Schutte, W. A., A. G. G. M. Tielens, and L. J. Allamandola, 1993, Astrophys. J. **415**, 397.

Seebauer, E. G., and C. E. Allen, 1995, Prog. Surf. Sci. **49**, 265.

Selegue, T. J., and J. M. List, 1994, J. Am. Chem. Soc. **116**, 4874.

Sellgren, K., 1984, Astrophys. J. **277**, 623.

Sellgren, K., K. I. Uchida, and M. W. Werner, 2007, Astrophys. J. **659**, 1338.

Sellgren, K., M. W. Werner, J. G. Ingalls, J. D. T. Smith, T. M. Carleton, and C. Joblin, 2010, Astrophys. J. Lett. **722**, L54.

Sha, X., and B. Jackshon, 2002, Surf. Sci. **496**, 318.

Sharp, R. G., N. J. Reilly, S. H. Kable, and T. W. Schmidt, 2006, Astrophys. J. **639**, 194.

Sheffer, Y., *et al.*, 2008, Astrophys. J. **687**, 1075.

Shen, C. J., J. M. Greenberg, W. A. Schutte, and E. F. van Dishoeck, 2004, Astron. Astrophys. **415**, 203.

Sheu, S.-Y., I.-P. Lee, Y. T. Lee, and H.-C. Chang, 2002, Astrophys. J. **581**, L55.

Shimajiri, Y., S. Takahashi, S. Takakuwa, M. Saito, and R. Kawabe, 2008, Astrophys. J. **683**, 255.

Sipilä, O., *et al.*, 2010, Astron. Astrophys. **509**, A98.

Sloan, G. C., *et al.*, 2007, Astrophys. J. **664**, 1144.

Smith, I. W. M., 2011, Annu. Rev. Astron. Astrophys. **49**, 29.

Smith, R. G., K. Sellgren, and A. T. Tokunaga, 1989, Astrophys. J. **344**, 413.

Smith, R. L., *et al.*, 2009, Astrophys. J. **701**, 163.

Sneden, C., A. Woszczyk, and J. Krelowski, 1991, Publ. Astron. Soc. Pac. **103**, 1005.

Snow, T. P., 2005, *Astrochemistry: Recent Successes and Current Challenges* (Cambridge University Press, Cambridge, England), Vol. 231, p. 175.

Snow, T. P., V. Le Page, Y. Keheyan, and V. M. Bierbaum, 1998, Nature (London) **391**, 259.

Snow, T. P., and B. J. McCall, 2006, Annu. Rev. Astron. Astrophys. **44**, 367.

Snow, Jr., T. P., 1977, Astrophys. J. **216**, 724.

Sonnentrucker, P., J. Cami, P. Ehrenfreund, and B. H. Foing, 1997, Astron. Astrophys. **327**, 1215.

Sonnentrucker, P., *et al.*, 2010, Astron. Astrophys. **521**, L12.

Souda, R., 2004, Phys. Rev. Lett. **93**, 235502.

Souda, R., H. Kawanowa, M. Kondo, and Y. Gotoh, 2003, J. Chem. Phys. **119**, 6194.

Speck, A. K., and M. J. Barlow, 1997, Astrophys. Space Sci. **251**, 115.

Stancil, P. C., *et al.*, 1999, Astron. Astrophys. Suppl. Ser. **140**, 225.

Stantcheva, T., P. Caselli, and E. Herbst, 2001, Astron. Astrophys. **375**, 673.

Stantcheva, T., and E. Herbst, 2004, Astron. Astrophys. **423**, 241.

Stantcheva, T., V. I. Shematovich, and E. Herbst, 2002, Astron. Astrophys. **391**, 1069.

Stein, S. E., 1978, J. Phys. Chem. **82**, 566.

Strazzulla, G., J. R. Brucato, M. E. Palumbo, and F. Spinella, 2007, Mem. Soc. Astron. Ital. **78**, 681.

Swings, P., and L. Rosenfeld, 1937, Astrophys. J. **86**, 483.

Szczepanski, J., J. Oomens, J. D. Steill, and M. T. Vala, 2011, Astrophys. J. **727**, 12.

Taquet, V., C. Ceccarelli, and C. Kahane, 2012a, Astron. Astrophys. **538**, A42.

Taquet, V., C. Ceccarelli, and C. Kahane, 2012b, Astrophys. J. Lett. **748**, L3.

Thompson, D. J., L. Baldini, and Y. Uchiyama, 2012, arXiv:1201.0988.

Thorburn, J. A., *et al.*, 2003, Astrophys. J. **584**, 339.

Thrower, J. D., *et al.*, 2011, EAS Publications Series **46**, 453.

Tielens, A. G. G. M., 1983, Astron. Astrophys. **119**, 177.

Tielens, A. G. G. M., 1990, in *Carbon in the Galaxy: Studies from Earth and Space*, edited by J. C. Tarter, S. Chang, and D. J. DeFrees (NASA Conference Publication No. 3061, p. 59.

Tielens, A. G. G. M., 2005, *The Physics and Chemistry of the Interstellar Medium* (Cambridge University Press, Cambridge, UK).

Tielens, A. G. G. M., 2008, Annu. Rev. Astron. Astrophys. **46**, 289.

Tielens, A. G. G. M, 2011, Proc. Int. Astron. Union **7**, 72 [*The Molecular Universe*, Proceedings of the IAU Symposium 280, Vol. 7 (Cambridge University Press, Cambridge, England, 2011), p. 72].

Tielens, A. G. G. M., and L. J. Allamandola, 1987, *Interstellar Processes* (Kluwer Academic Publishers, Dordrecht), Vol. 134, p. 397.

Tielens, A. G. G. M., and L. J. Allamandola, 2011, in *Physics and Chemistry at Low Temperatures*, edited by L. Khriachtchev (Pan Stanford, Singapore), p 341.

Tielens, A. G. G. M., and W. Hagen, 1982, Astron. Astrophys. **114**, 245.

Tielens, A. G. G. M., S. Hony, C. van Kerckhoven, and E. Peeters, 1999, *The Universe as Seen by ISO* (ESA), Vol. ESA-SP 427, p. 579.

Tielens, A. G. G. M., C. F. McKee, C. G. Seab, and D. J. Hollenbach, 1994, Astrophys. J. **431**, 321.

Tielens, A. G. G. M., M. M. Meixner, P. P. van der Werf, J. Bregman, J. A. Tauber, J. Stutzki, and D. Rank, 1993, Science **262**, 86.

Tielens, A. G. G. M., and T. P. Snow, 1995, *The Diffuse Interstellar Bands*, Astrophysics and Space Science Library (Kluwer Academic Publishers, Dordrecht), Vol. 202.

Tielens, A. G. G. M., A. T. Tokunaga, T. R. Geballe, and F. Baas, 1991, Astrophys. J. **381**, 181.

Tiné, S., *et al.*, 2003, Astrophys. Space Sci. **288**, 377.

Tuley, M., D. A. Kirkwood, M. Pachkov, and J. P. Maier, 1998, Astrophys. J. **506**, L69.

Turner, B. E., 1990, Astrophys. J. **362**, L29.

Turulski, J., and J. Niedzielskil, 1994, Int. J. Mass Spectrom. Ion Process. **139**, 155.

Tuthill, P. G., *et al.*, 2008, Astrophys. J. **675**, 698.

Ungerechts, H., and P. Thaddeus, 1987, Astrophys. J. Suppl. Ser. **63**, 645.

van der Tak, F. F. S., and E. F. van Dishoeck, 2000, Astron. Astrophys. **358**, L79.

van Diedenhoven, B., E. Peeters, C. Van Kerckhoven, S. Hony, D. M. Hudgins, L. J. Allamandola, and A. G. G. M. Tielens, 2004, Astrophys. J. **611**, 928.

van Dishoeck, E. F., and J. Black, 1988, Astrophys. J. **334**, 771.

van IJzendoorn, L. J., L. J. Allamandola, F. Baas, and J. M. Greenberg, 1983, J. Chem. Phys. **78**, 7019.

Van Winckel, H., M. Cohen, and T. R. Gull, 2002, Astron. Astrophys. **390**, 147.

Vaskonen, K., J. Eloranta, T. Kiljunen, and H. Kunttu, 1999, J. Chem. Phys. **110**, 2122.

Vastel, C., T. G. Phillips, and H. Yoshida, 2004, Astrophys. J. **606**, L127.

Vastel, C., *et al.*, 2006, Astrophys. J. **645**, 1198.

Vasyunin, A. I., D. A. Semenov, D. S. Wiebe, and Th. Henning, 2009, Astrophys. J. **691**, 1459.

Vasyunina, T., *et al.*, 2011, Astron. Astrophys. **527**, A88.

Vigren, E., *et al.*, 2012, Astrophys. J. **757**, 34.

Visser, R., E. F. van Dishoeck, and J. H. Black, 2009, Astron. Astrophys. **503**, 323.

Wakelam, V., and E. Herbst, 2008, Astrophys. J. **680**, 371.

Wakelam, V., *et al.*, 2010, Space Sci. Rev. **156**, 13.

Walmsley, C. M., D. R. Flower, and G. Pineau des Forts, 2004, Astron. Astrophys. **418**, 1035.

Wang, S., *et al.*, 2011, Astron. Astrophys. **527**, A95.

Ward-Thompson, D., *et al.*, 1994, Mon. Not. R. Astron. Soc. **268**, 276.

Watanabe, N., and A. Kouchi, 2008, Prog. Surf. Sci. **83**, 439.

Watanabe, N., *et al.*, 2010, Astrophys. J. Lett. **714**, L233.

Watson, J. K. G., 1994, Astrophys. J. **437**, 678.

Watson, W. D., 1973, Astrophys. J. **183**, L17.

Watson, W. D., 1974, Astrophys. J. **188**, 35.

Watson, W. D., 1976, Rev. Mod. Phys. **48**, 513.

Weisman, J. L., T. J. Lee, F. Salama, and M. Head-Gordon, 2003, Astrophys. J. **587**, 256.

Weselak, T., G. A. Galazutdinov, F. A. Musaev, and J. Krełowski, 2004, Astron. Astrophys. **414**, 949.

Westley, M. S., R. A. Baragiola, R. E. Johnson, and G. A. Baratta, 1995, Nature (London) **373**, 405.

Whittet, D. C. B., A. M. Cook, E. Herbst, J. E. Chiar, and S. S. Shenoy, 2011, Astrophys. J. **742**, 28.

Widicus Weaver, S. L., and D. N. Friedel, 2012, Astrophys. J. Suppl. Ser. **201**, 16.

Wigner, E., 1933, Z. Phys. Chem. B **23**, 28.

Winter, N. W., and F. H. Ree, 1998, J. Comput. Mater. Des. **5**, 279.

Wirström, E. S., S. B. Charnley, M. A. Cordiner, and S. N. Milam, 2012, Astrophys. J. Lett. **757**, L11.

Wirström, E. S., *et al.*, 2011, Astron. Astrophys. **533**, A24.

Woods, P. M., T. J. Millar, E. Herbst, and A. A. Zijlstra, 2003, Astron. Astrophys. **402**, 189.

Wooldridge, P. J., and J. P. Devlin, 1988, J. Chem. Phys. **88**, 3086.

Woon, D. E., 2002, Astrophys. J. **569**, 541.

Wouterloot, J. G. A., C. Henkel, J. Brand, and G. R. Davis, 2008, Astron. Astrophys. **487**, 237.

Wright, M. C. H., R. L. Plambeck, and D. J. Wilner, 1996, Astrophys. J. **469**, 216.

Young, E. D., 2007, Earth Planet Sci. Lett. **262**, 468.

Ysard, N., and L. Verstraete, 2010, Astron. Astrophys. **509**, A12.

Zapata, A., J. Schmid-Burgk, and K. M. Menten, 2011, Astron. Astrophys. **529**, A24.

Zecho, T., A. Güttler, X. Sha, B. Jackson, and J. Kuppers, 2002, J. Chem. Phys. **117**, 8486.

Zhang, W., L. Liu, and Y. Li, 2000, Phys. Rev. B **62**, 8276.

Zheng, G., S. Irle, and K. Morokuma, 2005, J. Chem. Phys. **122**, 014708.

Ziurys, L. M., 2006, Proc. Natl. Acad. Sci. U.S.A. **103**, 12 274.

Zolensky, M., *et al.*, 2008, Meteorit. Planet. Sci. **43**, 261.